Helsinki University of Technology, Electronic Circuit Design Laboratory
Report 42, Espoo 2006

DIGITAL MODULATORS WITH CREST FACTOR REDUCTION TECHNIQUES

Olli Väänänen

Dissertation for the degree of Doctor of Science in Technology to be presented with due permission of the Department of Electrical and Communications Engineering for public examination and debate in auditorium S4 at Helsinki University of Technology (Espoo, Finland) on the 17th of March, 2006, at 12 noon.

Helsinki University of Technology
Department of Electrical and Communications Engineering
Electronic Circuit Design Laboratory

Teknillinen korkeakoulu
Sähkö- ja tietoliikennetekniikan osasto
Piiritekniikan laboratorio

Distribution:
Helsinki University of Technology
Department of Electrical and Communications Engineering
Electronic Circuit Design Laboratory
P.O.Box 3000
FIN-02015 HUT
Finland
Tel. +358 9 451 2271
Fax. +358 9 451 2269

ISBN 951-22-8081-7
ISSN 1455-8440

Otamedia Oy
Espoo

Abstract

Many of the modulation methods currently in use suffer from a high Peak-to-Average power Ratio (PAR), also known as the Crest Factor (CF). The Global System for Mobile communication (GSM) is a widespread second-generation (2G) system that uses constant envelope Gaussian minimum shift keying modulation. The advantage achieved by constant envelope modulation is the possibility of using power-efficient power amplifiers (PAs). However, it might be beneficial to combine the carriers in a digital intermediate frequency in order to reduce the number of analogue components. The drawback with this is that the signal is no more a constant envelope signal, but it has a strongly fluctuating envelope with a high CF. Enhanced Data rates for GSM Evolution (EDGE) is an enhancement to the GSM system with the primary objective of tripling the on-air data rate while meeting essentially the same bandwidth occupancy of the original GSM signal. Also in the case of EDGE, if the carriers are combined prior to amplification we would end up with the same high CF problem.

Wideband Code Division Multiple Access (WCDMA) has been selected by the European Telecommunications Standards Institute for wideband wireless access to support third-generation (3G) services. Orthogonal Frequency Division Multiplexing (OFDM) is commonly considered to be a technical solution for fourth-generation (4G) services. In both cases, the transmitted signal is generated by adding together a large number of statistically independent signals, which leads to a signal with a high CF.

The high CF sets strict requirements for the linearity of the PA. In order to limit the adjacent channel leakage, it is desirable for the PA to operate in its linear region. High linearity requirements for the PA leads to low power efficiency and therefore to high power consumption. An alternative to the expense of a wide-dynamic-range PA is the use of deliberate clipping to digitally distort the signal so that the signal quality is still maintained at a sufficient level. As an extra advantage, the decreased CF gives rise to the possibility of utilizing the dynamic range of the digital circuitry and digital-to-analog converter efficiently.

This thesis discusses digital modulator design, concentrating on CF reduction algorithms. Two modulators, one capable of generating GSM, EDGE and WCDMA sig-

nals and one a very wideband OFDM modulator for 4G, are implemented. Several CF reduction algorithms are presented in the literature. Those most essential to this thesis are studied, and their applicability for the above mentioned transmission schemes is tested. The windowing method is developed further, concentrating on the implementational issues. Also, a new method for CDMA-based systems is presented and analysed. The method presented exploits the properties of the CDMA modulation in a way that, despite the high error measured by using error vector magnitude and peak code domain error, the receiving user does not experience any error. A specialised method to compensate the sinc distortion in the OFDM system is also presented.

Tiivistelmä

Monet nykyisin käytössa olevista ja käyttöön tulevista modulaatiomenetelmistä kärsivät suuresta signaalin huipputehon ja keskimääräisen tehon välisestä suhteesta ns. huippukertoimesta. Laajalle levinnyt GSM järjestelmä käyttää vakioverhokäyräistä modulaatiota, mikä mahdollistaa hyvän hyötysuhteen omaavien tehovahvistimien käytön. Toisaalta useiden GSM lähetteiden digitaalinen yhdistäminen ennen tehovahvistinta mahdollistaa muuten tehokkaiden lähetinrakenteiden toteuttamisen. Ongelmaksi tulee, että tässä tapauksessa signaali ei enää ole vakioverhokäyräinen vaan sen huippukerroin voi olla hyvinkin suuri. GSM:n kehittyneempi versio EDGE kärsii tästä samasta ongelmasta. Laajakaistainen koodijakoinen järjestelmä (WCDMA) on valittu kolmannen sukupolven matkapuhelinverkkojen perustaksi ja monikantoaaltomodulaatioon perustuvaa OFDM järjestelmää on kaavailtu neljännen sukupolven verkkoihin. Molemmissa tapauksissa lähetettävä signaali muodostetaan summaamalla useiden käyttäjien signaalit yhteen, mikä johtaa suureen huippukertoimeen.

Suuri huippukerroin asettaa suuria vaatimuksia tehovahvistimen lineaarisuudelle, mikä johtaa huonoon hyötysuhteeseen ja sitä kautta suureen tehonkulutukseen. Epälineaarinen tehovahvistin aiheuttaa signaalin vuotamista viereisille taajuuskaistoille. Vaihtoehtona paljon tehoa kuluttaville lineaarisille tehovahvistimille on signaalin tarkoituksellinen leikkaaminen. Tämä tarkoittaa signaalin huippuarvon keinotekoista pienentämistä kuitenkin siten, ettei toimenpiteen aiheuttama häiriötaso nouse liian suureksi. Signaalin huippukertoimen rajoittaminen mahdollistaa myös digitaalisten piirien sekä digitaali-analogia (D/A)-muuntimen dynaamisen alueen tehokkaan käytön.

Tässä työssä käsitellään digitaalisten modulaattorien suunnittelua keskittyen erityisesti signaalinleikkausalgoritmeihin. Kaksi digitaalista modulaattoria on suunniteltu ja toteutettu. Toteutetut modulaattorit ovat GSM/EDGE/WCDMA-monijärjestelmämodulaattori sekä erittäin laajakaistainen OFDM-modulaattori. Useita signaalinleikkausmenetelmiä on esitetty kirjallisuudessa. Niistä tämän työn kannalta oleellisimpien soveltuvuus yllämainittuihin modulaatiomenetelmiin on tutkittu. Ikkunointimenetelmää on kehitetty eteenpäin keskittyen piiritoteutuksen kannalta oleellisiin

näkökulmiin. Uusi menetelmä CDMA signaalin huippukertoimen pienentämiseksi ilman, että signaaliin aiheutetaan käyttäjään vaikuttavaa säröä, on esitetty. Lisäksi OFDM järjestelmään soveltuva menetelmä D/A-muuntimen aiheuttaman vääristymän korjaamiseksi on esitetty.

Preface

The research for this thesis has been carried out in the Electronic Circuit Design Laboratory (ECDL) of Helsinki University of Technology during the period 2000-2005. The work presented in the thesis is part of research projects funded by Nokia Networks, Nokia Research Center and the Finnish National Technology Agency (TEKES). During 2002-2005, I had the privilege of being a postgraduate student in the Graduate School in Telecommunication System-on-Chip Integration (TELESOC), which partially funded my studies. I also thank the following foundations for financial support: Nokia Foundation, the Finnish Society of Electronics Engineers (EIS), the Emil Aaltonen Foundation, the Foundation of Technology (TES) and the Finnish Cultural Foundation.

I would like to express my gratitude to my supervisor Prof. Kari Halonen for his guidance. Prof. Mike Faulkner and Prof. Markku Renfors are acknowledged for reviewing my thesis. I would also like to thank Prof. Jari Nurmi, the head of TELESOC, Dr. Timo Viero of Nokia Networks and Dr. Risto Kaunisto of Nokia Research Center.

The team I have been working with consists of Jaakko Ketola, Jonne Lindeberg, Johan Sommarek, Marko Kosunen, Jussi Pirkkalaniemi, Mikko Kaltiokallio, Mikko Talonen, Lasse Kantola and Jouko Vankka. I am grateful for their contribution to this work. I also want to thank my present and former roommates Jaakko, Johan, Aki Friman, Ilari Teikari and Lasse "Mikko" Aaltonen. I am also grateful to all the staff at ECDL for creating a relaxed and pleasant working atmosphere.

My friends deserve many thanks for the free-time activities that formed an excellent counterbalance for my work. Here, I especially want to thank Mr. Au and his family in Malaysia.

Most of all, I would like to thank my parents for all of their support of my educational and non-educational activities.

Espoo, February 2006
Olli Väänänen

This page is intentionally left blank.

Contents

This page is intentionally left blank.

Symbols and abbreviations

A	Maximum of the signal
a_k	Weighting coefficient
b	Windowed clipping function
$\mathbf{C}$	Code matrix
c	Multiplying clipping function
c_k	Spreading code
d_i	Rotation control sequence
d_k	Spread signal
$\mathbf{E}$	Error matrix
E	Error spectrum
E_b	Energy per bit
e	Error Signal
e'	Error signal after optimal scaling
$e_{d,k}$	Error signal projected onto code domain
F_r	Frequency control word
$F_{r,wl}$	Word length of F_r
f	Frequency
f_c	Carrier frequency
f_s	Sampling frequency
$f(x)$	Probability density function
G	Gain
g_{nl}	Non-linear function
$\mathbf{H}$	Unused channelisation code matrix
H	Frequency response
h	Impulse response
I	In-phase component

K	Number of active codes
$\mathbf{K}_n$	Walsh code matrix
K_{COR}	Number of CORDIC stages
K_i	CORDIC gain
K_{ROT}	Number of rotation stages
k	Scaling factor
k_i	Polynomial coefficients
N	FFT/IFFT size, number of carriers
N_b	Number of bits
N_w	Window length
P_c	Clipping probability
P_r	Residual signal power
P_s	Signal power
P_{sat}	Maximum output power of the power amplifier
Q	Quadrature component
r	Residual signal
S	Scrambling code
s	Ideal CDMA signal
s'	CDMA signal including error
$s_{d,k}$	CDMA signal projected onto code domain
s_i	Edge symbol
T	Duration of symbol
t	Time
$\mathbf{u}$	Data vector
u_k	Data waveform
V_{ref}	Reference voltage
V_{LSB}	Voltage corresponding to the least significant bit
W	Bandwidth
W_N	Twiddle factor
W_1	Bound of the sum-absolute value
W_∞	Bound of the sup-norm
$\mathbf{w}_n$	Weighting coefficient vector
w	Window function
x	Original signal
$\hat{x}$	Amplitude of x
x'	Clipped version of x
y	Distorted version of x
$\hat{y}$	Amplitude of y

α	Scaling factor
α_i	GSM data symbols
α_{rrc}	Roll-off parameter
γ	Signal to Noise Ratio
ΔCF	Reduction of Crest Factor
η	Efficiency
θ	Phase
μ	Fractional interval
σ	Standard deviation
σ^2	Variance
Φ	Rotation matrix
ϕ	Rotation angle
ω	Angular frequency
ACLR	Adjacent Channel Leakage power Ratio
ACP	Adjacent Channel Power
ASIC	Application Specific Integrated Circuit
BGA	Ball Grid Array
CDMA	Code Division Multiple Access
CF	Crest Factor
CMOS	Complementary Metal Oxid Semiconductor
CORDIC	Coordinate Rotation Digital Computer
CSD	Canonised Signed Digit
D/A	Digital to Analog
DC	Direct Current
DIF	Decimation In Frequency
DIT	Decimation In Time
DSP	Digital Signal Processing
ECDL	Electronic Circuit Design Laboratory
EDGE	Enhanced Data rates for GSM Evolution
ETSI	European Telecommunications Standards Institute
EVM	Error Vector Magnitude
FFT	Fast Fourier Transform
FHT	Fast Hartley Transform
FIR	Finite Impulse Response
FPGA	Field Programmable Gate Array
GMSK	Gaussian Minimum Shift Keying
GSM	Global System for Mobile communication

I	In-phase component
IF	Intermediate Frequency
IFFT	Inverse Fast Fourier Transform
LP	Linear Programming
LSB	Least Significant Bit
MSB	Most Significant Bit
NCO	Number-Controlled Oscillator
OBO	Output Back-Off
OFDM	Orthogonal Frequency Division Multiplexing
OSR	Oversampling Ratio
PA	Power Amplifier
PAR	Peak to Average Ratio
PCDE	Peak Code Domain Error
PDF	Probability Density Function
P/I	Pipelining/Interleaving
PSK	Phase Shift Keying
Q	Quadrature component
QAM	Quadrature Amplitude Modulation
QPSK	Quadrature Phase Shift Keying
RF	Radio Frequency
RMS	Root Mean Square
SF	Spreading Factor
SNR	Signal to Noise Ratio
VHDL	VHSIC Hardware Description Language
VHSIC	Very High Speed Integrated Circuits
WCDMA	Wideband Code Division Multiple Access
2G	Second Generation
3G	Third Generation
3GPP	Third Generation Partnership Project
4G	Fourth Generation

Chapter 1

Introduction

1.1 Motivation of the thesis

This thesis discusses digital modulator design, concentrating on CF reduction algorithms. Many of the modulation methods currently in use suffer from high Peak-to-Average power Ratio (PAR). The PAR is often measured by the Crest Factor (CF). There are several CF definitions presented in the literature, but the definition used in this thesis is

$$\mathrm{CF} = 10\log_{10}\left(\frac{\max(x^2)}{E[x^2]}\right), \tag{1.1}$$

where x is a real valued upconverted bandpass signal.

The Global System for Mobile communication (GSM) is a widespread second-generation (2G) system that uses constant envelope Gaussian Minimum Shift Keying (GMSK) modulation. The advantage achieved by constant envelope modulation is the possibility of using power efficient power amplifiers (PAs). However, it might be beneficial to combine the carriers in digital Intermediate Frequency (IF) in order to reduce the number of analogue components [1], [2]. The drawback with this is that the signal is no more a constant envelope signal, but one with a strongly fluctuating envelope with a high CF. Enhanced Data rates for GSM Evolution (EDGE) is an enhancement to the GSM system with the primary objective of tripling the on-air data rate while meeting essentially the same bandwidth occupancy of the original GSM signal. Also in the case of EDGE, if the carriers are combined prior to amplification, we would end up with the same high CF problem.

Wideband Code Division Multiple Access (WCDMA) has been selected by the European Telecommunications Standards Institute (ETSI) for wideband wireless access to support third-generation (3G) services. Orthogonal Frequency Division Multiplexing (OFDM) is commonly considered as a technical solution for fourth-generation

(4G) services. In both WCDMA and OFDM cases, the transmitted signal is generated by adding together a large number of statistically independent signals, which leads to a signal with a high CF.

The high CF sets strict requirements for the linearity of the PA. In order to limit the adjacent channel leakage and other distortion effects, it is desirable for the PA to operate in its linear region. High linearity requirements for the PA lead to low power efficiency and therefore to high power consumption (class A amplifier). In the base station, power consumption itself is not a problem as it is in mobiles, but the heat generated by high power consumption is. An alternative to the expense of a wide-dynamic-range power amplifier is the use of deliberate clipping to digitally distort the signal so that the signal quality is still maintained at a sufficient level. As an extra advantage, the decreased CF gives rise to the possibility of utilizing the dynamic range of the digital circuitry and Digital-to-Analog (D/A)-converter efficiently. In the following, the effect of the CF on the performance of PA and D/A-converter is discussed in more detail.

1.1.1 Power amplifier

Due to the nature of signal generation, WCDMA, OFDM and multicarrier GSM and EDGE signals have large CFs, which set high demands for the linearity of the PA. A non-linear transfer function causes regrowth of the spectrum and decreases the modulation accuracy.

PAs are divided into classes according to the biasing used. A class A amplifier is defined as an amplifier that is biased so that the current drawn from the battery is equal to the maximum output current. The class A amplifier is the most linear of all amplifier types, but the maximum efficiency of the amplifier is limited to 50%. In reality, due to the fact that the amplitude of the input signal is most of the time much less than its maximum value, the efficiency is much less than the theoretical maximum, i.e. only a few percent [3]. This poor efficiency causes high power consumption, which leads to warming in physical devices. This is a problem especially in a base station where the transmitted power is usually high.

To achieve a better efficiency, the amplifier can be biased so that current flows only half the time on either the positive or negative half cycle of the input signal. An amplifier biased like this is called a class B amplifier. The cost of the increased efficiency is worse linearity than in a class A amplifier. High demands on linearity make class B unsuitable for a system with high CF. On the other hand, the large scale of the input signal makes it difficult to bias an amplifier operating in class A. In practice, the amplifier is a compromise between classes A and B, and is called a class AB amplifier. [3]

1.1.1.1 Effect of the crest factor

The Output Back-Off (OBO) is defined as

$$\mathrm{OBO} = 10\log_{10}\left(\frac{P_{sat}}{E[g_{nl}(x)^2]}\right), \tag{1.2}$$

where g_{nl} is a non-linear function representing the non-linear gain response of the PA and P_{sat} is the maximum output power of the PA. The OBO defines how many decibels less than the maximum saturated output power the average output power is. This is clarified in Figure 1.1. If the PA is assumed to operate in the linear region, and the CF of the input signal is assumed to be high, i.e. the maximum output power is achieved, the OBO becomes

$$\mathrm{OBO} = 10\log_{10}\left(\frac{\max((\alpha x)^2)}{E[(\alpha x)^2]}\right) = 10\log_{10}\left(\frac{\max(x^2)}{E[x^2]}\right), \tag{1.3}$$

which is, in this case, the same as the CF of the input signal. In a real system, the gain characteristic is not linear near the saturation point. For this reason, equality between CF and OBO does not hold, but it can be assumed that

$$OBO \approx CF. \tag{1.4}$$

It is a well known fact that the efficiency of the PA is dependent on OBO [3], [4]. CF reduction enables the reduction of the OBO and, thereby, improves the efficiency. This gives a motivation to find methods for reducing the CF, which is the main topic of this thesis.

1.1.2 D/A-converter

A further advantage of the digital clipping is that the maximum of the clipped signal is known, which gives a possibility of scaling the clipped signal to full dynamic range. This makes the design of the D/A-converter easier because the number of bits needed can be reduced.

The Signal-to-Noise Ratio (SNR) at the output of the D/A-converter can be written as

$$\mathrm{SNR} = 10\log_{10}\left(\frac{E[x^2]}{E[e^2]}\right), \tag{1.5}$$

where x is the ideal waveform and e the quantization error. Assuming that the quantization error is uniformly distributed between $\pm V_{LSB}/2$ (V_{LSB} is the voltage corresponding to the Least Significant Bit (LSB)), and the signal is scaled to full swing

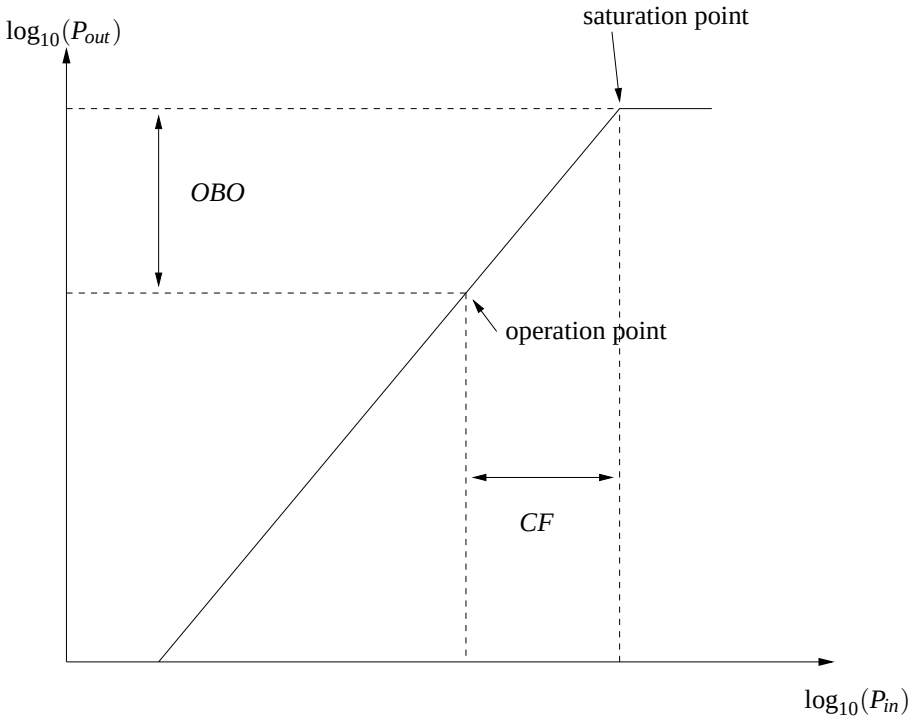

Figure 1.1 Definition of the Output Back-Off.

$\pm V_{ref}$, we obtain

$$\mathrm{SNR} = 10\log_{10}\left(\frac{V_{ref}^2/\mathrm{cf}}{V_{LSB}^2/12}\right), \tag{1.6}$$

where cf is the non-logarithmic presentation of the crest factor $\mathrm{CF} = 10\log_{10}(\mathrm{cf})$. Using the relation between V_{ref} and V_{LSB}, Equation 1.6 can be simplified to

$$\mathrm{SNR} = 20\log_{10}(2^{N_b-1}) + 10\log_{10}\left(\frac{12}{\mathrm{cf}}\right), \tag{1.7}$$

where N_b is the number of bits, and further to

$$\mathrm{SNR} = 6.02(N_b-1) + 10.8 - \mathrm{CF}. \tag{1.8}$$

In the derivation of Equation 1.8, the noise is integrated over the whole frequency band from zero to the Nyquist frequency ($f_s/2$). In order to find an equation for the Adjacent Channel Power (ACP), the noise must be integrated over a frequency band with a bandwidth equal to the signal bandwidth (W). This can be done as follows:

$$E[e_{bb}^2] = \sum_{m \in W} |E_m|^2 = \frac{W}{f_s/2} \sum_{m=0}^{M-1} |E_m|^2 = \frac{W}{f_s/2} \frac{1}{M} \sum_{m=0}^{M-1} |e_m|^2 = \frac{W}{f_s/2} E[e^2]. \quad (1.9)$$

The second equals sign is justified by assuming that the error spectrum (E) is flat, the third follows from Parseval's formula. In a manner similar to that of the previous case, we obtain

$$\text{ACP} = 6.02(N_b - 1) + 10.8 - \text{CF} + 10 \log_{10} \left(\frac{f_s}{2W} \right). \quad (1.10)$$

Equations 1.8 and 1.10 are tested through simulations and the results presented in Figures 1.2 and 1.3. The test signal is a multitone bandpass signal with a brickwall type spectrum. The relationship between the bandwidth and the sampling frequency is $f_s/W = 9.86$. This value was chosen because it corresponds to the OFDM modulator case presented in Chapter 9. In this example, the simulated values are very precisely in accord with the theoretical values. The simulations were repeated varying the f_s/W value between 8 and 80; the results were concordant with the case presented.

In practice, the CF can be reduced utilising various methods. Depending on the method chosen, the CF is normally reduced at the cost of the signal quality, i.e. reduced SNR and increased ACP. Therefore Equations 1.8 and 1.10 should not be assumed to give precise results in the real case when clipping is involved. Instead, they show the general relationship between the CF and signal quality. When the examination is limited to the D/A-converters quantization error, an adequate performance in terms of SNR and ACP can be achieved with lower number of bits when the CF is kept low.

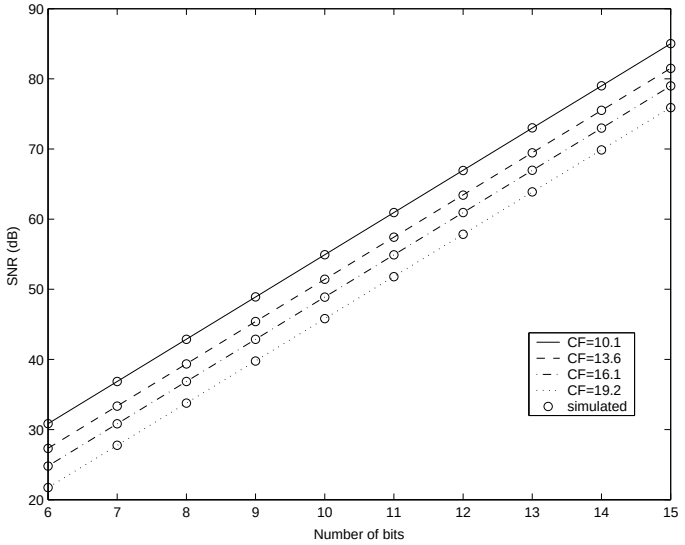

Figure 1.2 Simulated and theoretical SNR curves ($f_s/W = 9.86$).

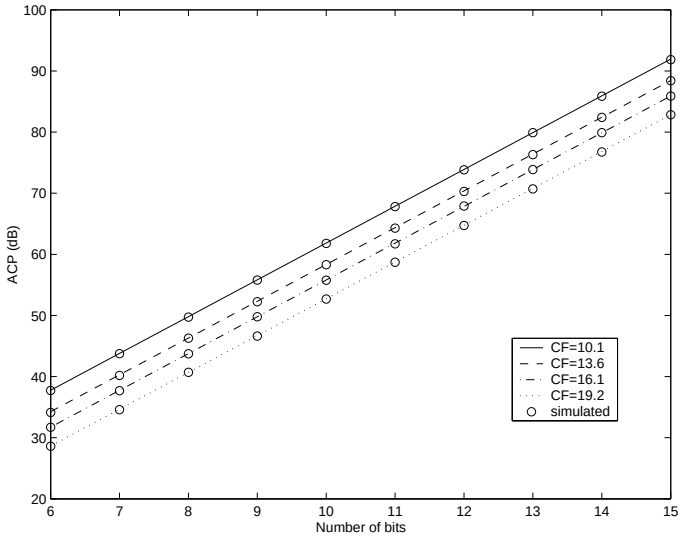

Figure 1.3 Simulated and theoretical ACP curves ($f_s/W = 9.86$).

1.2 Related work

As shown in previous sections, it is advantageous to minimise the CF. Several advanced CF reduction algorithms, in addition to the most obvious soft limiting [5]- [7], have been presented in the literature. These algorithms can be divided into two main categories. In the first category, the signal is deliberately distorted, still keeping the signal quality at sufficient level. The second category includes the algorithms that exploit the properties of the modulation in such a way that the signal quality is not deteriorated. In practice, this means a reduced payload, because a part of the signal is used for CF reduction or side information to be transmitted.

One problem with the soft limiting is that, as a non-linear operation, it causes spectral splattering. This can be prevented by filtering, e.g, placing the clipping operation before the channel filter. Unfortunately, the filtering tends to increase the CF, partly cancelling the effect of clipping. In [8], an algorithm to reduce the undesirable peak regrowth caused by filters is presented. Another problem is that when the sidebands are cleaned using filters, all the clipping noise is located at the signal band. In [9], a method to control the amount of clipping noise at the signal band is presented.

A windowing method that makes it possible to control the spectrum of the clipped signal by choosing a suitable window is presented in [10]- [14]. The idea is to multiply the original signal with a function composed of windows so that the wanted clipping result is achieved. The spectrum of the clipped signal can be controlled by the shape and length of the window in use.

A method to achieve a constant envelope in Code Division Multiple Access (CDMA) transmission is presented in [15]. This is an example of the method in which the payload is reduced in order to decrease the CF. In this method, only a part of the spreading codes is used for the transmission, while the rest of the codes are used for CF reduction. The unused codes are added to the transmitted signal with suitable weighting coefficients in order to keep the envelope of the composite signal constant. A tone reservation method for OFDM, based on an idea similar to that presented in [15], is presented in [16]. Instead of codes, a part of the subcarriers is reserved for CF reduction purposes.

One approach to the CF reduction problem is the use of specially chosen data, code and subcarrier sets. Examples of these methods are presented in [17]- [21]. Because these methods involve not only the modulator-level design but also the higher-level system design they are not discussed further.

Direct comparison of the modulators presented in this work to the state of the art modulators is difficult due to structural dissimilarities. [2] is an example of a GSM modulator with an on-chip D/A-converter. Published OFDM modulators, e.g. [22] and [23], are baseband-DSP processors without digital IF or on-chip DAC.

1.3 Research contribution and organisation of the thesis

This thesis discusses digital modulator design, concentrating on CF reduction algorithms. Two modulators, one capable of generating GSM, EDGE and WCDMA signals and one very wideband OFDM modulator for 4G are implemented.

Several CF reduction algorithms have been presented in the literature [5]- [21]. The most essential of those for this thesis are studied and their applicability for above mentioned transmission schemes is tested. The windowing method [10] is developed further, concentrating on the implementational issues. The presented implementation enables the windowing at high clock frequencies with a negligible processing delay. Also, based on [15], a new method for the CDMA system is presented and analysed. The method presented differs from [15] in that it does not aim for constant envelope signal. Instead, the target is only to reduce the CF by adding unused codes, which makes this method much more flexible than the one presented in [15]. The method presented is not comparable to the conventional clipping methods in terms of system specifications. The method presented exploits the properties of the CDMA modulation in a way that, despite the high error measured by using Error Vector Magnitude (EVM) and Peak Code Domain Error (PCDE), the receiving user does not experience any error.

A novel method to compensate the sinc distortion in the OFDM system caused the sample and hold circuit of the D/A-converter is presented. Conventionally, the sinc distortion is compensated by using filters [24], [25]. The compensation method presented is based on the properties of the OFDM modulation and is therefore applicable in the aforementioned system only.

The necessary signal quality metrics related to GSM, EDGE, WCDMA and OFDM transmission are discussed in Chapter 2. For GSM, EDGE and WCDMA signals, the quality metrics are specified in GSM and WCDMA standards. However, it is shown that, in the case of WCDMA, the quality metrics used do not guarantee an adequate signal quality for every user. Despite the fact presented, elsewhere in this thesis the quality metrics are used as they are specified in WCDMA standards. A mathematical model for signal quality metrics of the baseband clipped Gaussian distributed signal is presented in Chapter 3. Chapter 4 presents a new implementation for the windowing algorithm [10]. In Chapter 5, several clipping methods presented in the literature are discussed and compared in the case of WCDMA. An alternative method to decrease the CF of the CDMA signal, not comparable to methods discussed in Chapter 5 in terms of system specifications, is presented and tested in Chapter 6. The idea was developed jointly by the author and Dr. T. Viero while L. Kantola M.Sc assisted with the linear programming optimisation problem. Properties of GSM and EDGE mul-

ticarrier signals are discussed in Chapter 7 where the applicability of the windowing method is studied also.

Chapters 8 and 9 present a digital multimode modulator and an OFDM modulator, respectively, both designed at the Electronic Circuit Design Laboratory (ECDL). The algorithm design of the multimode modulator was done jointly by the author and Dr. J. Vankka. The electrical design of the digital part and the D/A-converter was carried out by J. Ketola M.Sc, J. Sommarek Lic.Sc and M. Kosunen Lic.Sc. The algorithm design of the OFDM modulator was done by the author and the electrical design was carried out by J. Lindeberg M.Sc. The D/A-converter was designed by J. Pirkkalaniemi M.Sc. In this design, the clipping algorithm is also implemented. Chapter 9 presents also a novel method to compensate the sinc distortion in the OFDM system. Finally, Chapter 10 presents the conclusions of the thesis.

This page is intentionally left blank.

Chapter 2

Quality parameters of the signal

This chapter presents the signal quality metrics used in this thesis. The relationship between EVM and PCDE is mathematically analysed; it is shown that there are deficiencies when the EVM and PCDE are used to measure the quality of the WCDMA signal. Section 2.3 is based on [26].

2.1 Spectrum of the signal

In order not to disturb the other communication systems, the power of the transmitted signal must be located within a limited frequency band. Due to the non-ideal transmitters and clipping, it is impossible to generate a signal with fully limited bandwidth. Instead, the maximum level of disturbance tolerated at the adjacent channels is defined.

For GSM and EDGE signals, the spectrum of the signal is calculated; it should fit to the mask specified in [27]. In the case of a WCDMA signal, the Adjacent Channel Leakage power Ratio (ACLR) is calculated; it should stay below the value specified in [28]. The ACLR is the ratio of the transmitted power to the power after a receiver filter in the adjacent channel. Both the transmitted power and the received power are measured through a matched filter (Root Raised Cosine) with a noise bandwidth equal to the chip rate 3.84 MHz [28].

2.2 Modulation accuracy

2.2.1 Error Vector Magnitude

The modulation accuracy of the WCDMA and EDGE signals is measured by Error Vector Magnitude. EVM is a measure for the difference between the theoretical wave-

form and modified version of the measured waveform. The measured waveform is modified by first passing it through a specified receiver measuring filter [27], [28]. The waveform is further modified by selecting the frequency, absolute phase, absolute amplitude and clock timing so as to minimize the error vector. The EVM result is defined as the square root of the ratio of the mean error vector power to the mean reference signal power expressed as a percentage. Mathematically, the error vector e can be written as

$$e = y - x, \tag{2.1}$$

where y is the modified measured signal and x the ideal transmitted signal. EVM can be defined as

$$\mathrm{EVM}_{rms} = \sqrt{\frac{E[|e|^2]}{E[|x|^2]}}. \tag{2.2}$$

2.2.2 Peak Code Domain Error

The quality of a WCDMA signal is also measured by the Peak Code Domain Error. PCDE is computed by projecting the power of the error vector (Equation 2.1) onto the code domain at a specific Spreading Factor (SF). The Code Domain Error for every code in the domain is defined as the ratio of the mean power of the projection onto that code to the mean power of the composite reference waveform. This ratio is expressed in dB. The Peak Code Domain Error is defined as the maximum value for the Code Domain Error for all codes [28].

The composite reference waveform s is equal to x in Equation (2.1). The projection of the error vector is calculated by despreading the error vector by all codes. After the despreading operation, there are SF error signals $e_{d,k}$. The PCDE is calculated from equation

$$\mathrm{PCDE} = 10\log_{10}\left(\frac{\max(E[|e_{d,k}|^2])}{E[|s|^2]}\right). \tag{2.3}$$

2.2.3 Phase error

The accuracy of the GMSK modulation is measured by computing the difference between the phase of the transmitted waveform and the phase of the expected one. The Root Mean Square (RMS) and peak value of the phase error shall not be greater than specified in [27].

2.3 Performance of EVM and PCDE in a WCDMA Downlink

In a WCDMA system, the downlink signal the base station transmits is designed to fulfil the specifications set in the Third-generation Partnership Project (3GPP) standard [28]. In this section, the performance of the EVM and PCDE quality metrics is impugned. It is shown that the limits of EVM and PCDE do not guarantee that the user will experience an adequate SNR.

Due to the high CF of the WCDMA downlink signal, it may be viable to distort the signal digitally, allowing some deterioration in the signal quality. The amount of distortion in the time domain is measured by EVM and PCDE. In base-station conformance testing, specialized test signals are used [28]. When the effect of clipping is studied, it may cause problems if these signals alone are tested. In a real system, the number of users and the relative power levels between users vary. Keeping the EVM and PCDE at some predefined level does not necessarily lead to a situation in which the SNR for each user, after the despreading operation, is sufficient. A mathematical model for the behaviour of the SNR as a function of the PCDE and the number of active codes is presented in the following. It is shown that the SNR is strongly dependent on the number of active codes, not only the PCDE, as it would be if it were assumed that fulfilling the PCDE requirements leads to an adequate signal quality in every case.

2.3.1 Mathematical analysis

In a WCDMA system, the base station spreads and sums the baseband signals intended for different users. The signal intended for user k can be written in the complex domain as

$$d_k(m) = u_k(m)c_k(m), \tag{2.4}$$

where u_k is the data waveform and the c_k the spreading waveform, known as a channelization code. The Quadrature Phase Shift Keying (QPSK) modulation is assumed, so the complex symbols u_k have a constant amplitude. The composite baseband signal can be written as

$$s = \sum_{k=1}^{K} a_k d_k, \tag{2.5}$$

where K is the number of active codes and a_k the weighting coefficient proportional to the power of the code channel k. At the transmitter, noise is added as a result of clipping and other non-idealities. The transmitted signal s' can be expressed as

$$s' = s + e, \tag{2.6}$$

where e is an error signal. The signal quality is measured by the EVM and PCDE [28] presented in Equations 2.2 and 2.3 respectively. When the number of active codes K is large enough, according to the central limit theorem, the composite signal s becomes normally distributed. In this case, as it will be shown in Chapter 3, the relationship between the EVM and the PCDE can be written as

$$\mathrm{PCDE} = 10\log_{10}\left(\frac{1}{\mathrm{SF}}\mathrm{EVM}^2\right), \tag{2.7}$$

where SF is the spreading factor used.

The signal quality experienced by the user k can be measured by SNR γ, defined as

$$\gamma_k = \frac{E[|s_{d,k}|^2]}{E[|e_{d,k}|^2]}, \tag{2.8}$$

where $s_{d,k}$ is the despread version of the signal s when the code k is used in the despreading operation. Using Equation 2.5, we get the power of the despread signal so Equation 2.8 can be written as

$$\gamma_k = \frac{a_k^2}{E[|e_{d,k}|^2]}. \tag{2.9}$$

This equation shows how the SNR of the user k is strongly dependent on the power level of the user in question. When the EVM is kept at some specified level and a fixed spreading factor is used, according to Equation 2.7, the PCDE can be calculated by using these two quantities. When the error signal e is additive white Gaussian noise, the variance of the despread error signal does not depend much on the code k used. If all users have equal power levels ($a_k = 1$), the composite signal is simply a sum of binary random variables with variance K [29]. In this case, the PCDE can be written as

$$\mathrm{PCDE} = 10\log_{10}\left(\frac{E[|e_{d,k}|^2]}{K}\right), \tag{2.10}$$

and, assuming that all active channels have approximately equal behaviour, this can be further written as

$$\mathrm{PCDE} = 10\log_{10}\left(\frac{1}{K\gamma}\right), \tag{2.11}$$

from which the SNR can be solved:

$$\gamma = \frac{10^{-\mathrm{PCDE}/10}}{K}. \tag{2.12}$$

This can be expressed in decibels as

$$\mathrm{SNR} = -\mathrm{PCDE} - 10\log_{10}(K). \tag{2.13}$$

The simulated SNR and the SNR calculated from Equation 2.13 are presented in Figure 2.4 as a function of the number of the active channel codes when the PCDE is -35 dB. The spreading factor of 256 is used and all the active codes have equal powers. The results show that the behaviour of the SNR is as Equation 2.13 predicts. The error signal is generated by clipping the original transmitted signal at the baseband.

The SNR experienced by a user depends strongly on the power level of the user in question, while the EVM and PCDE still fulfil the specifications. In the WCDMA conformance testing [28], the measurements of the EVM and PCDE are limited in a few cases when the specified test signals are used. In the PCDE measurements, there are two possible test signals, one with 16 active channels and the other with 32 active channels. The larger of these two options that can be supported by the equipment being tested should be used. In both cases, the PCDE specification is the same, -33 dB. According to Equation 2.13, this leads to unequal user SNR between these two cases.

The main issue in the preceding review is to show that the specified EVM and PCDE levels do not guarantee that the user has an adequate signal quality. The presented case is simplified by assuming that all users have the same power level, in which case only the number of users affects the SNR, through the fact that the total power is distributed among the users. If power control is used, i.e. unequal power levels are used, the situation is more complicated, but the problem remains the same. The main problem is whether the EVM and PCDE are adequate performance parameters when the transmitter is designed. Especially when clipping is being studied, the specified test signals [28] are not suitable and, as shown, in general, the performance of the single code channel cannot be measured by using only EVM and PCDE.

2.4 Conclusions

The essential signal quality metrics are presented and a problem related to the EVM and PCDE specifications is discussed. It is shown that the SNR experienced by the user is not dependent only on the EVM and PCDE, as it would be if it were assumed that fulfilling the requirements leads to an adequate signal quality. This limits the usage of the EVM and PCDE in a few specified cases [28]. Unfortunately, when clipping is studied, more test signals are needed; therefore it might be beneficial to change the definition of the PCDE so that the error projected to the specified code is compared to the power of the corresponding code channel instead of the power of the composite signal.

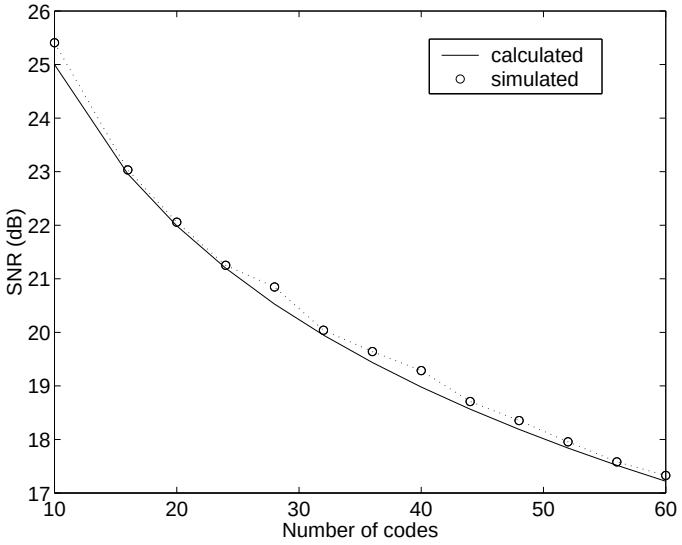

Figure 2.1 From Equation 2.13 calculated and simulated SNR.

Chapter 3

Effect of baseband clipping

In this chapter, the effect of baseband clipping on signal quality is analysed. It is assumed that the In-phase (I) and Quadrature (Q) branches of the complex signal to be clipped are Gaussian distributed. This assumption is valid for signals that are generated by adding several statistically independent signals, e.g. CDMA and OFDM signals. A mathematical model for EVM and PCDE as a function of the clipping ratio is presented in two cases. At first, I and Q components are clipped independently, after which the complex envelope is clipped. The evaluation of the EVM is valid for all Gaussian distributed signals, but the use of the PCDE is restricted to CDMA signals only.

The clipping takes place before the pulse shaping filtering and, therefore, the spectral splattering is not a problem. In this analysis, the modulation and demodulation are assumed to be ideal and the clipping is the only source of error. Due to the peak regrowth caused by the pulse shaping filtering, this analysis cannot give accurate results for the relationship between the CF of the IF signal and the clipping level. However, these results give a straightforward way to minimise the clipping ratio within given signal-quality constraints which, if it is assumed that the peak regrowth is independent of clipping, leads to minimised CF at IF. This Chapter is based on [30].

3.1 Clipping I and Q independently

Signals I and Q are clipped independently so that the maximum amplitude of I and Q is A. This is presented in Figure 3.1. Signals I and Q can be modelled as independent Gaussian distributed random variables with zero mean and variance σ^2. The Probability Density Function (PDF) of the random variable x, presenting both I and Q

is

$$f(x) = \frac{1}{\sqrt{2\pi}\sigma} e^{-x^2/2\sigma^2}. \tag{3.1}$$

Using x, the clipping can be written as

$$x' = \begin{cases} A & x > A \\ x & |x| \leq A \\ -A & x < -A. \end{cases} \tag{3.2}$$

Probability P_{c+} that clipping occurs at the positive side is

$$P_{c+} = P(x > A) = \frac{1}{\sqrt{2\pi}\sigma} \int_A^\infty e^{-x^2/2\sigma^2} dx \tag{3.3}$$

$$= \frac{1}{2} \mathrm{erfc}(\frac{A}{\sigma\sqrt{2}}).$$

Let us define an error signal e as

$$e = \begin{cases} x - A & x > A \\ 0 & x \leq A. \end{cases} \tag{3.4}$$

By using the conditional PDF,

$$f(x|x > A) = \frac{f(x)}{\int_A^\infty f(x)dx} = \begin{cases} \frac{2f(x)}{\mathrm{erfc}(\frac{A}{\sigma\sqrt{2}})} & x \geq A \\ 0 & x < A \end{cases} \tag{3.5}$$

we can calculate the first and the second conditional moment for error signal e as follows

$$E[e|x > A] = \sqrt{\frac{2}{\pi}} \frac{1}{\sigma \mathrm{erfc}(\frac{A}{\sigma\sqrt{2}})} \int_A^\infty (x - A) e^{-x^2/2\sigma^2} dx \tag{3.6}$$

$$= \sqrt{\frac{2}{\pi}} \frac{\sigma}{\mathrm{erfc}(\frac{A}{\sigma\sqrt{2}})} e^{-A^2/2\sigma^2} - A$$

$$E[e^2|x > A] = \sigma^2 + A^2 - \sqrt{\frac{2}{\pi}} \frac{\sigma A}{\mathrm{erfc}(\frac{A}{\sigma\sqrt{2}})} e^{-A^2/2\sigma^2}. \tag{3.7}$$

Because PDF 3.1 is symmetrical, in the case that the clipping occurs both at the negative and positive side, we can assume that

$$P_c = P(|x| > A) = 2P(x > A) = \mathrm{erfc}(\frac{A}{\sigma\sqrt{2}}), \tag{3.8}$$

$$E[e\big||x| > A] = 0, \tag{3.9}$$

$$E[|e|\big||x|>A] = E[e\big|x>A], \tag{3.10}$$

$$E[e^2\big||x|>A] = E[e^2|x>A]. \tag{3.11}$$

The average power of the error signal can now be calculated by multiplying the conditional second moment with the clipping probability

$$E[e^2] = P_c E[e^2\big||x|>A] \tag{3.12}$$

$$= (\sigma^2+A^2)\text{erfc}(\frac{A}{\sigma\sqrt{2}}) - \sigma A\sqrt{\frac{2}{\pi}}e^{-A^2/2\sigma^2}.$$

Similarly, we get the average absolute value of the error signal

$$E[|e|] = \sigma\sqrt{\frac{2}{\pi}}e^{-A^2/2\sigma^2} - A\text{erfc}(\frac{A}{\sigma\sqrt{2}}). \tag{3.13}$$

3.1.1 Error Vector Magnitude

The received signal y can be written as

$$y = x - e, \tag{3.14}$$

where x is the ideal transmitted signal and e the error signal. The EVM is calculated by comparing the received signal y to the reference signal x', which is a scaled version from signal x. The error is calculated from equation

$$e' = x' - y = \alpha x - y = (\alpha-1)x + e, \tag{3.15}$$

where α is the scaling factor. EVM is defined as

$$\text{EVM} = \sqrt{\frac{E[e'^2]}{E[x'^2]}} = \sqrt{\frac{E[e'^2]}{\alpha^2 E[x^2]}}. \tag{3.16}$$

The scaling factor α must be chosen so that EVM is minimized. Combining Equations 3.15 and 3.16, we get

$$\text{EVM} = \sqrt{\frac{(\alpha-1)^2E[x^2] + 2(\alpha-1)E[xe] + E[e^2]}{\alpha^2 E[x^2]}}, \tag{3.17}$$

which is minimized when

$$\alpha = \frac{1 - 2\frac{E[xe]}{E[x^2]} + \frac{E[e^2]}{E[x^2]}}{1 - \frac{E[xe]}{E[x^2]}}. \tag{3.18}$$

The term $E[xe]$ can be written as

$$E[xe] = E[(A+|e|)|e|] = AE[|e|] + E[e^2]. \tag{3.19}$$

Combining Equations 3.12, 3.13, 3.16, 3.18 and 3.19, α becomes

$$\alpha = \frac{1 + (\frac{A^2}{\sigma^2} - 1)\text{erfc}(\frac{A}{\sigma\sqrt{2}}) - \frac{A}{\sigma}\sqrt{\frac{2}{\pi}}e^{-A^2/2\sigma^2}}{1 - \text{erfc}(\frac{A}{\sigma\sqrt{2}})}, \tag{3.20}$$

and EVM can be written in the form

$$\text{EVM} = \frac{1}{\alpha}\Big[(\alpha-1)^2 + [(2\alpha-1) + \frac{A^2}{\sigma^2}]\text{erfc}(\frac{A}{\sigma\sqrt{2}}) \tag{3.21}$$

$$-\frac{A}{\sigma}\sqrt{\frac{2}{\pi}}e^{-A^2/2\sigma^2}\Big]^{1/2}.$$

The EVM calculated from Equation 3.21 and the simulated EVM are presented in Figure 3.2. The test data is a combination of 67 code channels with a spreading factor of 128, and the number of samples is 128000.

3.1.2 Peak Code Domain Error

At first, the error signal e' is projected onto the code domain. The PCDE is the ratio of the mean power of the projected error signal to the mean power of the reference waveform x' expressed in decibels. The mean power of the reference waveform equals the variance $\alpha^2\sigma^2$ of the signal x'. It is assumed that descrambling has no effect on the distribution of the error signals.

The projection of the error vector e' onto the code domain can be expressed as

$$e_{d,k}(n) = \frac{1}{\text{SF}}\sum_{i=1}^{\text{SF}} c_k(i)e'(n\text{SF}+i), \tag{3.22}$$

where c_k is the spreading code. Defining

$$e_i(n) = e'(n\text{SF}+i), \tag{3.23}$$

$e_{d,k}$ can be modelled as a sum of random variables $e_i, i = 1,2,..,\text{SF}$. Because e' has zero mean, also $e_{d,k}$ and e_i have zero mean. For a zero mean signal, the power of the

signal (second moment) is equal to variance. Variance of the $e_{d,k}$ is

$$E[e_{d,k}^2] = \frac{1}{\mathrm{SF}^2}\Big[\sum_{i=1}^{\mathrm{SF}} c_k(i)^2 E[e_i^2] + \sum_{i\neq j} c_i c_j \mathrm{Cov}[e_i, e_j]\Big] \tag{3.24}$$

$$= \frac{E[e'^2]}{\mathrm{SF}} + \frac{1}{\mathrm{SF}^2}\sum_{i\neq j} c_i c_j \mathrm{Cov}[e_i, e_j] = \frac{1}{\mathrm{SF}}(E[e'^2] + C_{ij}).$$

The PCDE can be written in the form

$$\mathrm{PCDE} = 10\log_{10}\Big(\frac{E[e_{d,k}^2]}{E[x'^2]}\Big) \tag{3.25}$$

$$= 10\log_{10}\Big(\frac{1}{\mathrm{SF}\alpha^2 E[x^2]}(E[e'^2] + C_{ij})\Big).$$

If random variables $e_i, i = 1, 2, .., \mathrm{SF}$ are assumed to be independent, the covariance term C_{ij} is zero. Using Equation 3.16, Equation 3.25 can be written as a function of EVM

$$\mathrm{PCDE} = 10\log_{10}\Big(\frac{1}{\mathrm{SF}}\frac{E[e'^2]}{\alpha^2 E[x^2]}\Big) \tag{3.26}$$

$$= 10\log_{10}\Big(\frac{1}{SF}\mathrm{EVM}^2\Big).$$

The PCDE calculated from Equation 3.26 and the simulated PCDE are presented in Figure 3.3. The difference at high clipping rations can be explained by the fact that, due to the calculation of the PCDE, a Gaussian distributed test signal cannot be used. Instead, a CDMA signal with a limited peak value is used, which means that, with high clipping ratios, the probability of exceeding the clipping threshold is considerably smaller than in the case of an ideally Gaussian distributed signal. Therefore, the simulated results are slightly better than the calculated.

3.2 Clipping complex envelope

The complex baseband signal

$$x = I + jQ \tag{3.27}$$

is clipped so that the maximum absolute value of the x is A. This is illustrated in Figure 3.1. As was the case earlier, I and Q are Gaussian distributed with zero mean and variance σ^2 and independent. Amplitude $\hat{x}$ is defined as

$$\hat{x} = \sqrt{I^2 + Q^2} \tag{3.28}$$

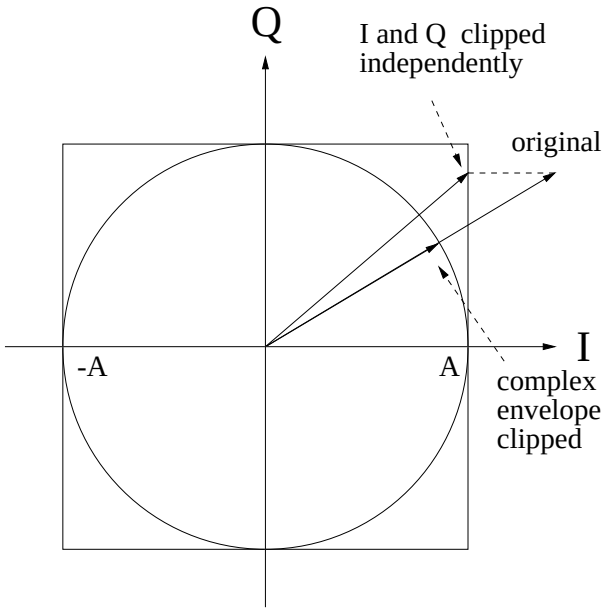

Figure 3.1 Constellation of the clipped signal.

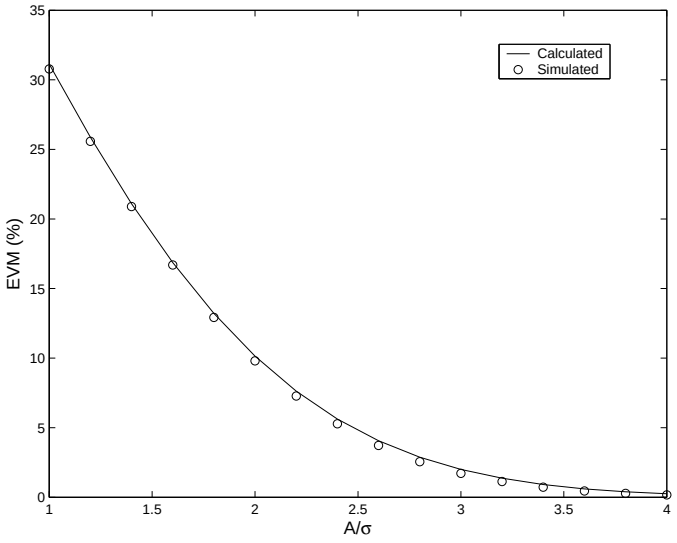

Figure 3.2 Calculated and simulated EVM with 67 code channels.

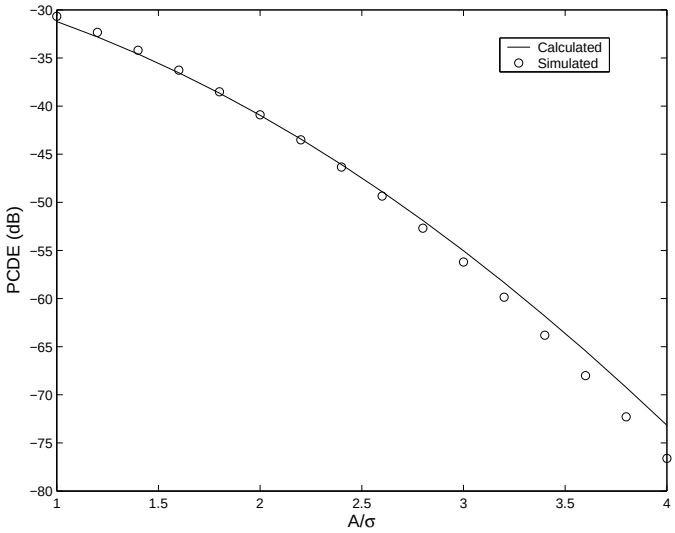

Figure 3.3 From Equation 3.26 calculated and simulated PCDE.

which has the Rayleigh PDF [31]

$$f(\hat{x}) = \frac{\hat{x}}{\sigma^2} e^{-\hat{x}^2/2\sigma^2} \varepsilon(\hat{x}). \tag{3.29}$$

The first and second moments of $\hat{x}$ are

$$E[\hat{x}] = \sqrt{\frac{\pi}{2}}\sigma \tag{3.30}$$

and

$$E[\hat{x}^2] = 2\sigma^2. \tag{3.31}$$

Phase θ is defined as

$$\theta = \arctan\left(\frac{Q}{I}\right) \tag{3.32}$$

which has PDF given by

$$f(\theta) = \frac{1}{2\pi}. \tag{3.33}$$

Clipping can be expressed in mathematical form

$$\hat{x}' = \begin{cases} A & \hat{x} > A \\ \hat{x} & \hat{x} \leq A. \end{cases} \tag{3.34}$$

Phase θ is not changed in this kind of clipping operation. Clipping probability P_c can be calculated from Equation 3.29.

$$P_c = P(\hat{x} > A) = \int_A^\infty \frac{\hat{x}}{\sigma^2} e^{-\hat{x}^2/2\sigma^2} d\hat{x} = e^{-\frac{A^2}{2\sigma^2}} \tag{3.35}$$

Let us define an error signal e as

$$e = \begin{cases} \hat{x} - A & \hat{x} > A \\ 0 & \hat{x} \leq A. \end{cases} \tag{3.36}$$

By using the conditional PDF

$$f(\hat{x}|\hat{x} > A) = \frac{f(\hat{x})}{\int_A^\infty f(\hat{x}) d\hat{x}} = \begin{cases} e^{A^2/2\sigma^2} f(\hat{x}) & \hat{x} \geq A \\ 0 & \hat{x} < A \end{cases} \tag{3.37}$$

the first and the second conditional moment for error signal e becomes

$$E[e|\hat{x} > A] = \sigma\sqrt{\frac{\pi}{2}} e^{A^2/2\sigma^2} \operatorname{erfc}(\frac{A}{\sigma\sqrt{2}}) \tag{3.38}$$

$$E[e^2|\hat{x} > A] = 2\sigma^2 - 2\sigma A\sqrt{\frac{\pi}{2}} e^{A^2/2\sigma^2} \operatorname{erfc}(\frac{A}{\sigma\sqrt{2}}). \tag{3.39}$$

The average power and the mean value of the error signal can be calculated as earlier

$$E[e^2] = 2\sigma^2 e^{-A^2/2\sigma^2} - 2\sigma A\sqrt{\frac{\pi}{2}} \operatorname{erfc}(\frac{A}{\sigma\sqrt{2}}) \tag{3.40}$$

$$E[e] = \sigma\sqrt{\frac{\pi}{2}} \operatorname{erfc}(\frac{A}{\sigma\sqrt{2}}). \tag{3.41}$$

3.2.1 Error Vector Magnitude

The amplitude of the received signal y can be written as

$$\hat{y} = \hat{x} - e, \tag{3.42}$$

where $\hat{x}$ is the amplitude of the ideal transmitted signal and e the amplitude of the error signal. The EVM is calculated by comparing the received signal y to the reference signal $\hat{x}'$, which is a scaled version of signal $\hat{x}$. The error is calculated from equation

$$e' = \hat{x}' - \hat{y} = \alpha\hat{x} - \hat{y} = (\alpha - 1)\hat{x} + e, \tag{3.43}$$

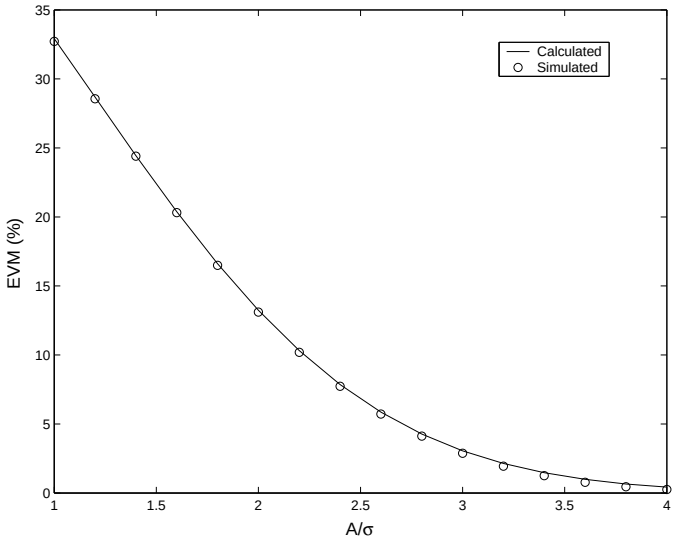

Figure 3.4 Calculated and simulated EVM with 67 code channels.

The EVM can be calculated using amplitudes only, because, in this case, the clipping does not have an effect on the phase of the complex signal. After a derivation similar to that in Section 3.1.1, we get

$$\alpha = \frac{1 - e^{-A^2/2\sigma^2}}{1 - e^{-A^2/2\sigma^2} + \frac{A}{2\sigma}\sqrt{\frac{\pi}{2}}\mathrm{erfc}(\frac{A}{\sigma\sqrt{2}})} \tag{3.44}$$

and

$$\begin{aligned} \mathrm{EVM} &= \frac{1}{\alpha}\Big[(\alpha-1)^2 + (2\alpha-1)e^{-A^2/2\sigma^2} \\ &\quad -\alpha\frac{A}{\sigma}\sqrt{\frac{\pi}{2}}\mathrm{erfc}(\frac{A}{\sigma\sqrt{2}})\Big]^{1/2}. \end{aligned} \tag{3.45}$$

The EVM calculated from Equation 3.45 and the simulated EVM is presented in Figure 3.4. The test data is a combination of 67 code channels with a spreading factor of 128, and the number of samples is 128000.

3.2.2 Peak Code Domain Error

All the following calculations are done using the in-phase component I. It is assumed that behaviour of the quadrature component Q is similar. The mean power of the reference waveform equals the variance $\alpha^2\sigma^2$ of the scaled signal αI.

First we have to project the power of the error signal e' onto the I-plane. The error signal e' has PDF $f_{e'}$, which does not have to be known exactly. The projected error

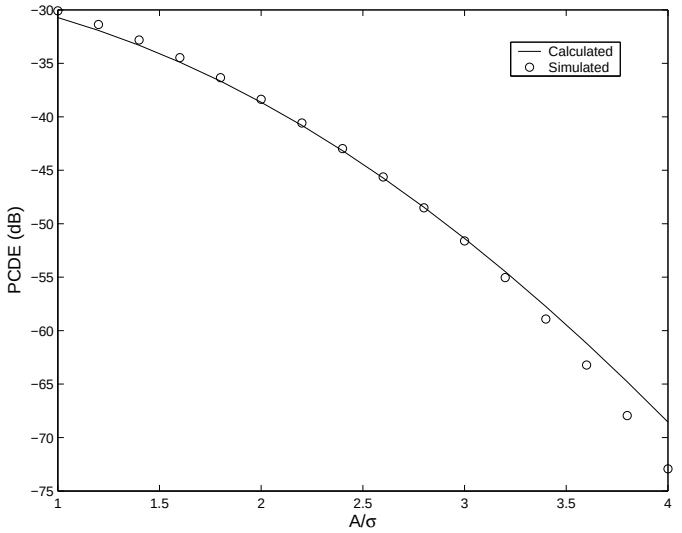

Figure 3.5 From Equation 3.48 calculated and simulated PCDE.

signal can be expressed as

$$e_p = e' \cos(\theta). \tag{3.46}$$

Because clipping has no effect on θ in this case, the PDF of the θ is given in Equation 3.33. The power of the projected error signal can be written as

$$E[e_p^2] = \int_{-\infty}^{\infty} \int_0^{2\pi} e'^2 \cos^2(\theta) f_{e'}(e') \frac{1}{2\pi} d\theta de' \tag{3.47}$$

$$= \frac{1}{2} \int_{-\infty}^{\infty} e^2 f_{e'}(e') de' = \frac{1}{2} E[e'^2].$$

Similarly, it can be shown that the signal e_p has zero mean. Mathematical formulation of the PCDE is similar to that presented in Section 3.1, and the PCDE becomes

$$\text{PCDE} = 10 \log_{10} \left(\frac{1}{\text{SF}} \frac{E[e'^2]}{2\alpha^2\sigma^2} \right) \tag{3.48}$$

$$= 10 \log_{10} \left(\frac{1}{SF} \text{EVM}^2 \right).$$

The PCDE calculated from Equation 3.48 and the simulated PCDE are presented in Figure 3.5.

3.3 Conclusions

A mathematical model for EVM and PCDE was derived in the case of baseband clipping. The signal is assumed to be Gaussian distributed and the clipping is performed in both branches, I and Q, either independently or jointly. The presented model is tested through simulations and seen to be valid. The results can be used for adjusting the clipping level in a WCDMA base station, or in any transmitter that has Gaussian distributed signals, so that the downlink signal still fulfils the specifications. Unfortunately, this theory cannot predict the CF of the IF signal because of the peak regrowth caused by the following filters. It is possible to evaluate the worst case increment caused by the filters, but, due to the very small probability of occurrence, it does not give reasonable results, and therefore it is not considered further.

This page is intentionally left blank.

Chapter 4

Windowing method

This chapter presents an efficient implementation for the peak windowing method [10]- [14]. Conventional clipping, which is expressed mathematically in Equation 3.2 causes sharp corners in a clipped signal, which leads to an unwanted out-of-band radiation (increased ACP). To smooth these corners and overcome the out-of-band power problem, the clipping is implemented by multiplying the original signal with a suitable function. The procedure is called windowing. The difference between the conventional clipping and windowing is presented in Figure 4.1. The advantage of windowing compared to the methods combining conventional clipping and filtering is the absence of the peak regrowth, which is a common problem when filtering is involved. Also, the windowing can be applied as well to a single carrier as to a multi-carrier signal.

Keeping in mind that the multiplication in the time domain corresponds to convolution in the frequency domain, it is obvious that the spectral widening of the clipped signal can be controlled by adjusting the spectral properties of the multiplying signal. In theory, the multiplying signal can be any arbitrary signal that gives a wanted result, but, in practice, the signal must be generated in a systematic way. In the peak windowing algorithms, the multiplying signal is a sum of window functions [10]. In the following, a systematic and simple algorithm to form the multiplying function based on the window function is presented not involving any exhaustive or iterative optimisation processes. A very straightforward algorithm can be implemented with a specialised Finite Impulse Response (FIR) filter structure. This algorithm was first published in [32].

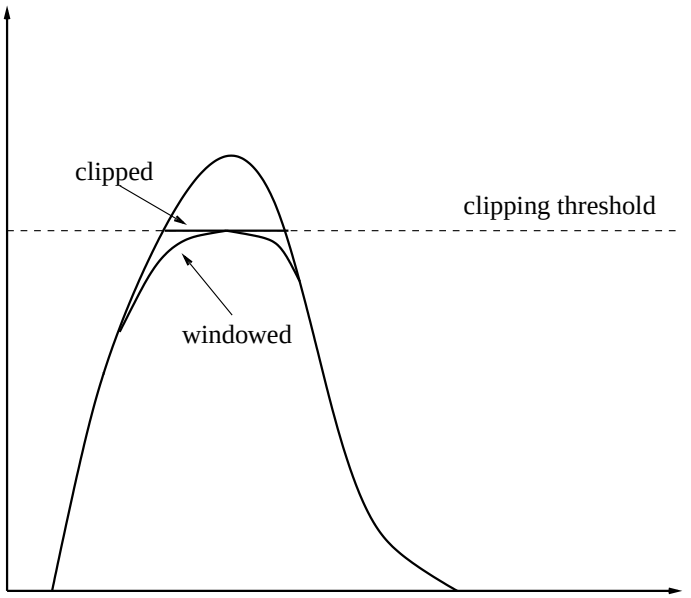

Figure 4.1 Clipped signal and windowed signal.

4.1 Windowing algorithm

Instead of using Equation 3.2 the conventional clipping can be expressed as a multiplication

$$x'(n) = c(n)x(n), \tag{4.1}$$

where

$$c(n) = \begin{cases} 1 & , |x(n)| \leq A \\ \frac{A}{|x(n)|} & , |x(n)| > A, \end{cases} \tag{4.2}$$

where A is the maximum amplitude allowed for the clipped signal. The idea of the windowing method is to replace the function $c(n)$ with the function

$$b(n) = 1 - \sum_{k=-\infty}^{\infty} a_k w(n-k), \tag{4.3}$$

where $w(n)$ is the window function and a_k a weighting coefficient. The block diagram of the windowing method is presented in Figure 4.2. To achieve the wanted clipping level, the function $b(n)$ must satisfy the inequality

$$1 - \sum_{k=-\infty}^{\infty} a_k w(n-k) \leq c(n), \tag{4.4}$$

for all n.

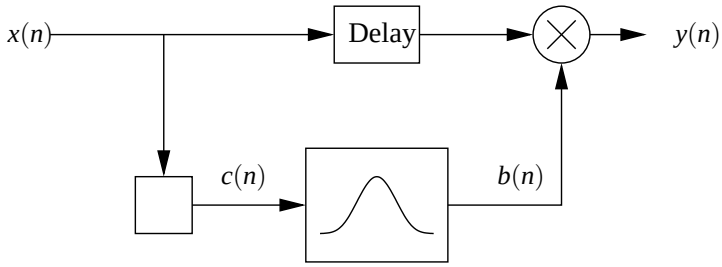

Figure 4.2 Block diagram of the windowing method.

To minimize the error in the time domain, i.e. to minimise the difference between $c(n)$ and $b(n)$, inequality 4.4 must be as near equality as possible. The difference between $c(n)$ and $b(n)$ depends on the shape of the window, the window length N_w defined as a number of samples $w(n)$ that are not equal to zero, weighting coefficients a_k and, of course, the clipping threshold. Spectral properties of the clipped signal depend on the shape and the length of the window. In order to keep the algorithm simple enough to be implemented, the shape and the length of the window and the clipping threshold should be fixed. Choosing the parameters mentioned above is discussed in the following section. The only parameters that cannot be predetermined are the coefficients a_k. After the shape and the length of the window is chosen, weighting coefficients a_k need to be optimised. Instead of calculating a_k explicitly, $b(n)$ is formed from $c(n)$ directly, as presented in the following.

If it is assumed that clipping probability and window length are so low that windows do not overlap in the time domain, the easiest way to form the function $b(n)$ is to find the part

$$\sum_{k=-\infty}^{\infty} a_k w(n-k) \tag{4.5}$$

by convolving the function $1-c(n)$ with the window $w(n)$, when $b(n)$ becomes

$$b(n) = 1 - \sum_{k=-\infty}^{\infty} [1-c(k)]w(n-k). \tag{4.6}$$

The convolution can be implemented as an FIR filter structure.

In a real system, windows unfortunately overlap, and, as a result of convolution, the signal is clipped much more than needed, which leads to a high error and gain reduction. In the worst case, the sign of function $b(n)$ may become negative, which is fatal for the system. The effect of the overlapping windows can be seen in Figure 4.4. Hence, another way to form the function $b(n)$ must be found. A simple solution to the problem mentioned above is to combine the conventional FIR structure with a

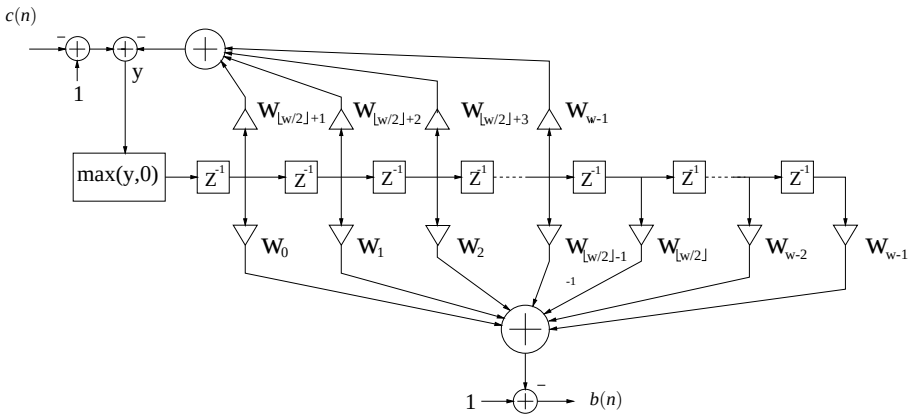

Figure 4.3 FIR filter structure with feedback.

feedback structure, which scales down the incoming value if necessary. This reduces the overlapping effect caused by consecutive large samples. The proposed structure is presented in Figure 4.3, where '$\lfloor\ \rfloor$' denotes the floor operation. The impulse response of the filter (coefficients w_n) is equal to the window function w. Based on the previous values, the feedback loop calculates a correction term, which can be subtracted from input while the output still satisfies inequality 4.4. If the correction term is larger than the input value, signal y (Figure 4.3) becomes negative after the subtraction, which leads to an unwanted clipping result. This is prevented by adding a block that replaces negative values with zero. Figure 4.4 presents function $b(n)$ formed with and without the feedback loop. This example clearly shows the problem caused by overlapping windows and it also shows the benefit achieved by using feedback.

4.2 Window selection

As mentioned earlier, the multiplication in the time domain corresponds to convolution in the frequency domain. In order to limit the spectral widening, the window function should have a narrow spectrum. However, the strict localisation in the frequency domain leads to a wide response in the time domain, which means that the effect of the clipping is spread to the samples adjacent to the sample to be clipped, increasing the EVM. It can be concluded that the choosing of the window is a trade off between the EVM and the spectral properties. The optimal choice depends heavily on the system in which the windowing is applied.

As an example, we consider the use of some well-known windows [33] in reducing the CF of a WCDMA signal. The CF of the unclipped signal is 14.86 dB when an Oversampling Ratio (OSR) of 16 is used. In each case, the window length is constant

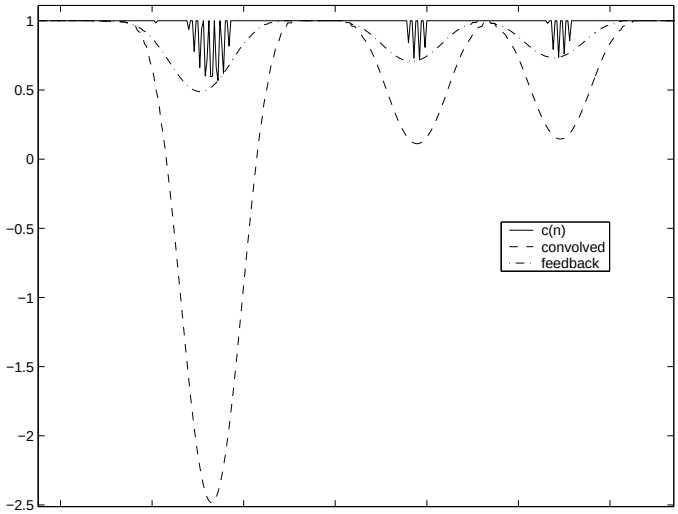

Figure 4.4 Function $b(n)$ formed by convolution (4.6) and by presented algorithm (Figure 4.3).

(N_w=67) and the clipping threshold is chosen to reduce the CF down to 10 dB. Kaiser5 refers to a Kaiser window with a beta value of 5. The resulting spectra are presented in Figure 4.5 and the EVM and ACLR results in Table 4.1. In this case, the Hamming and Kaiser windows stand out and, foreseeably, the triangular window gives the worst performance.

In Figures 4.6 and 4.7, the ACLR and EVM are presented respectively as a function of the window length. The window used is a Hamming window and the test signal is equal to the one in the previous case. This result supports the assumption about the trade off between ACLR and EVM.

The purpose of this section is not to find the optimal window, but only to demonstrate and discuss the effect of the related parameters. Another topic, not considered in this section, is the implementational issues of the algorithm. As an IF clipping method, the windowing may need to operate at high frequency. This can set requirements for the shape of the window also. An example of this is discussed in more detail in Chapter 9.

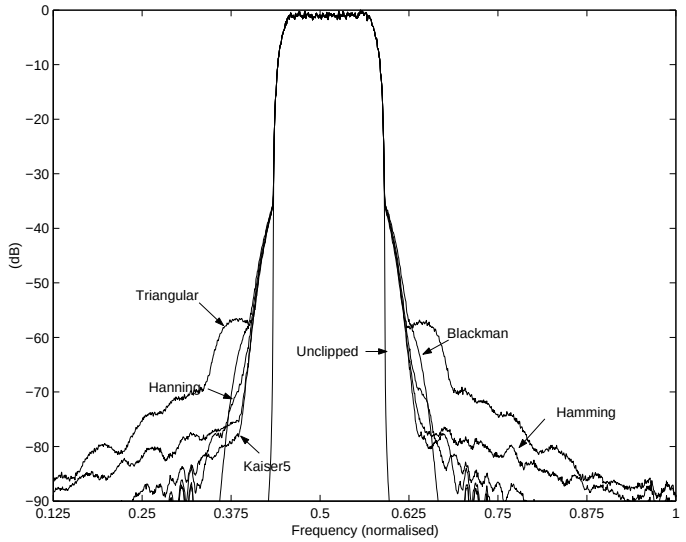

Figure 4.5 Spectra of the windowed signals.

Table 4.1 Window comparison.

Window	EVM (%)	ACLR (dB)
Hamming	4.46	66.4
Hanning	4.43	64.5
Blackman	4.28	61.5
Kaiser5	4.45	66.9
Triangular	4.40	59.4

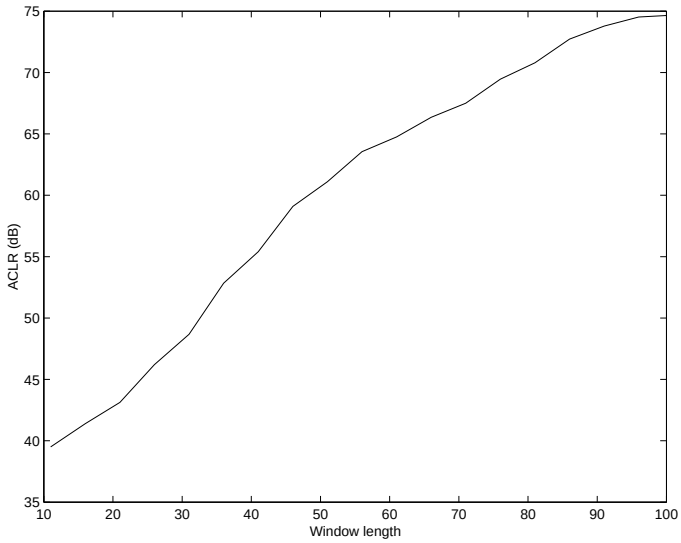

Figure 4.6 ACLR as a function of the window length (Hamming).

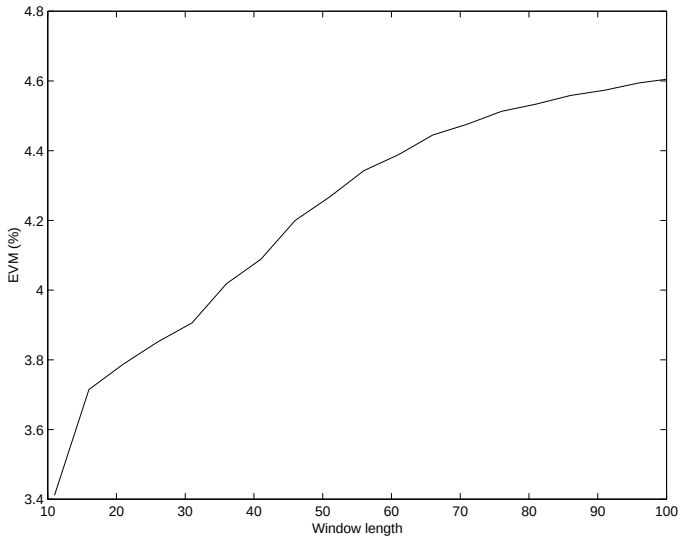

Figure 4.7 EVM as a function of the window length (Hamming).

4.3 Conclusions

An efficient algorithm to implement the peak windowing method is presented. Its applicability in different transmission techniques is discussed later in this thesis. Here, the main objective is to keep the computational complexity of the algorithm low enough for high-speed implementations and avoid iterative processes causing delay. Most probably, this does not lead to an optimal performance in terms of CF, ACP and EVM and, therefore, it would be beneficial to take another kind of approach, not so implementation oriented, and, for example, study whether the method can be improved by using self-adjustable window length or some other trick.

Chapter 5

Effect of clipping in WCDMA system

A WCDMA signal is a sum of signals intended for different users, as presented in Figure 5.1, where u_k is the complex data of the user k, c_k a spreading code, b_k a weighting factor, s a complex scrambling sequence and ω the angular frequency of the carrier. When statistically independent signals are summed, according to the central limit theorem, the I and Q parts of the resulting signal are Gaussian distributed, which leads to a high CF. The following root raised cosine filtering tends to increase the CF further. If several carriers are combined in the digital domain the situation becomes even worse. To avoid the problems caused by the high CF, an efficient CF reduction method is needed.

In this chapter, the effects of several different clipping methods on the EVM, PCDE and ACLR in the WCDMA system are derived through simulations. The performances of different clipping methods are compared in terms of CF reduction, while the signal quality meets the WCDMA specifications. The clipping methods discussed are limited to those that can be applied without any modifications to the transmission and reception procedure. Methods excluded for this reason are, for example, methods based on code selection and the method presented in Chapter 6. This Chapter is based on [32] and [34].

5.1 Clipping methods

5.1.1 Baseband clipping

In baseband clipping, the I and Q signals are modified either independently or jointly. The independent clipping of I and Q leads to the situation where the constellation

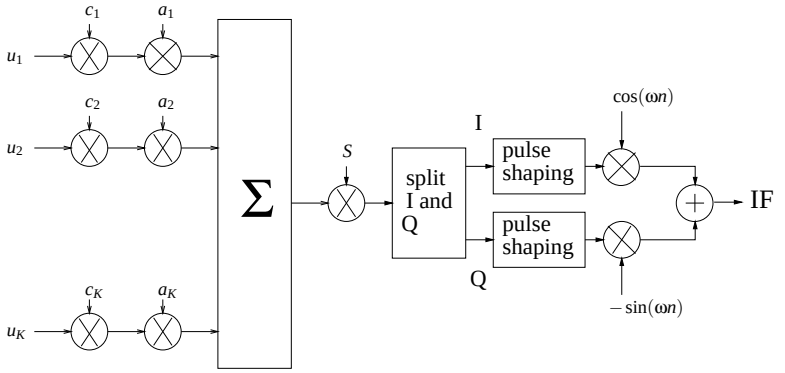

Figure 5.1 WCDMA modulator.

of the baseband symbols is circumscribed by a square. In the following text, Square refers to this method. In the joint clipping, the amplitude of the complex symbol is clipped, but the angle remains unchanged. In this case, the constellation is circumscribed by a circle. This method is referred to as Circle. The clipping takes place before the pulse shaping filtering and, therefore, it is obvious that it has no effect on the ACLR. A mathematical analysis of the behaviour of the EVM and PCDE as a function of the clipping ratio was presented in Chapter 3. The theory presented gives an accurate relationship between the CF of the baseband signal and the error metrics, but due to the following pulse shaping filter, simulations are needed for a reliable evaluation of the CF at the IF.

5.1.2 Adaptive baseband clipping

The problem of the baseband clipping is that the pulse shaping filter (root raised cosine) tends to increase the CF and partially cancels the effect of clipping. An adaptive peak suppression algorithm to prevent the peak regrowth is presented in [8]. Here the same idea is used in the following way. We assume that an oversampling ratio of 2 is used in the filtering, i.e. that the input signal is zero-padded with a factor of 2 before the filter, and the filter "fills in" the zero-valued samples with interpolated sample values. The clipping threshold after filtering is specified to be A. The algorithm is as follows:

1. The unclipped signal is filtered and analyzed.
2. If the threshold is exceeded there are two options:
    - If the peak is not an interpolated sample, the corresponding sample of the unfiltered signal is scaled down by factor $k = A/A_s$, where A_s is the amplitude of the peak.

- If the peak is an interpolated sample, the two adjacent samples of the corresponding sample of the unfiltered signal is scaled down by factor $k = A/A_s$.

3. After scaling operations, the new version of the unfiltered signal is filtered.

As it can be seen, this clipping algorithm requires at least one iteration loop. The optimal way to apply this algorithm is to use many iteration loops and decrease the clipping level step by step. In practice, the complexity and the processing delay restrict the number of the iteration loops. This method is simulated in two cases. In the first case, referred to as Adaptive, the presented algorithm is used with one iteration loop. The block diagram of this is presented in Figure 5.2. In the second case, referred to as Iterative, the presented algorithm is used with 20 iteration loops. This example is not meant to be a practical solution but is presented to test the concept. In a practical design, i.e. in the one presented in Chapter 8, the implementation of 20 iteration loops would require 21 pulse shaping filters (37 taps), causing a filtering delay of 200 chips and some processing delay.

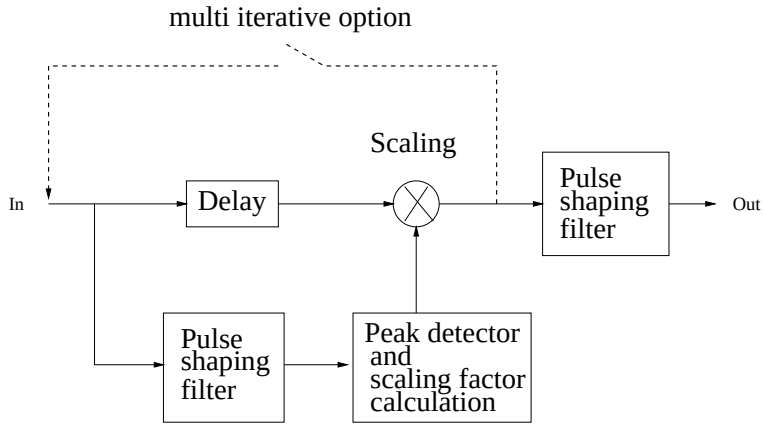

Figure 5.2 Block diagram of the adaptive baseband clipping structure.

5.1.3 IF clipping

Another way to clip the signal is to operate with the IF signal. As a nonlinear operation, the clipping obviously distorts the signal and the ACLR is decreased. The ACLR can be increased by bandpass filtering after the clipping operation. The peak regrowth caused by the filter is a problem, as it is in the baseband case. In theory, the adaptive clipping can be used in the IF case also. However, it is not discussed in this thesis, mainly for two reasons. Even in the baseband case, the iteration is a complex procedure, and, at the IF where the sampling frequency is higher, the implementation

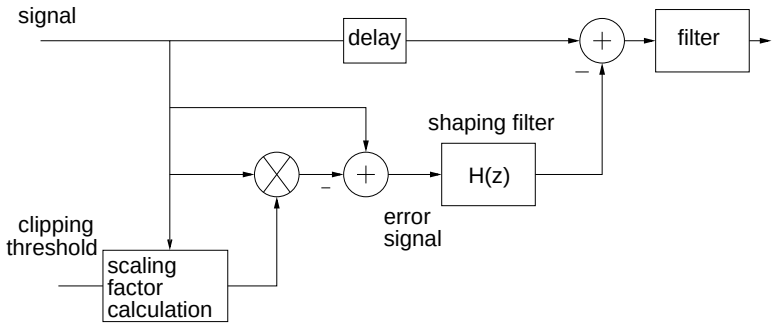

Figure 5.3 Error shaping.

becomes even more difficult and unpractical. Another reason is that, when several IF carriers are combined, all filtering base solutions become unpractical.

The IF clipping, with and without a bandpass filter, is simulated. Also, two more advanced clipping methods, error shaping [9] and windowing method [10], are simulated. The windowing method is discussed in detail in Chapter 4. It can be shown that most of the clipping noise is located at the signal band [35]. The ACLR can be increased by bandpass filtering, but then the EVM and PCDE becomes restrictive. In [9], a method for shaping the noise spectrum caused by clipping is presented. The purpose of the error shaping is to reduce the error in the signal band that leads to reduced EVM and PCDE, enabling the decrease of the clipping ratio. The block diagram is presented in Figure 5.3.

5.2 Simulation model

All simulations were carried out by using Matlab. The test data is generated according to [28]. The generation of the WCDMA signal is presented in Figure 5.1.

The block diagram of the modulator model used is presented in Figure 5.4. The pulse shaping filter is Root Raised Cosine FIR filter with 1001 coefficients. The number of coefficients is chosen to be high, so that the clipping is the only significant source of error. The interpolation ratio of the pulse shaping filter is two. After the pulse shaping filter there are 3 half band filters. The function of the half band filters is to increase the sampling rate. Every half band filter interpolates by a factor of two, so the OSR at the IF becomes 16. The ACLR and CF are calculated for the IF signal in Figure 5.4.

Calculation of the EVM and PCDE is performed as presented in [28]. In the multicarrier case, the EVM and PCDE are calculated for the carrier with the highest frequency. The ACLR is calculated by using the adjacent channel above the highest

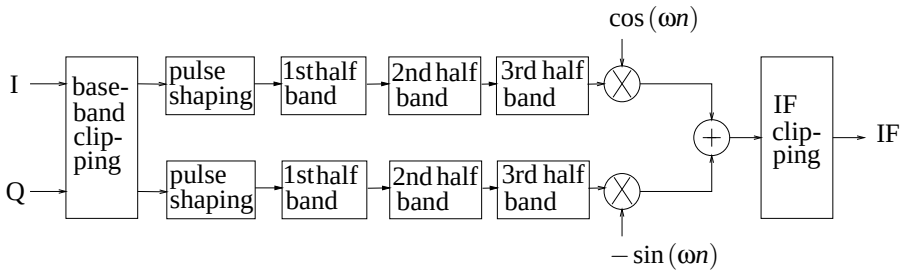

Figure 5.4 Simulation model used.

frequency channel used.

Simulations are performed using two different specifications. In the first case, the CF is minimized so that the ACLR, EVM and PCDE still fulfil the system specifications ACLR more than 50 dB, EVM less than 17.5% and PCDE less than -33 dB [28]. In the second case, there is some margin left for the error caused by the following analogue parts. ACLR is specified to be more than 65 dB, EVM less than 3% and PCDE less than -49 dB.

5.3 Results

5.3.1 Single carrier

The single carrier case is simulated using two different test data generated as presented in the WCDMA base station conformance testing specification [28] (Test Model 3). Simulation results for Test Model 3 with 32 active codes and three control channels are presented in Tables 5.1 and 5.2. The CF before clipping is 15.418 dB. Results for Test Model 3 with 16 active codes and three control channels are presented in Tables 5.3 and 5.4. The CF before clipping is 15.414 dB. In both cases the spreading factor is 256.

In the baseband clipping, Circle method seems to be more efficient than Square method, even if the clipping ratio for Square is less than the clipping ratio for Circle. This can be explained by using the equation

$$\mathrm{IF} = I\cos(\omega t) - Q\sin(\omega t) = \sqrt{I^2+Q^2}\cos(\omega t+\phi) \tag{5.1}$$

which shows that the envelope of the signal IF is linearly dependent on the amplitude of the complex baseband signal. When the I and Q are clipped independently to value A, the critical maximum amplitude of the complex baseband signal becomes $\sqrt{2}A$. If one of the signals (I or Q) is below the clipping level, and the other is clipped to value A, the amplitude of the complex symbol becomes less than $\sqrt{2}A$. Because the critical

point is the limiting factor from the CF point of view, it can be said that, in most of the cases, the amplitude of the complex signal is clipped too much without gaining any advantage, and the EVM is increased. The region clipped in vain is presented in Figure 5.5. Taking into account the fact that, in the case of method Circle, the angle of the complex phasor does not change, which can be a useful property in the receiver, the Circle method is more suitable for baseband clipping than the Square method.

Adaptive clipping has better efficiency than the conventional baseband clipping methods. When a high level of error is tolerated the efficiency of the Adaptive method can be increased by using more iteration loops (the Iterative method). In this case, the efficiency of the Iterative method becomes about same as the efficiency of the IF clipping with filtering. For high clipping levels, i.e. for a low tolerated error level, the efficiency of the adaptive clipping does not improve when the number of iterations is increased.

Clipping at IF is slightly less efficient than conventional baseband clipping. However, by combining the IF clipping with bandpass filtering, the efficiency can be significantly improved. When clipping is performed at IF, the ACLR is the limiting parameter. By using the bandpass FIR filter with 50 coefficients, the ACLR can be increased so that the EVM and PCDE become the limiting parameters. The problem of this method is the regrowth of the CF after the clipping operation and the fact that it is difficult to find the optimal combination of the clipping ratio and the band pass filter.

As the results in Tables 5.1 and 5.2 show, no advantage is achieved by using error shaping. The idea of the error shaping is to remove clipping noise from the signal band so that the clipping ratio can be decreased. Most of the clipping noise is located at the signal band [35]; filtering it out leads to a situation where the CF is increased. Even if the filter has a maximum attenuation of no more than 1.5 dB in the stop band, the decrease of the clipping ratio cannot compensate the increase of the CF.

The windowing method is the most efficient of the presented clipping methods. The window used is a Hamming window with the length of 75. In Chapter 4, the properties of some common window functions are compared and it seems that the Hamming window has a good relationship between the EVM and ACLR. Choosing a window length is a problematic issue. Results show that, in most cases, the EVM or PCDE is the limiting parameter and that there is some margin for ACLR. In theory, reducing the window length decreases the EVM, PCDE and ACLR, which leads to a situation where the clipping ratio could be decreased. Simulations showed that, in this case, the CF increased, so no advantage was achieved. Another reason that makes the windowing method more attractive than IF clipping with filtering is that the windowing method can be easily applied to a multicarrier system and, further, the clipped signal does not exceed the threshold value, which is not the case when the

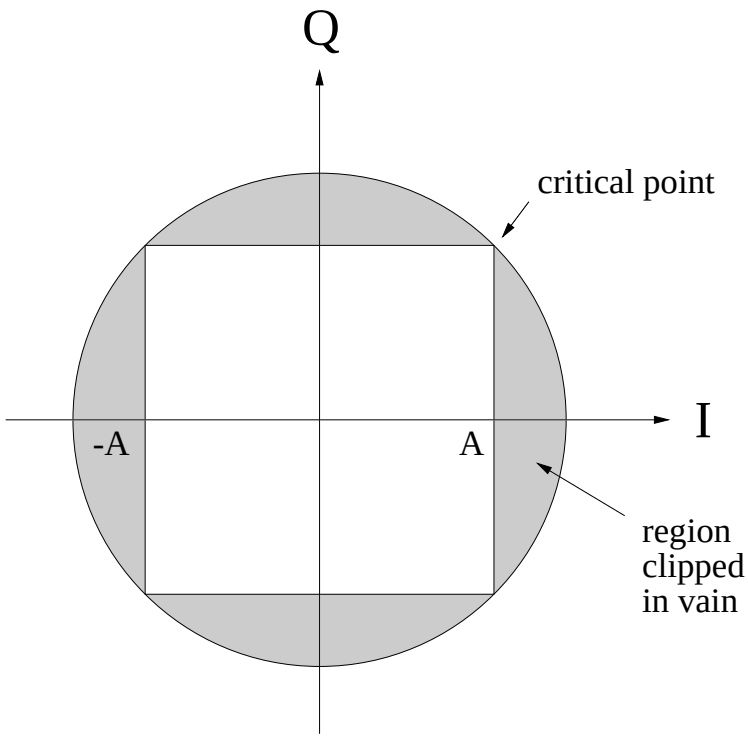

Figure 5.5 Region clipped in vain when *I* and *Q* clipped independently.

filtering is involved. This gives rise to the possibility of utilizing the whole dynamic range of the following digital circuitry and D/A-converter.

5.3.2 Multicarrier

The multicarrier signal is simulated by adding together four signals after the upconversion. All four signals are generated by using independent data and an equal number of codes. Baseband clipping is performed independently for each baseband signal with an equal clipping ratio. IF clipping is done after carriers are combined. Results for data with 32 code channels are presented in Tables 5.5 and 5.6. The CF before clipping is 13.745 dB. It is counter intuitive that the CF in the multicarrier case is smaller than in the corresponding single carrier case, but the explanation is that, in this specific example, the peaks are cancelled out in the summation. In theory, it could be the opposite.

In all cases, both baseband clipping methods are inefficient and no advantage is achieved. When different signals are combined at IF, high peaks of the individual signals can be cancelled out and correspondingly new peaks can be generated to the

Table 5.1 Simulation results for test data with 32 active codes and 3 control channels.

Method	Δ*CF*	EVM	PCDE	ACLR
Square	3.22 dB	16.2 %	-33.1 dB	92.0 dB
Circle	4.33 dB	17.5 %	-33.5 dB	92.0 dB
Adaptive	5.46 dB	17.5 %	-34.2 dB	92.0 dB
Iterative	6.15 dB	17.5 %	-33.6 dB	92.0 dB
IF	3.05 dB	0.73 %	-58.6 dB	50.1 dB
IF+filt	6.10 dB	16.4 %	-33.0 dB	52.6 dB
Error Shaping	5.48 dB	15.8 %	-33.0 dB	51.8 dB
Windowing	7.35 dB	17.5 %	-33.4 dB	56.1 dB

Table 5.2 Simulation results for test data with 32 active codes and 3 control channels. High margin.

Method	Δ*CF*	EVM	PCDE	ACLR
Square	1.80 dB	3.0 %	-50.8 dB	92.0 dB
Circle	2.05 dB	3.0 %	-50.8 dB	92.0 dB
Adaptive	2.33 dB	3.0 %	-51.0 dB	92.0 dB
Iterative	2.33 dB	3.0 %	-50.1 dB	92.0 dB
IF	1.00 dB	0.3 %	-58.9 dB	65.1 dB
IF+filt	2.57 dB	3.0 %	-51.5 dB	67.4 dB
Error Shaping	2.45 dB	3.0 %	-51.5 dB	66.5 dB
Windowing	3.65 dB	3.0 %	-49.9 dB	72.0 dB

Table 5.3 Simulation results for test data with 16 active codes and 3 control channels.

Method	Δ*CF*	EVM	PCDE	ACLR
Square	3.37 dB	9.9 %	-33.1 dB	92.0 dB
Circle	3.61 dB	10.1 %	-33.1 dB	92.0 dB
Adaptive	4.50 dB	11.4 %	-33.0 dB	92.0 dB
Iterative	4.71 dB	10.4 %	-33.0 dB	92.0 dB
IF	3.69 dB	0.7 %	-57.5 dB	50.0 dB
IF+filt	4.62 dB	8.4 %	-33.0 dB	57.3 dB
Windowing	6.17 dB	9.7 %	-33.0 dB	61.5 dB

Table 5.4 Simulation results for test data with 16 active codes and 3 control channels. High margin.

Method	ΔCF	EVM	PCDE	ACLR
Square	2.47 dB	3.0 %	-49.2 dB	92.1 dB
Circle	2.48 dB	3.0 %	-49.3 dB	92.1 dB
Adaptive	2.93 dB	3.0 %	-49.8 dB	92.0 dB
Iterative	2.93 dB	3.0 %	-49.7 dB	92.0 dB
IF	1.35 dB	0.3 %	-57.8 dB	65.1 dB
IF+filt	3.03 dB	3.0 %	-49.0 dB	65.9 dB
Windowing	4.09 dB	2.8 %	-50.0 dB	72.8 dB

Table 5.5 Multicarrier signal with 4 carriers, 32 code channels per carrier.

Method	ΔCF	EVM	PCDE	ACLR
Square	0.07 dB	17.5 %	-34.6 dB	90.1 dB
Circle	-0.03 dB	17.5 %	-34.4 dB	90.1 dB
IF	1.52 dB	0.41 %	-65.1 dB	50.0 dB
Windowing	5.57 dB	17.5%	-34.7 dB	51.1 dB

composite signal. For this reason, the adaptive baseband clipping is not considered in this context. An effective baseband clipping method would require a feedback structure, which, however, would be very complex and hard to implement.

As in the single carrier case, the ACLR is a limiting parameter in the IF clipping. Because it is difficult to apply filtering in the case of a multicarrier signal, the windowing method becomes the most interesting. Results show that, by using the windowing method, the CF can be reduced significantly. The major problem, as in the single carrier case, is still choosing the window length. In simulations, efforts were made to minimize the CF.

Table 5.6 Multicarrier signal with 4 carriers, 32 code channels per carrier. High margin.

Method	ΔCF	EVM	PCDE	ACLR
Square	-0.06 dB	3.0 %	-50.0 dB	90.1 dB
Circle	-0.06 dB	3.0 %	-50.7 dB	90.1 dB
IF	0.48 dB	0.3 %	-66.5 dB	65.0 dB
Windowing	3.03 dB	3.0 %	-50.5 dB	65.0 dB

5.4 Conclusions

The effects of several different clipping methods on the EVM, PCDE and ACLR are derived through simulations. In simulations, different types of test data are used and both single carrier and multicarrier signals are considered. It is shown that a significant CF reduction can be achieved using different methods. Which method is the best depends on, of course, the modulator structure. However, the windowing method stands out with its performance in both the single carrier and multicarrier case.

Chapter 6

Projection method

As presented earlier, several advanced clipping methods can be applied in a CDMA system. However, typically, the signal quality is degraded in the clipping operation. In this chapter, a clipping method that minimizes the error experienced by the user is presented. In a CDMA system, user separation is based on the usage of the orthogonal channelization codes. The main idea of the presented clipping algorithm is that the error signal caused by clipping is orthogonal to all the active channel codes and therefore, in the ideal case, it does not introduce any error at the receiver. In a real system, the non-ideal modulation and the non-ideal channel partly destroy the orthogonality, but, if the power of the added signal is relatively low, some advantage can be achieved compared to conventional methods (Chapter 5) in which the error power is uncontrollably distributed among the active and non-active channel codes.

At first, the idea of the method is presented and some practical implementations are proposed and tested through simulations. Then, the same problem is studied as a mathematical multivariable problem in order to find the optimal solution to be used as a reference when the performance of the practical algorithms is evaluated. This chapter is mainly based on [36] and [37].

6.1 Clipping algorithm

In [15], an idea of using reserved channel codes for achieving a constant amplitude modulation is presented. The main idea is to use only a part of the orthogonal codes for data transmission and combine the remaining codes to the composite signal so that the amplitudes of the symbols become constant. However, this may be complex and may set limitations to code selection, especially when the spreading factor is large. Also, when the power control is used, the constant amplitude cannot be achieved. The algorithm presented here also uses the idea of exploiting the unused channel codes.

At first, a residual signal, which will be subtracted from the composite signal for achieving the wanted clipping result, is generated. The generation of the residual signal is discussed in detail in Section 6.2. Then the residual signal is estimated by using the unused channelization codes, which means that the estimate is orthogonal to all the active channel codes. The orthogonality makes the residual signal in the ideal case invisible for receivers, and at the same time the CF of the composite signal is reduced. The algorithm is presented in detail in the following.

The base station spreads and sums the baseband signals intended for different users. The spreading and summation is presented in Equations 2.4 and 2.5 and in Figure 5.1. It is assumed that the channelization codes are orthogonal and have a fixed length SF equal to the spreading factor. In this case, there are SF orthogonal codes. Also, it is assumed that only some of the codes are active simultaneously. The clipping algorithm presented here processes real and imaginary parts of the signal independently. In the following, all signals are assumed to be real.

We define a residual signal r by equation

$$s' = s - r, \tag{6.1}$$

where s' is the clipped version of the composite signal s. The exact derivation of the residual signal is discussed later. The main idea of this clipping method is that the residual signal added is orthogonal to the composite signal. We consider the set of channelization codes as a vector space with dimension SF, where every code represents a basis vector.

The continuous chip sequence is cut into blocks of SF chips and each block is processed independently. The n^{th} block of the orthogonal residual signal r' can be derived from the n^{th} block of the non-orthogonal residual signal r by projecting r to the subspace of unused codes. The first step is to calculate the weighting coefficients corresponding to the unused codes, according to the equation

$$\mathbf{w}_n = \frac{1}{\mathrm{SF}}\mathbf{H}\mathbf{r}_n, \tag{6.2}$$

where $\mathbf{H}$ is a matrix in which every row represents an unused channelization code, $\mathbf{r}_n$ is the n^{th} block of the r and $\mathbf{w}_n$ is a vector of weighting coefficients corresponding to the code matrix $\mathbf{H}$. An estimate for $\mathbf{r}_n$ can be calculated by summing unused channelization codes with corresponding weighting coefficients according to the equation

$$\mathbf{r}'_n = \mathbf{H}^T\mathbf{w}_n = \frac{1}{\mathrm{SF}}\mathbf{H}^T\mathbf{H}\mathbf{r}_n \tag{6.3}$$

As Equation 6.3 shows, the whole operation can be performed in one step using projection matrix $\mathbf{H}^T\mathbf{H}$. The continuous estimate r' for the residual signal is composed

of the blocks $\mathbf{r}'_n$ and the clipped composite signal becomes

$$s_{clip} = s - r'. \tag{6.4}$$

It is obvious that r' is orthogonal to s. At the receiver, the despreading operation can be written as

$$\mathbf{u}_n = \frac{1}{\mathrm{SF}}\mathbf{C}\mathbf{s}_{clip,n} = \frac{1}{\mathrm{SF}}(\mathbf{C}\mathbf{s}_n - \mathbf{C}\mathbf{r}'_n) = \frac{1}{\mathrm{SF}}\mathbf{C}\mathbf{s}_n, \tag{6.5}$$

where $\mathbf{C}$ is a matrix composed of the channelization codes used and $\mathbf{u}_n$ is a vector of received data symbols. The result shows that clipping has no effect on the received data symbols when the system is assumed to be ideal.

6.2 Residual signal

Four possible ways to derive the residual signal are presented. In the first case, later referred as Algorithm 1, I and Q branches are clipped independently, which leads to the situation when the constellation of the baseband symbols is circumscribed by a square. The residual signal is defined by equation

$$r = \begin{cases} s - A & , s > A \\ 0 & , |s| \leq A \\ s + A & , s < -A, \end{cases} \tag{6.6}$$

where A is the clipping level and s denotes the real valued signal either in I or Q branch.

In the second case (Algorithm 2), the amplitude of the complex symbol is clipped but the angle remains unchanged. In this case, the constellation is circumscribed by a circle and the residual signal can be written as

$$r = \begin{cases} s(1 - \frac{A}{\sqrt{I^2+Q^2}}) & , \sqrt{I^2+Q^2} > A \\ 0 & , \sqrt{I^2+Q^2} \leq A, \end{cases} \tag{6.7}$$

where A and s are defined as earlier.

The problem with the methods described earlier is that the pulse shaping filter tends to increase the CF and partially cancels the effect of clipping (see Section 5.1.2). An adaptive peak suppression algorithm [8] is used in order to prevent the peak regrowth, as presented in Section 5.1.2. This clipping algorithm requires at least one iteration loop. The optimal way to apply this algorithm is to use many iteration loops and decrease the clipping level step by step. In reality, the complexity and the pro-

cessing delay restrict the number of iteration loops. In these simulations, 20 iterations are used.

In the third case (Algorithm 3), the I and Q are clipped independently and the aforementioned algorithm is used to prevent the peak regrowth in the filtering operation. The residual signal is the difference between the original and the clipped waveforms. The fourth case (Algorithm 4) is similar to the third case, except the complex envelope is clipped.

6.3 Results

The presented clipping algorithm is simulated by using all four of the presented residual signal definitions. The simulation model used is presented in Figure 5.1. After the clipping operation, the signal is filtered and upconverted. Oversampling is included in the filtering operation. The CF is calculated from the real valued IF signal. The CF reduction achieved is presented in Table 6.1 for input signals with a varying number of active channel codes. In these simulations, the active codes are chosen randomly and the modulating data is a pseudorandom QPSK signal. Each code channel has a randomly chosen relative weighting coefficient between 0.2 and 1. The spreading factor is 256 in each case. Another presented quantity P_r/P_s is the ratio of the residual signal power to the composite signal power. This is an important quantity when the system is not assumed to be ideal and when there is cross correlation between the channel codes. It can be assumed that the real error due to clipping is more or less the same as the error in the situation when the unused codes are used as normal data channels with relative power P_r/P_s. In every case, the results show that the power of the residual signal is relatively low, less than 6 % of the composite signal power. In each case, the clipping level is set to minimize the CF.

Ignoring some minor exceptions, possibly caused by the random nature of the simulations, some general remarks regarding the results can be made. With the exception of one case (128 active codes), it is more efficient to clip the complex envelope (Algorithm 2) than I and Q independently (Algorithm 1). The same observation can be made also when the effect of the pulse shaping filter is taken into account (Algorithm 3 compared with Algorithm 4). The explanation for this is similar to that presented in Chapter 5.

By taking into account the effect of the pulse shaping filter (Algorithm 3 compared with Algorithm 1 and Algorithm 4 compared with Algorithm 2) the reduction of the CF can be enhanced. There is one exception, however: the difference in favour of Algorithm 1 compared with Algorithm 3 is negligible. The cost of the enhanced clipping result is the increased residual signal power.

It is obvious that the number of active codes affects the efficiency of the presented

clipping method. Excluding the simulation result with 16 active codes, and one case with Algorithm 4, the CF reduction is reduced when the number of active codes is increased, which is the anticipated result. The selection of the active codes plays a major role and is discussed in Section 6.5.

6.4 Optimal method

In the previous sections, a straightforward algorithm to utilise unused channelization codes in order to reduce the CF of the composite signal is presented. To keep the algorithm simple enough for practical implementations, the performance of the clipping method is compromised. In order to evaluate the performance of the presented algorithm, an optimal solution is found and compared with the algorithm presented. To keep the problem simple enough, only the independent clipping of I and Q corresponding to case 1 in the previous section is studied. The clipping procedure can be considered as a multivariable optimisation problem and can be solved using Linear Programming (LP) methods [38].

As earlier, the clipped signal can be written as a sum of original signal and residual signal

$$\mathbf{s}' = \mathbf{C}^T\mathbf{u} - \mathbf{H}^T\mathbf{w}. \tag{6.8}$$

To find a residual signal that minimises the CF, the elements of vector $\mathbf{w}$ are considered as variables of a multivariable optimisation problem. The CF of one data block can be written as

$$\mathrm{CF} = \frac{||\mathbf{s}'||_\infty^2}{\frac{1}{\mathrm{SF}}\mathbf{s}'^T\mathbf{s}'}. \tag{6.9}$$

Using Equation 6.8, the denominator of Equation 6.9 can be written as

$$\frac{1}{\mathrm{SF}}\mathbf{s}'^T\mathbf{s}' = \mathbf{u}^T\mathbf{u} + \mathbf{w}^T\mathbf{w} = P_s + P_r \tag{6.10}$$

when Equation 6.9 becomes

$$\mathrm{CF} = \frac{||\mathbf{C}^T\mathbf{u} - \mathbf{H}^T\mathbf{w}||_\infty^2}{P_s + P_r}. \tag{6.11}$$

In order to minimise the CF, the numerator should be minimised and the denominator maximised. However, the denominator can be maximised only by increasing the residual signal power P_r, which is undesirable for the reason explained earlier. Therefore, instead of minimising the CF, only the maximum peak is minimised while the power

Table 6.1 Simulated crest factor reduction.

Number of codes	CF (dB)	Algorithm 1		Algorithm 2		Algorithm 3		Algorithm 4	
		ΔCF (dB)	P_r/P_s	ΔCF (dB)	P_r/P_s	ΔCF (dB)	P_r/P_s	ΔCF (dB)	P_r/P_s
16	12.86	2.55	0.044	2.92	0.026	2.53	0.052	3.08	0.023
32	13.26	2.89	0.036	3.01	0.019	3.33	0.060	3.83	0.057
64	13.22	2.52	0.037	3.09	0.029	2.81	0.048	4.21	0.040
128	13.06	1.79	0.014	1.67	0.018	2.31	0.022	2.78	0.013
192	14.18	0.99	0.007	1.04	0.005	1.07	0.005	1.54	0.008
224	12.95	0.31	0.005	0.40	0.005	0.35	0.005	0.51	0.006
240	13.08	0.13	0.003	0.24	0.002	0.22	0.001	0.32	0.001

of the residual signal is constrained. Ideally, limiting the residual signal power means that the squared Euclidean norm $||\mathbf{w}||_2^2$ is limited, which leads to a quadratic constraint and convex programming problem. To retain linearity, the power of the residual signal is controlled using linear constraints sum-absolute-value $||\mathbf{w}||_1$ and sup-norm $||\mathbf{w}||_\infty$. The minimisation problem can be written as

$$\begin{aligned} \text{minimise} \quad & \|\mathbf{C}^T\mathbf{u} + \mathbf{H}^T\mathbf{w}\|_\infty \\ \text{subject to} \quad & \|\mathbf{w}\|_1 \leq W_1 \\ & \|\mathbf{w}\|_\infty \leq W_\infty, \end{aligned} \tag{6.12}$$

where W_1 and W_∞ are control parameters for sum-absolute-value and sup-norm, respectively. It is possible that there are several solutions in the sense that the peak is minimised and, in order to keep the power ratio P_r/P_s small, the cost function needs to be modified. This is achieved by adding $\|\mathbf{w}\|_1$ to the cost function with a suitable small coefficient δ, which means that the lowest possible peak may not be reached, but a proper choice for δ will keep the solution close enough to the optimum. Now the final optimisation problem can be written in the form

$$\begin{aligned} \text{minimise} \quad & \|\mathbf{C}^T\mathbf{u} + \mathbf{H}^T\mathbf{w}\|_\infty + \delta\|\mathbf{w}\|_1 \\ \text{subject to} \quad & \|\mathbf{w}\|_1 \leq W_1 \\ & \|\mathbf{w}\|_\infty \leq W_\infty. \end{aligned} \tag{6.13}$$

In a matrix form, a general linear problem can be expressed as [38]

$$\begin{aligned} \text{maximise / minimise} \quad & \mathbf{c}^T\mathbf{x} \\ \text{subject to} \quad & \mathbf{A}\mathbf{x} \begin{bmatrix} \leq \\ = \\ \geq \end{bmatrix} \mathbf{b} \\ & \mathbf{l} \leq \mathbf{x} \leq \mathbf{t}, \end{aligned} \tag{6.14}$$

where $\mathbf{x}$ is the variable vector $\mathbf{l}$, $\mathbf{t}$ and $\mathbf{b}$ are limit vectors and $\mathbf{c}$ and $\mathbf{A}$ contain coefficients for the objective and constraint functions. Notation $\mathbf{a} < \mathbf{b}$ means that every element of $\mathbf{a}$ is smaller than the corresponding element of $\mathbf{b}$. The next task is to write problem 6.13 in the form of 6.14. First we remove the sup-norm from the objective function and replace it with a new variable t so the problem becomes

$$\begin{aligned} \text{minimise} \quad & t + \delta\|\mathbf{w}\|_1 \\ \text{subject to} \quad & \mathbf{C}^T\mathbf{u} + \mathbf{H}^T\mathbf{w} \leq t\mathbf{1} \\ & \mathbf{C}^T\mathbf{u} + \mathbf{H}^T\mathbf{w} \geq -t\mathbf{1} \\ & \|\mathbf{w}\|_1 \leq W_1 \\ & \|\mathbf{w}\|_\infty \leq W_\infty \\ & t \geq 0, \end{aligned} \tag{6.15}$$

where $\mathbf{1}$ is a vector of ones the same size as $\mathbf{w}$. In the following, the size of $\mathbf{1}$ depends on the mathematical context. The next step is to get rid of the sum absolute value of $\mathbf{w}$. This can be done by splitting the vector into two components $\mathbf{w} = \mathbf{w}_+ - \mathbf{w}_-$ so that the elements of $\mathbf{w}_+$ and $\mathbf{w}_-$ are non-negative. Further, W_∞ limit can be written without sup-norm when the problem becomes

$$\begin{aligned} \text{minimise} \quad & t + \delta(\mathbf{w}_+ + \mathbf{w}_-)^T\mathbf{1} \\ \text{subject to} \quad & \mathbf{C}^T\mathbf{u} + \mathbf{H}^T(\mathbf{w}_+ - \mathbf{w}_-) \leq t\mathbf{1} \\ & \mathbf{C}^T\mathbf{u} + \mathbf{H}^T(\mathbf{w}_+ - \mathbf{w}_-) \geq -t\mathbf{1} \\ & \mathbf{w}_+^T\mathbf{1} + \mathbf{w}_-^T\mathbf{1} \leq W_1 \\ & \mathbf{w}_+ \leq W_\infty\mathbf{1} \quad \text{and} \quad \mathbf{w}_- \leq W_\infty\mathbf{1} \\ & t, \mathbf{w}_+, \mathbf{w}_- \geq 0. \end{aligned} \tag{6.16}$$

Now, the objective function and the constraint functions are linear, and the variables, coefficients and limits can be collected as follows

$$\begin{aligned} \text{minimise} \quad & [\delta\mathbf{1}, 1] \begin{bmatrix} \mathbf{w}_+ \\ \mathbf{w}_- \\ t \end{bmatrix} \\ \text{subject to} \quad & \begin{bmatrix} \mathbf{H}^T & -\mathbf{H}^T & -\mathbf{1} \\ -\mathbf{H}^T & \mathbf{H}^T & -\mathbf{1} \\ \mathbf{1} & \mathbf{1} & 0 \end{bmatrix} \begin{bmatrix} \mathbf{w}_+ \\ \mathbf{w}_- \\ t \end{bmatrix} \leq \begin{bmatrix} -\mathbf{C}^T\mathbf{u} \\ \mathbf{C}^T\mathbf{u} \\ W_1 \end{bmatrix} \\ & 0 \leq \begin{bmatrix} \mathbf{w}_+ \\ \mathbf{w}_- \\ t \end{bmatrix} \leq \begin{bmatrix} W_\infty\mathbf{1} \\ W_\infty\mathbf{1} \\ \infty \end{bmatrix}. \end{aligned} \tag{6.17}$$

Now the problem is in the form of 6.14 and can be solved. There are several algorithms and tools for solving LP problems [38], but the details are not discussed here.

Table 6.2 Crest factor reduction without power constraints.

Number of codes	CF	CF_{LP}	ΔCF_{LP}	P_r/P_s
16	12.87 dB	8.59 dB	4.27 dB	0.4328
32	13.26 dB	8.37 dB	4.89 dB	0.5131
64	13.22 dB	8.78 dB	4.44 dB	0.5016
128	13.06 dB	9.46 dB	3.59 dB	0.4519
192	14.18 dB	10.23 dB	3.95 dB	0.4048
224	12.95 dB	10.46 dB	2.48 dB	0.3257
240	13.08 dB	10.91 dB	2.17 dB	0.2373

6.4.1 Results

The LP optimisation algorithm is tested and the results are presented in Tables 6.2 and 6.3. The test signals are similar to the test signals used in Section 6.3. The control parameter δ is chosen by decreasing its value step by step until it has no significant effect on the result. The signal is divided into blocks of SF=256 chips corresponding to one symbol and each block is processed separately. The CF is calculated for filtered and upconverted signals.

In Table 6.2, the LP algorithm is applied without any constraints to evaluate the optimal CF reduction. A significant CF reduction can be achieved, even if the number of active codes is as high as 240. However, this is achieved at the cost of a high P_r/P_s power ratio and it should be noted that this example is presented only in order to test the concept, not as a practical solution. Based on the results presented in Section 6.3, it can be assumed that the reduction of the CF could be even higher if the complex envelope is minimised instead of minimising I and Q independently. That kind of minimisation problem is no more solvable by the means of LP, and therefore it is not studied further.

In Table 6.3, the power of the residual signal is limited to be equal to the reference case. The reference power limits are obtained by using projection method case 1. The clipping level is chosen to minimise the CF and the power ratio P_r/P_s is calculated, after which the constraints W_1 and W_∞ are chosen by trial and error. The projection method seems to give a higher CF reduction, but this is only because the LP optimisation is carried out for each block, even when there is no need for clipping. This increases the P_r/P_s power ratio, while no advantage is gained. Extensive and very time consuming computer simulations are needed to achieve the maximal CF reduction using LP optimisation with power constraints. Therefore, this subject is excluded from this thesis.

Table 6.3 Crest factor reduction with power constraints.

Number of codes	CF	ΔCF_{proj}	$\Delta\text{CF}_{LP,lim}$	P_r/P_s
16	12.86 dB	2.55 dB	1.88 dB	0.044
32	13.26 dB	2.89 dB	2.72 dB	0.036
64	13.22 dB	2.52 dB	2.67 dB	0.037
128	13.06 dB	1.79 dB	1.90 dB	0.014
192	14.18 dB	0.99 dB	0.74 dB	0.007
224	12.95 dB	0.31 dB	0.21 dB	0.005
240	13.08 dB	0.13 dB	0.24 dB	0.003

6.5 Code selection

An important topic related to the clipping method presented is the selection of the active codes. In simulations, the best results are achieved when the active codes are chosen randomly from the code space. When the active codes are taken from one branch of the code tree, only the performance of the clipping is degraded. This can be explained by taking a look at the code matrices. The Walsh code matrix $\mathbf{K}_n$ can be generated iteratively:

$$\mathbf{K}_{2n} = \begin{bmatrix} \mathbf{K}_n & \mathbf{K}_n \\ \mathbf{K}_n & -\mathbf{K}_n \end{bmatrix} \quad \text{, where} \quad \mathbf{K}_1 = [1] \tag{6.18}$$

If the first half of the codes are active in data transmission, we get

$$\mathbf{C} = \begin{bmatrix} \mathbf{K}_n & \mathbf{K}_n \end{bmatrix} \quad \text{and} \quad \mathbf{H} = \begin{bmatrix} \mathbf{K}_n & -\mathbf{K}_n \end{bmatrix} \tag{6.19}$$

and the resulting coded signals become

$$\mathbf{C}^T\mathbf{u} = \begin{bmatrix} \mathbf{K}_n^T\mathbf{u} \\ \mathbf{K}_n^T\mathbf{u} \end{bmatrix} \quad \text{and} \quad \mathbf{H}^T\mathbf{w} = \begin{bmatrix} \mathbf{K}_n^T\mathbf{w} \\ -\mathbf{K}_n^T\mathbf{w} \end{bmatrix}. \tag{6.20}$$

Due to the symmetry, if the highest peak of $\mathbf{K}_n^T\mathbf{u}$ denoted by $\check{s}$ is present in row i it is also found in row $i+n$. Now, if the i^{th} row of the residual signal $\mathbf{H}^T\mathbf{w}$ is r_i, row $i+n$ becomes $-r_i$. In order to reduce the highest peak $\check{s}$, the following inequalities should both be true.

$$|\check{s}+r_i| < |\check{s}| \quad \text{and} \quad |\check{s}-r_i| < |\check{s}| \tag{6.21}$$

Since the conditions can not be met at the same time, we can conclude that it is indeed impossible to reduce peaks generated from the first half of the code matrix by using the second half of the code matrix. This should be taken into account when the codes

are allocated and, if there are freedoms in the code selection, the active codes should be chosen so that the different branches of the code tree are represented as widely as possible.

6.6 Conclusions

The principle for a clipping method that exploits the unused channel codes is presented. In an ideal case, this clipping method does not introduce any error at the receiver. In reality, it can be said that the clipping does not introduce more error than would be the case by adding new users with relatively low power levels into the system.

Several possible algorithms are presented and tested through simulations. The most simple clipping problem is solved also as a mathematical multivariable problem in order to test the real potential of the presented idea. Results show that the CF can be reduced some dBs, depending on the number of active codes and the definition used for the residual signal. The mathematical solution shows that there is still a margin between the optimal solution and the solution achieved by the presented methods: this gives fertile ground for further research.

This page is intentionally left blank.

Chapter 7

Reducing the crest factor of multicarrier GSM and EDGE signals

The GSM is a widespread 2G system that uses GMSK modulation. The advantage of this modulation method is the constant envelope signal, which makes it possible to use power-efficient power amplifiers. EDGE is an enhancement to the GSM system. The primary objective for the EDGE signal is to triple the on-air data rate while meeting essentially the same bandwidth occupancy of the original GMSK signal. The EDGE system uses $3\pi/8$-shifted 8-Phase Shift Keying (PSK) modulation, which is not a constant envelope modulation.

In conventional base station solutions, transmitted carriers are combined after power amplifiers. An alternative to this is to combine the carriers in the digital IF domain [1] [2]. This saves a large number of analogue components and, because there is no analogue I/Q modulator, many problems, i.e. DC offset and mismatch of the components can be avoided. The major drawback to combining the digital carriers is a strongly varying envelope of the composite signal. When a number of carriers are combined, according to the central limit theorem, the envelope of the composite signal becomes Gaussian distributed with high CF. In this chapter, at first the properties of the GSM and EDGE multicarrier signals are discussed and then the conventional IF clipping (Equation 3.2) and windowing method presented in Chapter 4 are applied in both cases. This chapter is based on [34] and [39].

7.1 Signal model

In both cases, GSM and EDGE, a single carrier IF signal is generated using the burst format specified in [40]. The oversampling ratio of 240 is used at the IF. This corresponds to 65 MHz sampling frequency in the digital modulator, because the symbol rate is 270.833 ksym/s in GSM/EDGE. The oversampling ratio must be chosen high in order to achieve an IF frequency high enough to enable the digital combining of a large number of carriers. A multicarrier signal is generated by combining several single carrier signals at IF, using 600 kHz channel spacing. All combined signals are generated by using independent random data and the initial phase of the carrier is chosen randomly.

The CF of the real single carrier GSM IF signal is approximately equal to the CF of the sinusoidal signal, 3.01 dB. Simulations have shown that the CF of the corresponding EDGE signal is about 6.18 dB.

If all the carriers are assumed to be statistically independent, the power of the composite signal is doubled when the number of carriers is doubled. In the worst case, all the carriers have their maximum simultaneously, which means that, when the number of carriers is doubled, the maximum of the composite signal is doubled and the peak power is multiplied by four. In this case, the PAR is doubled, which means an about 3 dB increment in the CF. In reality, it is very unlikely that all the carriers reach their maximum simultaneously, and the CF does not increase as much as predicted. Simulated CFs for composite signals with different numbers of carriers are presented in Table 7.1. The results show that the CF does not increase as much as in the worst possible case, but, anyway, for a large number of carriers it becomes very high in both cases, GSM and EDGE.

In the future, it will be possible to transmit GSM and EDGE signals simultaneously using the same power amplifier. The CFs of the signal with 16 carriers when the number of EDGE carriers is varied is presented in Table 7.2.

Table 7.1 Simulated CFs for signals with different number of carriers

Number of carriers	CF GSM	CF EDGE
1	3.010 dB	6.176 dB
2	6.020 dB	8.969 dB
4	9.012 dB	11.102 dB
8	11.397 dB	12.956 dB
16	14.258 dB	15.747 dB
32	17.395 dB	18.649 dB

Table 7.2 Crest Factor of the signal with 16 carriers when the number of EDGE carriers is varied

Number of EDGE carriers	CF
1	14.372 dB
2	14.391 dB
4	14.266 dB
8	14.372 dB
12	14.783 dB

7.2 Results

The clipped signal must fulfil the system specifications [27]. In the case of GSM, the signal quality is measured by phase error, and, in the case of EDGE, the signal quality is measured by EVM. In both cases, the spectrum of the signal must fit the spectrum mask.

7.2.1 GSM

At first, different window types are compared. The spectrum of the unclipped signal, the spectrum of the clipped signal and the spectra of the windowed signals are presented in Figure 7.1. The window length of 551 is used. Results for Hanning and Blackman windows are presented. Other common window functions, i.e. Kaiser, Hamming and Gaussian, are also investigated; the Hanning and Blackman windows are found to be better than the other windows.

The test signal consists of 16 carriers and the CF of the unclipped signal is 14.26 dB. In each case, the signal is clipped so that the Crest Factor becomes 10 dB. Figure 7.1 shows that the conventional clipping causes very high out-of-band radiation and therefore it is not applicable in the case of GSM transmission. A Blackman window seems to give better spectral properties than a Hanning window.

The effect of the window length (Blackman) used is presented in Figure 7.2 and in Table 7.3. The CF of the test signal is clipped to 12 dB. In this example, the window length of 240 corresponds to the length of one symbol (an oversampling ratio of 240 is used). It is obvious that a long window gives better spectral properties than a short window, but the interesting result is that the long window gives a better phase error performance than a short window. This is surprising, because, when the window length increases, the difference between the transmitted and the ideal waveform increases, and therefore, intuitively, the phase error should increase.

The achieved CF reduction (ΔCF) in the case of 8, 16 and 32 carriers is presented in Table 7.4. The window length used is 601 and the clipping level is set so that the

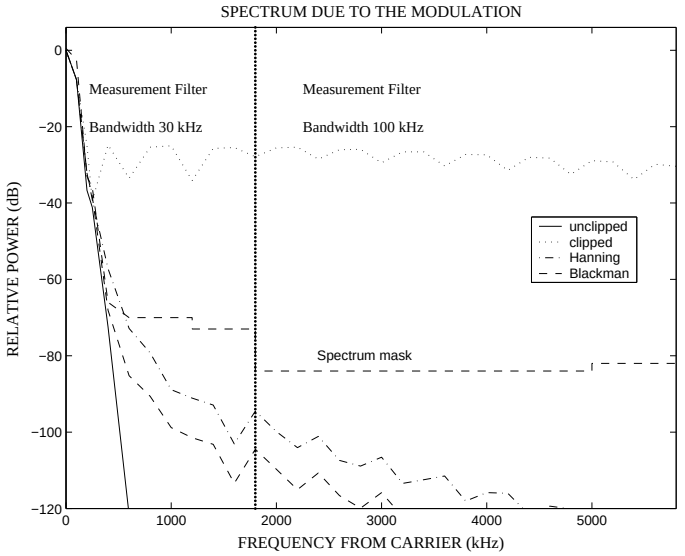

Figure 7.1 Spectrum of the GSM signal when different clipping methods are used.

spectrum is the limiting element. The results show that the CF of the multicarrier GSM signal can be reduced significantly while the distortion is still kept at tolerable level. The phase error specifications are 5° for RMS and 20° for peak error [27]. In practice, implementing the windowing algorithm presented in [32] with a window length of 601 might be very difficult and lead to high area and power consumption in the circuit implementation. The window length required can be decreased by decreasing the OSR, but, as mentioned earlier, this limits the number of carriers combined digitally.

Table 7.3 Phase error of the GSM signal as a function of the window length.

Window length	rms	peak
101	0.957°	5.049°
201	1.033°	5.567°
401	0.667°	3.308°
601	0.157°	0.818°

7.2.2 EDGE

Again different window types are compared. The spectrum of the unclipped signal, the spectrum of the clipped signal and the spectra of the windowed signals are presented in Figure 7.3. Two different windows, Hanning and Blackman, are used. In both cases, the window length is 525. The test signal consists of 16 carriers and the CF

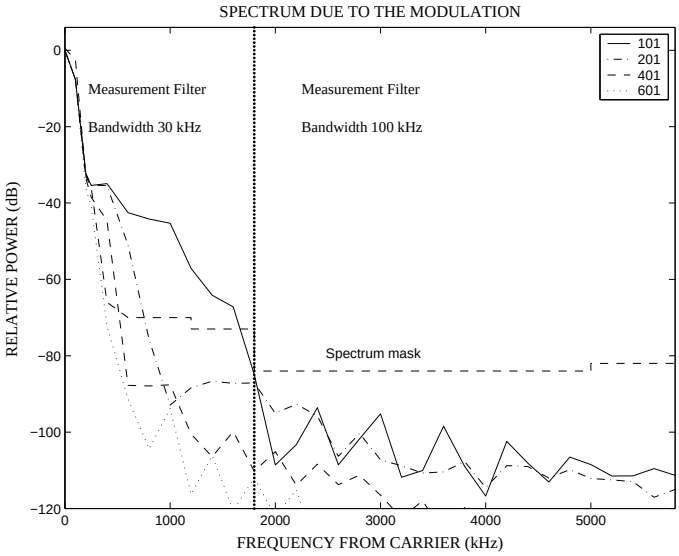

Figure 7.2 Spectrum of the GSM signal as a function of the window length.

Table 7.4 Crest Factor reduction in the case of multicarrier GSM signal.

number of carriers	CF	ΔCF	rms	peak
8	9.131 dB	2.266 dB	0.199°	0.866°
16	10.207 dB	4.051 dB	0.230°	1.212°
32	10.658 dB	6.737 dB	0.360°	2.805°

of the unclipped signal is 15.75 dB. In every case, the signal is clipped so that the CF becomes 12 dB. Figure 7.3 shows that, as earlier, the conventional clipping causes very high out-of-band radiation and therefore it is not applicable in the case of EDGE transmission. A Blackman window seems to give better spectral properties than a Hanning window.

The effect of the window length (Blackman) is presented in Figure 7.4 and in Table 7.5. The CF of the test signal is clipped one decibel. The longer window gives better spectral behaviour but the EVM becomes high. A window long enough to meet the spectral specifications causes an EVM which is very near or above the EVM specifications: 7% for RMS and 24% for peak value [27]. In a real digital modulator EVM, this high cannot be tolerated, because some margin must be left for the following analogue parts. In conclusion, it can be said that neither of the clipping methods discussed here can be used for EDGE clipping. Even one decibel reduction in CF leads to an intolerable error. Generally, EDGE signals seem to be very sensitive to clipping errors, which

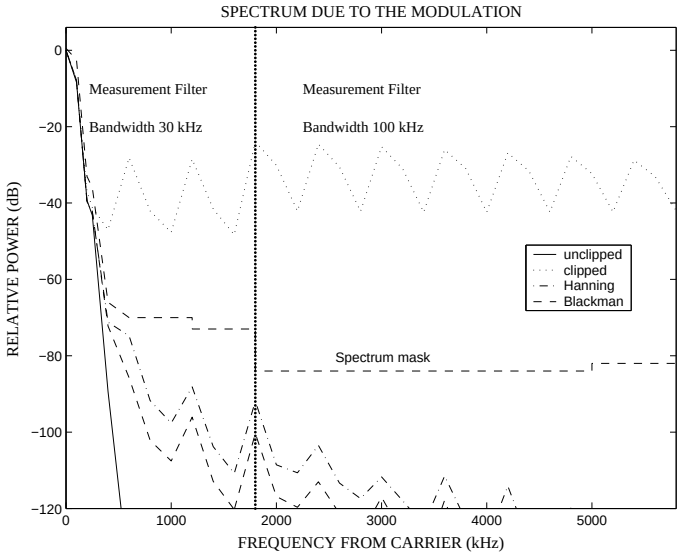

Figure 7.3 Spectrum of the EDGE signal when different clipping methods are used.

makes the CF reduction a very challenging problem.

The reason for the poor performance of the EDGE clipping is that the clipping seems to affect more the amplitude of the signal than the phase of the signal. Because the distortion in the case of the EDGE signal is measured by both amplitude error and phase error, the error metric EVM becomes high. In the case of GSM clipping, the error is measured by phase error only, and therefore the signal can be clipped significantly. If we down-convert the clipped GSM signal and divide it into the in phase and quadrature branches and calculate the EVM, as in the case of EDGE, it can be seen that, while the phase error remains low, the EVM can be high. For the signal with 0.19 degrees RMS and 0.88 degrees peak phase error, the corresponding EVM values are 5.4% and 19.6%, respectively.

Table 7.5 EVM of the clipped EDGE signal as a function of the window length.

Window length	rms EVM	peak EVM
101	2.763 %	11.526 %
201	3.683 %	15.156 %
401	5.690 %	21.920 %
601	6.944 %	24.783 %

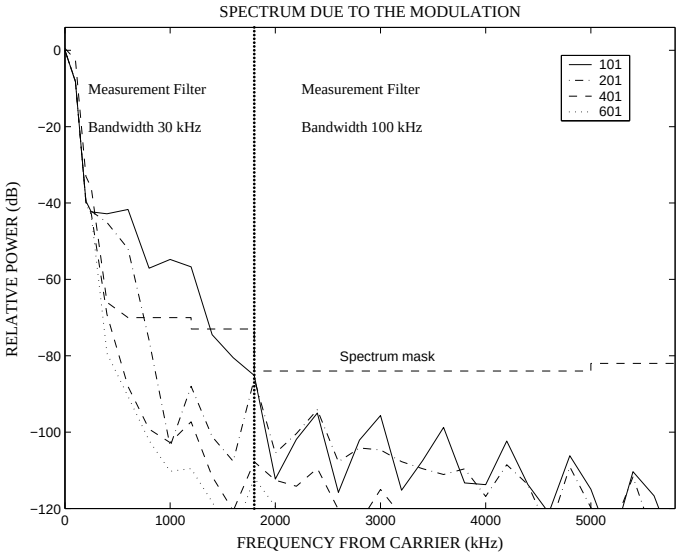

Figure 7.4 Spectrum of the clipped EDGE signal as a function of the window length.

7.2.3 GSM/EDGE

As shown earlier, the EDGE clipping is much more complicated than the GSM clipping, so it can be assumed that, when the GSM and EDGE carriers are transmitted simultaneously, the performance of the EDGE signals restrict the clipping. When a signal with 15 GSM carriers and one EDGE carrier is clipped by using the windowing method, the CF is reduced about 1.5 dB from 14.37 dB to 12.88 dB. In this case, the RMS EVM is 3.1 % and the peak EVM is 21.5 %, which fulfils the specifications, but the values are intolerably high. When the number of the EDGE carriers is varied, the results are of the same kind; especially the peak EVM seems to be problematic.

7.3 Conclusions

Two different clipping methods, conventional IF clipping and the windowing method, are applied to GSM and EDGE multicarrier signals in order to reduce the CF. In the case of GSM, the windowing method is shown to be efficient and the CF is reduced significantly, while the distortion is still kept at a tolerable level. In the case of EDGE, both clipping methods are proved to be inapplicable.

This page is intentionally left blank.

Chapter 8

Multimode modulator

As mentioned earlier, GSM is a widespread 2G system and its enhanced variant, EDGE, is a step towards 3G systems. WCDMA has been selected by ETSI for wideband wireless access to support 3G services. Because it is obvious that the existing networks will not be replaced at one attempt, it is desirable that the first generation of the 3G base station modulator should support all of the modulation methods mentioned. Instead of three separate modulators, it is reasonable to implement one programmable modulator.

In this chapter, a digital multimode GSM/EDGE/WCDMA modulator is presented. First, the modulation methods are discussed, after which the algorithms to generate the modulations in question are presented. All the building blocks are designed to give an adequate signal quality with minimal complexity. In practice, this means that the word lengths, number of filter taps etc. are chosen in a way that the non-idealities of the D/A-converter, which are the common bottlenecks of this kind of system, are dominating the total performance. Extensive Matlab simulations were carried out in order to minimise the amount of hardware needed. In this thesis, only the system-level design is considered. The details of the Application Specific Integrated Circuit (ASIC) implementation can be found in [1], [42] and [43]. Finally, measurement results are presented and compared with specifications.

8.1 Modulation methods

8.1.1 GSM

In GSM transmission, GMSK modulation is used [40]. Differentially encoded data symbols ($\alpha_i \in \{-1, 1\}$) at rate $270,833$ kbit/s are filtered using a filter with impulse response

$$h_{gsm}(t) = g(t) * \text{rect}(\frac{t}{T}), \tag{8.1}$$

where

$$\text{rect}(\frac{t}{T}) = \begin{cases} \frac{1}{T} & |t| < \frac{T}{2} \\ 0 & \text{otherwise} \end{cases} \tag{8.2}$$

The pulse $g(t)$ is defined by

$$g(t) = \frac{\exp(\frac{-t^2}{2\delta^2 T^2})}{\sqrt{2\pi}\delta T}, \tag{8.3}$$

where

$$\delta = \frac{\sqrt{\ln(2)}}{2\pi BT} \text{ and } BT = 0.3. \tag{8.4}$$

B is the 3 dB bandwidth of the filter and T is the duration of one input symbol. The phase of the modulated signal is

$$\phi(t) = \sum_i \alpha_i \pi h \int_{-\infty}^{t-iT} g(u)du, \tag{8.5}$$

where the modulating index $h = 1/2$. The modulated Radio Frequency (RF) carrier can be expressed as

$$RF_{gsm}(t) = \sqrt{\frac{2E_c}{T}} \cos(2\pi f_c t + \phi(t) + \phi_0), \tag{8.6}$$

where E_c is the energy per modulating bit, f_c the centre frequency and ϕ_0 a random phase that is constant during one burst.

8.1.2 EDGE

The primary target of the EDGE is to triple the data rate of the GSM transmission. The EDGE signal is generated by using an 8-PSK modulation with $3\pi/8$ symbol rotation and filtering the symbols with a linearised GMSK filter [40]. The modulating bits are mapped in groups of three to 8PSK symbols, according to the rule

$$s_i = e^{j2\pi l/8}, \tag{8.7}$$

where l is given by Table 8.1. The symbol rate becomes $\frac{812.5}{3}$ kbit/s $= 270.833$ kbit/s, which is equal to the symbol rate of GSM. The symbols are continuously rotated according to the equation

Table 8.1 Mapping between modulating bits and the 8PSK symbol parameter.

$d_{3n}, d_{3n+1}, d_{3n+2}$	0,0,0	0,0,1	0,1,0	0,1,1	1,0,0	1,0,1	1,1,0	1,1,1
l	3	4	2	1	6	5	7	0

$$\hat{s_i} = s_i \cdot e^{ji3\pi/8}. \tag{8.8}$$

Input symbols for the modulator follows Equation 8.8 i.e. the symbol mapping is performed off-chip.

The impulse response of the linearised GMSK filter is defined as

$$h_{edge}(t) = \begin{cases} \prod_{i=0}^{3} S(t+iT) & 0 \le t \le 5T \\ 0 & \text{otherwise} \end{cases} \tag{8.9}$$

where

$$S(t) = \begin{cases} \sin(\pi \int_0^t g(u)du) & 0 \le t \le 4T \\ \sin(\frac{\pi}{2} - \pi \int_0^{t-4T} g(u)du) & 4T \le t \le 8T \\ 0 & \text{otherwise} \end{cases} \tag{8.10}$$

and

$$g(t) = \frac{1}{2T}(Q(2\pi \cdot 0.3\frac{t-5T/2}{T\sqrt{\log(2)}}) - Q(2\pi \cdot 0.3\frac{t-3T/2}{T\sqrt{\log(2)}})). \tag{8.11}$$

T is the symbol period. The error function $Q(t)$ is defined as

$$Q(t) = \frac{1}{\sqrt{2\pi}} \int_t^{\infty} e^{-\frac{\tau^2}{2}} d\tau. \tag{8.12}$$

The baseband signal becomes

$$x(t) = \sum_i \hat{s_i} \cdot h(t - iT + \frac{5}{2}T). \tag{8.13}$$

The In-phase (I) and Quadrature (Q) signals are the real and imaginary parts of $y(t)$, respectively.

$$I(t) = \Re\{x(t)\} = \sum_i \cos(\phi_i) \cdot h(t - iT + \frac{5}{2}T) \tag{8.14}$$

$$Q(t) = \Im\{x(t)\} = \sum_i \sin(\phi_i) \cdot h(t - iT + \frac{5}{2}T) \tag{8.15}$$

where $\phi_i = \text{angle}(\hat{s_i})$. The modulated RF carrier becomes

$$RF_{edge}(t) = I(t)\cos(2\pi f_c t) - Q(t)\sin(2\pi f_c t) \tag{8.16}$$

8.1.3 WCDMA

In WCDMA, the data intended for different users is spread and scrambled using specific codes [44]. This is not included in this modulator implementation. The complex spread and scrambled symbols with symbol rate $3,84$ Mbit/s are divided to I- and Q-branches. Both branches are filtered with a Root Raised Cosine filter [45] with impulse response

$$h_{wcdma}(t) = \frac{4\alpha_{rrc}}{\pi(1-\alpha_{rrc})+4\alpha_{rrc}} \times \left[\frac{T\sin(\frac{\pi}{T}(1-\alpha_{rrc})t)}{4\alpha_{rrc}t} + \frac{\cos(\frac{\pi}{T}(1+\alpha_{rrc})t) + \frac{4\alpha_{rrc}t}{T}\sin(\frac{\pi}{T}(1-\alpha_{rrc})t)}{1-(\frac{4\alpha_{rrc}t}{T})^2}\right], \tag{8.17}$$

when $t = \pm\frac{T}{4\alpha_{rrc}}$. $h_{wcdma}(0) = 1$ and

$$h_{wcdma}(\pm\frac{T}{4\alpha_{rrc}}) = \frac{4\alpha_{rrc}}{\pi(1-\alpha_{rrc})+4\alpha_{rrc}} \times \left[\frac{T\sin(\frac{\pi}{4\alpha_{rrc}}(1-\alpha_{rrc}))}{2} + \frac{\cos(\frac{\pi}{4\alpha_{rrc}}(1+\alpha_{rrc})) + \sin(\frac{\pi}{4\alpha_{rrc}}(1-\alpha_{rrc}))}{4\sqrt{2}}\right]. \tag{8.18}$$

T is the symbol duration and $\alpha_{rrc} = 0.22$ is the roll-off parameter defining the bandwidth used. The modulated RF carrier is generated according to the equation

$$RF_{wcdma}(t) = I(t)\cos(2\pi f_c t) - Q(t)\sin(2\pi f_c t) \tag{8.19}$$

8.2 Modulator structure

The digital modulator consists of a programmable pulse shaping filter, two interpolating halfband filters, a programmable interpolator and a COordinate Rotation DIgital Computer (CORDIC) rotator to generate a digital IF signal. After the CORDIC rotator, an inverse sinc filter is placed to compensate the distortion caused by the D/A-converter. Finally, there is a ramp generator in front of the D/A-converter. The ramp generator is needed to implement the burst format in the GSM and EDGE transmission. A block diagram of the multimode modulator is presented in Figure 8.1. The area enclosed by the dashed line is included in the chip.

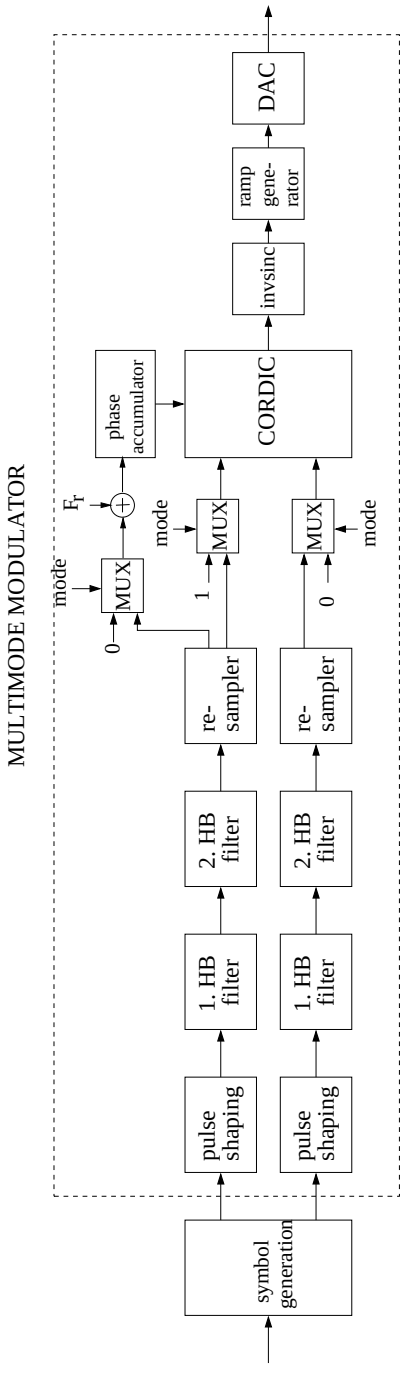

Figure 8.1 Block diagram of the modulator.

8.2.1 Filtering

The filter section consists of a pulse shaping filter and two halfband filters. The purpose of the halfband filters is to increase the oversampling ratio with a factor of four. To relax the complexity of the following fractional rate interpolator, the pulse shaping filter is also interpolating by a factor of two when the oversampling ratio of the whole filter chain becomes 8.

An interpolating filter can be decomposed into its polyphase components [46]. In this case, the filters are divided into two subfilters, one including the odd taps and the other including the even taps. This halves the computational rate and makes it easier to use the pipelining/interleaving (P/I) technique. All filters are implemented using Canonic Signed Digit (CSD) coefficients, which enables a multiplier free structure. The idea of the CSD coefficients is to present the multiplying constant as a sum of powers of two. Then the multiplication can be performed using shift and add operations only. Because all the filters to be implemented are symmetrical, it is possible to use folding. The amount of hardware can be reduced further using the P/I technique, which enables the filtering of the several data streams using one filter only [47]. In this case, *I* and *Q* signals are interleaved and only one filter chain is needed (unlike the case shown in Figure 8.1). This is performed at the expense of some additional logic and a doubled sampling frequency, leading to slightly increased power consumption.

In order to realise all the three modulations described above, the coefficients of the pulse shaping filter must be programmable. The pulse shaping filter is implemented as a 37 tap FIR filter, which means that the impulse responses defined in Equations 8.1, 8.9 and 8.17 are truncated and sampled.

In the case of GSM and EDGE, the input signal is oversampled by four, which makes it easy to add the 8.25 symbols long guard period needed [48]. This means that three zeros must be placed between the incoming symbols before the filtering. Instead of using Equation 8.1, the coefficients of the GSM pulse shaping filter are calculated using Equation 8.3. The convolution with rectangular pulse in Equation 8.1 is implemented by combining the rectangular waveform directly to the incoming symbols. In practice, this means that the signal is not zero-padded, but the symbols are repeated four times to form the rectangular waveform. The coefficients of the EDGE pulse shaping filter are calculated according to Equation 8.9, and the coefficients of the WCDMA filter according to Equation 8.17. The folded direct form structure is chosen for the pulse shaping filter because it must be possible to change the modulation scheme from GSM to EDGE, or vice versa, between adjacent time slots. The folded transposed direct form structure [49] has less complex hardware and better speed performance, but the changing of the taps cannot be seen at the output immediately.

Both half band filters are implemented using folded transposed direct form archi-

tecture [49]. The first filter has 23 taps and the second has 11 taps. In both cases, the even taps, excluding the centre tap, are zero, which means that, in the polyphase decomposition, the second subfilter becomes extremely simple, including only one tap.

In the filtering chain as well as in the following parts, the scaling of the signal must be considered carefully. In order to prevent overflows, the signal level must be low enough; on the other hand, a margin that is too large leads to an inefficient use of the dynamic range of the equipment. Therefore, the scaling of the signal was decided after extensive computer simulations.

8.2.2 Fractional rate interpolation

After the filter chain described earlier, the GSM/EDGE sampling rate is increased by a factor of 24 and the WCDMA sampling rate by a factor of 8, which leads to sampling frequencies of 6.5 MHz and 30.72 MHz, respectively. Because the sampling frequency of the D/A-converter is fixed, a programmable interpolator is needed to make the conversion between the different symbol rates and the fixed output symbol rate. Furthermore, because there is no common integer ratio multiple for both symbol rates at the reachable frequencies, the interpolation rate must be a rational number.

The output instant for the interpolant is controlled by the fractional interval

$$\mu = \frac{kT_i - mT_s}{T_s}, \tag{8.20}$$

where T_s is the sampling interval, T_i the output interval and n the largest integer for which $nT_s \leq kT_i$. In practice, μ is calculated using a Number-Controlled Oscillator (NCO) [50]. Furthermore, the Most Significant Bit (MSB) of the NCO can be used as the sampling clock for the interpolator and the preceding filter chain.

The interpolated signal can be written as

$$y(kT_i) = \sum_{i=-N/2}^{N/2-1} x[(m-i)T_s]h[(i+\mu)T_s], \tag{8.21}$$

where $x[(m-i)T_s]$ are the N input samples, i.e. basepoints of the input signal, and $h[(i+\mu)T_s]$ are the N samples from the continuous impulse response of the interpolation filter [50].

Equation 8.21 shows that the impulse response of the digital interpolation filter depends on μ, which is varying. This means that a new set of filter coefficients is needed for every output sample. For arbitrary sampling rates, a huge memory is needed to store the precalculated impulse responses or a very complex computational block to calculate the coefficients real time. To avoid this problem, a polynomial based solu-

tion is chosen [51]. Using a third degree Lagrange polynomial, the interpolated signal can be written as

$$y_k = \sum_{i=-2}^{1} C_i x_{(m-1-i)}, \tag{8.22}$$

where

$$\begin{aligned} C_{-2} &= \tfrac{1}{6}\mu^3 - \tfrac{1}{6}\mu \\ C_{-1} &= -\tfrac{1}{2}\mu^3 + \tfrac{1}{2}\mu^2 + \mu \\ C_0 &= \tfrac{1}{2}\mu^3 - \mu^2 - \tfrac{1}{2}\mu + 1 \\ C_1 &= -\tfrac{1}{6}\mu^3 + \tfrac{1}{2}\mu^2 - \tfrac{1}{3}\mu \end{aligned} \tag{8.23}$$

Equation 8.22 is implemented using a Farrow structure [52] shown in Figure 8.2. A Farrow structure can be found for any polynomial-based filter. In this work, the target was to find an interpolator that can keep the signal quality at a sufficient level with minimal complexity. Starting from a linear polynomial, simulations pointed out that at least a third-order polynomial is needed. Here, the limiting factor is the WCDMA signal, which has a significantly wider bandwidth than a GSM or EDGE signal.

The performance of the interpolator, as well as the other non-idealities in the transmitter, are evaluated by comparing the generated signal to the ideal one. The reference signal is generated by using an interpolating filter structure with variable coefficients. In the case of EDGE, calculating the impulse response, as defined in Equation 8.9, is computationally very demanding; it is therefore reasonable to find a suitable approximation.

8.2.2.1 Approximation of the linearised GMSK pulse

As mentioned earlier, in the simulations, the coefficients for the interpolation filter must be calculated for every output sample separately, which is extremely impractical and time consuming. Therefore, an approximation with a low computational complexity is needed. We start by moving the crest of the pulse to the origin. This makes the pulse

$$h'_{edge}(t) = h_{edge}(t + \frac{5}{2}T), \tag{8.24}$$

symmetrical about the origin; it can then be approximated using an exponential function

$$h'_{edge}(t) \approx e^{P(t)}, \tag{8.25}$$

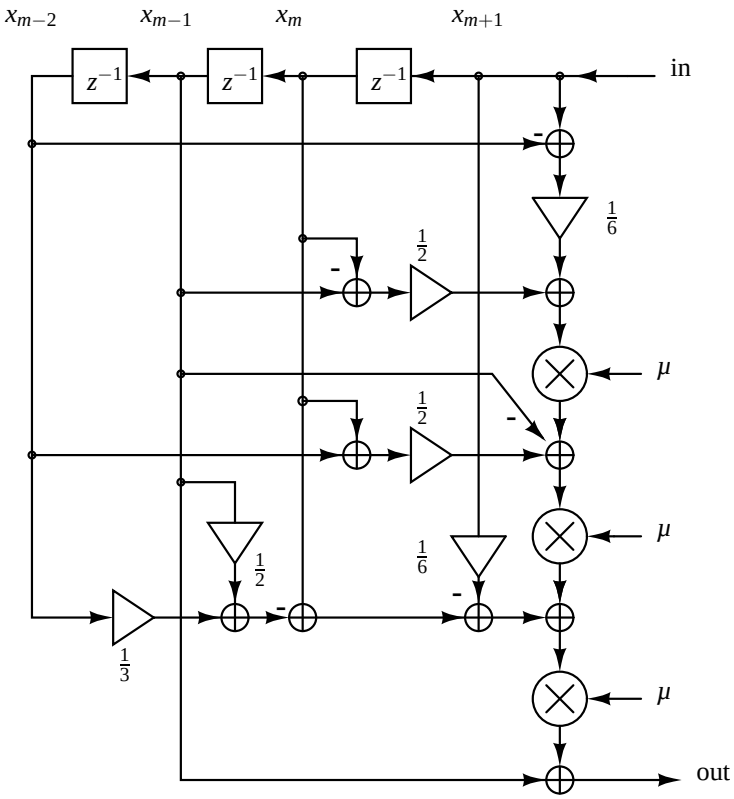

Figure 8.2 Farrow structure of cubic Lagrange interpolator

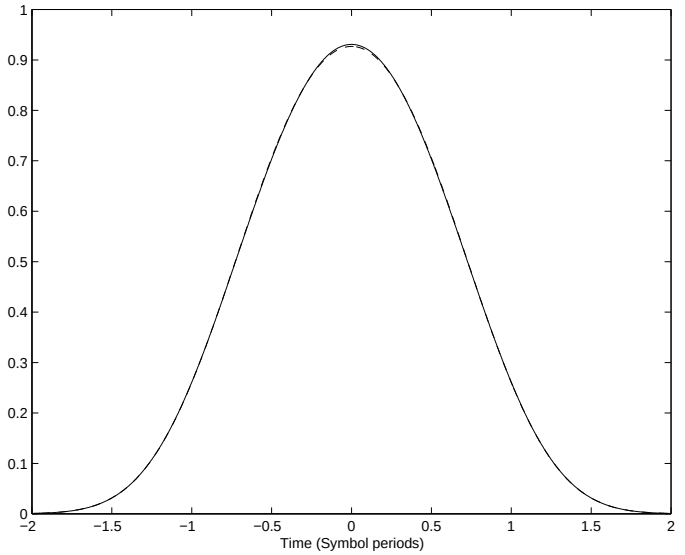

Figure 8.3 The original and approximated pulse.

where $P(t)$ is a polynomial of Nth degree . Because the pulse has an even symmetry, we can assume that the odd power coefficients are zero. The even power coefficients are obtained by calculating $h'_{edge}(t)$ using Equation 8.9, taking the natural logarithm from the result and fitting a Nth degree polynomial to the data. When $N = 6$, we obtain

$$P(t) = 0.007837(t/T)^6 + 4.31e^{-16}(t/T)^5 - 0.2117(t/T)^4$$
$$-1.705e^{-15}(t/T)^3 - 1.0685(t/T)^2 + 8.4805^{e-16}(t/T) - 0.0717. \quad (8.26)$$

It is noticeable that the coefficients of the odd powers are significantly smaller than the coefficients of the even powers. To guarantee the symmetry of the pulse, the odd coefficients are set to zero. In this case, the approximation becomes

$$h'_{edge}(t) \approx \exp[0.007837(t/T)^6 - 0.2117(t/T)^4 - 1.0685(t/T)^2 - 0.0717]. \quad (8.27)$$

In Figure 8.3, the pulse calculated using Equation 8.9 is compared to the pulse calculated using Equation 8.27. The root mean square and the peak value of the approximation error over the interval $-5T/2 \leq t \leq 5T/2$ are 0.27% and 1.6%, respectively. However, because it is difficult to estimate the error caused by the limited numerical accuracy (e.g. in numerical integration) when evaluating Equation 8.9, it seems justified to use the approximation presented.

8.2.3 Upconversion

A CORDIC rotator is utilised to implement upconversion [53]. The advantage of the CORDIC rotator is that no hardware-consuming multipliers are needed. Instead, the vector rotation is performed iteratively, using binary shifts and additions. The in-phase and quadrature components of the CORDIC rotator are

$$\begin{aligned} I_{out} &= I(n)\cos(\omega_c n) - Q(n)\sin(\omega_c n) \\ Q_{out} &= Q(n)\cos(\omega_c n) + I(n)\sin(\omega_c n) \end{aligned} \tag{8.28}$$

respectively. The actual iterative rotation is performed according to the equation

$$\begin{aligned} I_{i+1} &= K_i[I_i - Q_i d_i 2^{-i}] \\ Q_{i+1} &= K_i[Q_i + I_i d_i 2^{-i}] \\ \phi_{i+1} &= \phi_i - d_i \arctan(2^{-i}), \end{aligned} \tag{8.29}$$

where

$$d_i = -1 \quad \text{if} \quad \phi_i < 0, \quad 1 \quad \text{otherwise} \tag{8.30}$$

and

$$K_i = \frac{1}{\sqrt{1+2^{-2i}}}. \tag{8.31}$$

If the product of K_i's is removed, the algorithm can be implemented using shift and add operations only. The resulting gain, dependent on the number of iterations, can be treated as a part of the system's total gain. The phase value ϕ_{in}, corresponding to the desired rotation angle, can be calculated using a phase accumulator with a control word

$$F_r = \frac{f_c \cdot 2^{F_{r,wl}}}{f_s}, \tag{8.32}$$

where f_c is the desired carrier frequency, f_s the sampling frequency and $F_{r,wl}$ the word length of the control word. When i is an integer, $\arctan(2^{-i})$ can only get values $[0, \pi/4]$: therefore the possible rotations are limited between $\pm\pi/2$. To enable rotations between $\pm\pi$, an additional rotation is needed. This initial rotation is performed according to the equation

$$\begin{aligned} I_0 &= -d_0 Q_{in} \\ Q_0 &= d_0 I_{in} \\ \phi_0 &= \phi_{in} - d_0 \pi/2, \end{aligned} \tag{8.33}$$

where

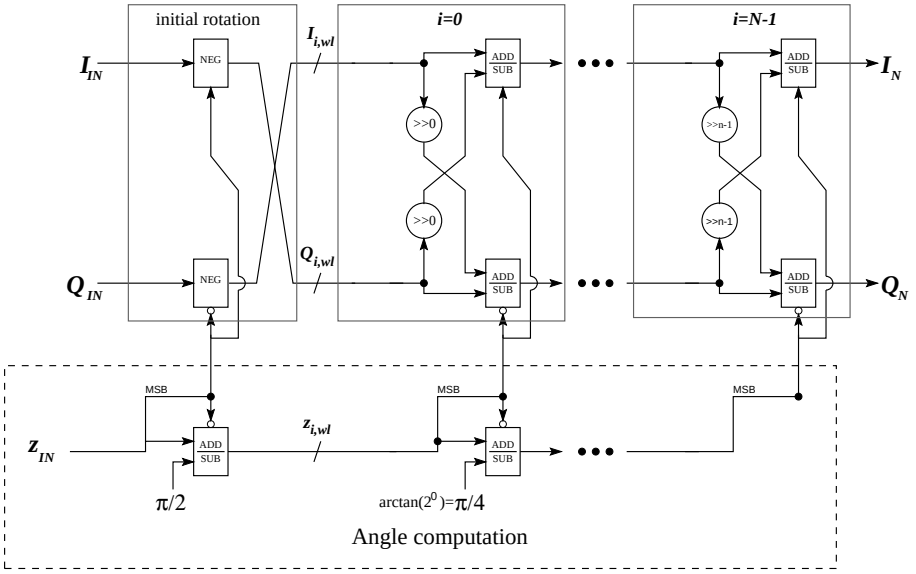

Figure 8.4 Block diagram of the CORDIC rotator.

$$d_0 = -1 \quad \text{if} \quad \phi_{in} < 0, \quad 1 \quad \text{otherwise} \tag{8.34}$$

To achieve an adequate signal quality, 14 iteration stages are needed. A block diagram of the CORDIC rotator is presented in Figure 8.4.

When I and Q are pulse shaped EDGE or WCDMA symbols, the in-phase output of the CORDIC rotator is equivalent to Equations 8.16 and 8.19. In the GSM mode, the CORDIC inputs I and Q are set to 1 and 0, respectively. When the properly-scaled pulse shaped data is added to the carrier frequency control word, the in-phase output of the CORDIC rotator becomes

$$I_{out} = cos(\omega_c n + \theta(n)), \tag{8.35}$$

where $\theta(n)$ is the information-bearing component of the phase. This is equivalent to Equation 8.6.

8.2.4 Inverse sinc and power control

In order to reduce the sinc effect caused by the D/A-converter, a 7-tap compensation filter is placed after the CORDIC rotator. The coefficients of the compensation filter were found in [24]. It is possible to generate a multicarrier signal by adding the IF outputs of the several digital modulators. Digital power control must be implemented to enable the adjusting of a single carrier with respect to the others. The GSM and

EDGE signals are transmitted in bursts, which requires a digital ramp generator. In this modulator, a programmable ramp generator capable of generating a Blackman window was utilised. The power control is performed by scaling the ramp curve.

The digital IF signal is D/A-converted by using a 14-bit on-chip D/A-converter. The wordlength was chosen according to the high dynamic range of the multicarrier signal. The exact implementation of the ramp generator and D/A-converter is not in the scope of this thesis, but the more detailed description can be found in [43].

8.3 Results

The modulator was implemented with $0.35\mu m$ Complementary Metal Oxid Semiconductor (CMOS) technology and the performance was evaluated using a specially-made test board and computer program. The output spectra of the GSM, EDGE and WCDMA signals are shown in Figures 8.5,8.6 and 8.7, respectively. The GSM and EDGE signals meets the spectrum mask requirements [27] and the ACLR of the WCDMA signal satisfies specification [28]. The summary of the spectral properties is presented in Table 8.2.

The EVM and phase error measured at the digital output and the D/A-converter output are presented in Table 8.3. All the results satisfy the specification. In fact, the signal quality is much better than the specification. This is because the following analogue transmission stages distort the signal. The errors are generated more in D/A-conversion than in the digital domain.

8.4 Conclusions

A digital multimode modulator for a 3G base station was designed and implemented. The modulator can operate in GSM, EDGE and WCDMA systems. It is shown in measurements that the solutions chosen work and the modulator meets the GSM, EDGE and WCDMA standards easily. The margin between the specification and the signal quality achieved is reserved for the following analogue stages.

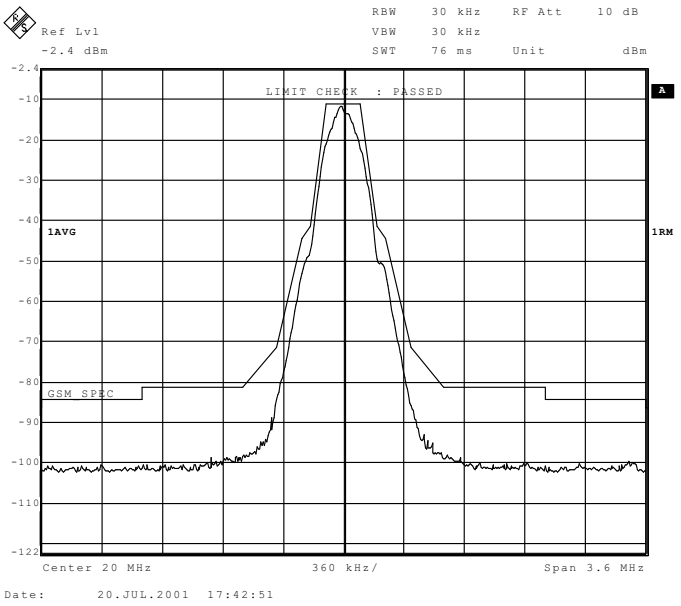

Figure 8.5 Power spectrum of GSM signal.

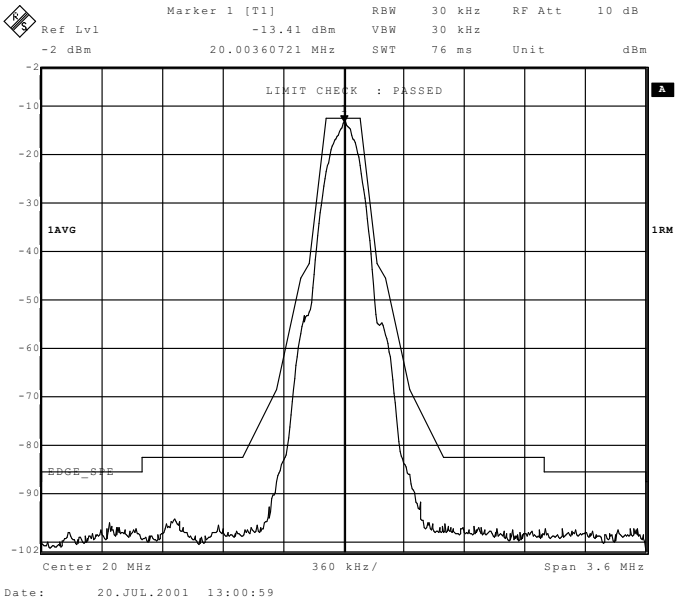

Figure 8.6 Power spectrum of EDGE signal.

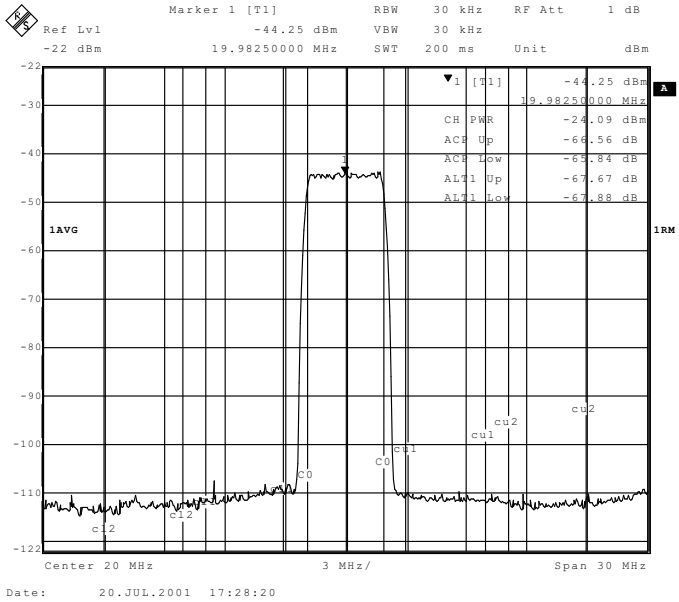

Figure 8.7 Power spectrum of WCDMA signal.

Table 8.2 Spectral properties summary

	GSM	EDGE	WCDMA	
	600 kHz offset (dB)	600 kHz offset (dB)	ACLR1 (dB)	ACLR2 (dB)
Digital output	-100	-90	72.9	73.3
D/A-converter output	-87.3	-84.6	65.8	67.7
Specification	-70	-70	45	50

Table 8.3 Signal quality summary

	GSM phase error		EDGE EVM (%)		WCDMA EVM (%)
	peak	rms	peak	rms	rms
Digital output	0.75	0.29	1.26	0.27	1.11
D/A-converter output	1.71	0.74	1.55	0.37	1.18
Specification	20	5	22	7	17.5

This page is intentionally left blank.

Chapter 9

OFDM modulator

OFDM is widely considered as a technical solution for the 4G wireless communication systems. In this chapter a digital OFDM modulator is presented.

The modulator consists of IFFT block, upsampling filters, upconversion included in the upsampling operation and clipper. The block diagram of the implemented modulator is presented in Figure 9.1. and the specifications for the modulator are presented in Table 9.1. A 2048-point IFFT is utilised to generate the baseband multicarrier OFDM signal. The number of the active carriers modulated by 16-Quadrature Amplitude Modulation (QAM) symbols is 1664. The rest of the carriers, as well as the DC carrier, are nulled to enable the half band filtering included in upsampling. After the IFFT, the signal is divided in I and Q branches and upsampled by a factor of two. A half band FIR filter is used to remove the images. In the next stage, the I and Q signals are upsampled by a factor of four; because the carrier frequency is chosen to be one quarter of the clock frequency, the upconversion can be included in the polyphase filtering. This is presented in detail in Section 9.3. The digital IF signal is clipped in order to reduce the high CF of the OFDM signal. The clipping algorithm used is discussed in Section 4.

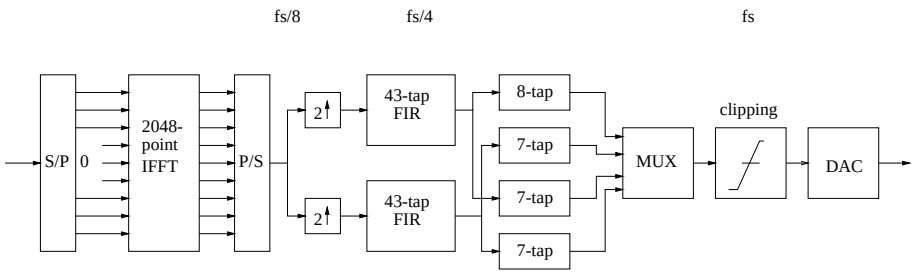

Figure 9.1 Block diagram of the OFDM modulator.

Table 9.1 Modulator specifications.

Channel separation	102.4 MHz
Signal bandwidth	83.2 MHz
Subcarrier spacing	50 kHz
Number of subcarriers	2048
Subcarriers in use	1664
ACLR	45 dB
EVM	-25 dB
Modulation	16-QAM

9.1 IFFT algorithm

An Inverse Discrete Fourier Transform is needed to generate the OFDM signal. Mathematically it can be expressed as

$$x(k) = \frac{1}{N}\sum_{n=0}^{N-1} X(n)W_N^{nk} \quad 0 \leq k < N, \tag{9.1}$$

where $W = \exp(j2\pi/N)$ and is known as a twiddle factor, $X(n)$ is the symbol sequence to be transmitted and $x(k)$ the corresponding time domain waveform. Factor $1/N$ affects the gain of the transmitter chain only and therefore it can be neglected.

A large number of Fast Fourier Transform (FFT) algorithms have been developed over the years. The Cooley-Tukey algorithm [54], nowadays known as radix-2, can be considered as the first breakthrough in the implementation of FFT. It was shortly followed by radix-4 and mixed radix algorithms. The idea of the radix algorithms is to decompose the original transform into smaller independent transforms, until the resulting transform is trivial to calculate. Also, algorithms based on different approaches, e.g. Fast Hartley Transform (FHT) [55] and Winograd algorithm [56], have been developed. FFT algorithms can be benchmarked using different criteria [57]-[59]. In this design, the main selection criteria for the algorithm are the minimal multiplicative complexity, a sufficiently simple control and the possibility of using pipelined architectures. A radix-2^2 IFFT algorithm [60] is chosen because it is a good compromise between the properties mentioned above. It has a relatively low multiplicational complexity and can be easily divided into stages (butterflies) so that a pipelined structure can be utilised.

The butterfly structure of the chosen radix-2^2 FFT is shown in Figure 9.2. The FFT butterfly can be easily converted to IFFT by changing the sign of the twiddle factor W. Here, it must be noticed that this concerns not only the complex multipliers, but also the trivial multiplications included in the butterfly. To implement a 2048-point transform, six butterfly stages and five complex multipliers between the stages are

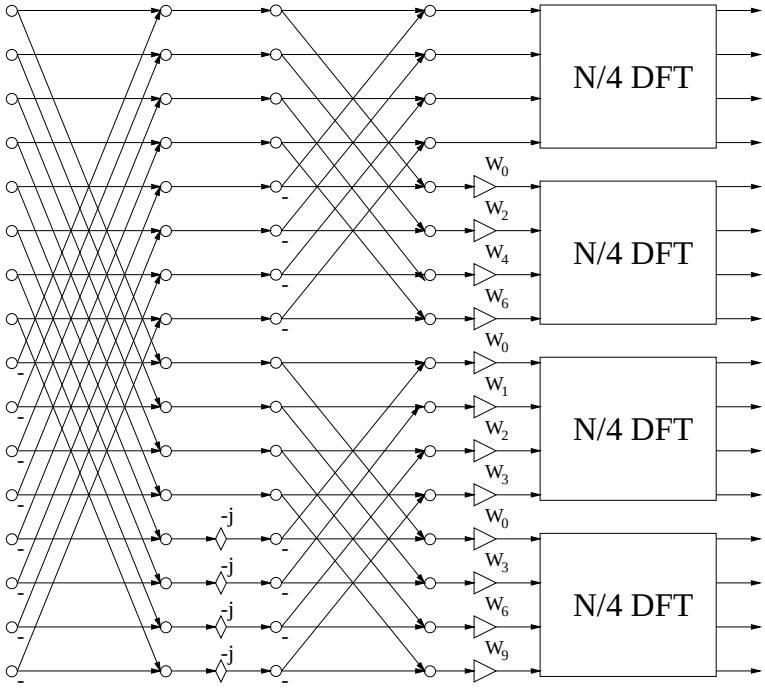

Figure 9.2 Structure of the radix-2^2 butterfly.

needed. The multipliers are used in serial mode in order to reduce the hardware.

In one butterfly stage, four statistically independent samples are added together and rotated: this yields a maximum gain of $4\sqrt{2}$. This worst case scenario must be taken into account in order to prevent overflows. However, scaling down with a factor of $4\sqrt{2}$ without increasing the noise floor needs three extra bits added at each stage. This is avoided by decreasing the scaling factor and allowing the signal to be saturated. In the first stages, where the saturation is more probable, the scaling factor is chosen high enough to keep the distortion at a sufficiently low level. In the later stages, the probability of the worst-case addition is negligible and the scaling factor can be low.

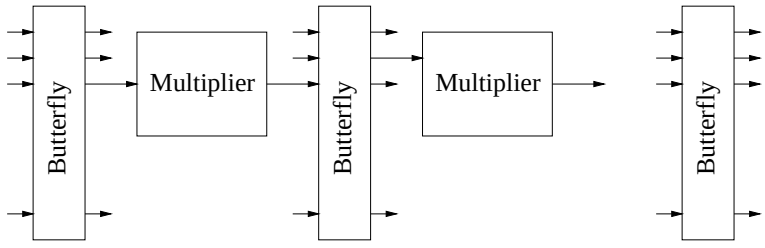

Figure 9.3 Structure of the IFFT.

The distortion caused by the signal saturation can be observed as an increased EVM and ACP. The succeeding half band filter can be used to clean the distortion from the sidebands: the inband distortion must be kept low enough. Anyway, the signal is deliberately clipped in the following stages and the saturation error in the IFFT can be included in the error caused by clipping. Further, the saturation in the IFFT limits the peak value of the signal and therefore relieves the need for clipping.

If the radix-2^2 algorithm is implemented as presented in Figure 9.2, the output samples are in bit-reverse-order and therefore an additional sorting block is needed. This type of algorithm is called a Decimation-In-Frequency (DIF) algorithm. The sorting block is implemented using memory and the memory needed is dependent on the word length. The minimization of memory determines the silicon area and therefore a smaller word length in the sorting operation reduces the silicon area drastically. The DIF implementation can be converted to decimation-in-time (DIT) implementation, in which the samples are fed to the system in bit-reverse-order and come out in order [49]. The DIT implementation is very close to the DIF implementation, but the butterflies are in reverse order. In the DIT implementation, the sort operation can be done before the IFFT. For this implementation, the input word size was 3-bits, which is enough for 16-QAM modulation, and the output was 12-bits. The memory size reduces to 1/4 when the sorting is completed before the IFFT. For this reason, the DIT implementation is chosen.

9.1.1 Complex rotator

A special effort is made to minimise the complexity of the complex multipliers. In the IFFT algorithms, one of the multiplicands is always $e^{j\omega}$, i.e. the multiplication is reduced to complex rotation.

In the Radix2^2 algorithm, the original IFFT is divided into four smaller IFFTs with a quarter of the size of the original transform. In each stage, the rotations needed can be written as

$$X' = Xe^{j2\pi\frac{n}{N}}, n = 0, ...N-1 \tag{9.2}$$

where X is a complex symbol and N the number of points in the transform in question. In this design, the rotation angles needed are

$$\phi = 2\pi\tfrac{n}{N} \quad , n = 0, ..., N-1 \tag{9.3}$$

where $N \in \{2048, 512, 128, 32, 8\}$. To implement a multiplier free complex rotator, the rotation is performed in steps. A CORDIC rotator [53] is a well-known solution to implement a multiplier free complex rotator. The elementary rotations of the CORDIC

rotator are

$$\begin{aligned} \phi_1 &= \pi/2 \\ \phi_i &= \arctan(2^{-(i-2)}), \quad i = 2,3,... \end{aligned} \tag{9.4}$$

and the rotation angle becomes

$$\phi_{COR} = \sum_{i=1}^{K_{COR}} d_i \phi_i \quad , d_i \in \{-1,1\}, \tag{9.5}$$

where d_i is the control sequence corresponding ϕ_{COR}. Setting ϕ equal to ϕ_{COR}, it can be seen that the resulting equation has no exact solution, but the number of stages K_{COR} must be chosen high enough to ensure a sufficient accuracy.

Instead of using CORDIC, it is reasonable to choose a solution where the sum of elementary rotations match the needed rotation with a minimal number of stages. This is done by choosing the elementary rotations as

$$\phi_i = \frac{\pi}{2^{(i-1)}}, \tag{9.6}$$

when the rotation angle becomes

$$\phi_{ROT} = \sum_{i=1}^{K_{ROT}} d_i \phi_i \quad , d_i \in \{0,1\}. \tag{9.7}$$

In this case, the equation $\phi = \phi_{ROT}$ can be solved for $N = 2048, 512, 128, 32, 8$ exactly, when the number of stages becomes $11, 9, 7, 5$ and 3, respectively.

A rotation of angle ϕ can be expressed by the matrix equation

$$\begin{bmatrix} I' \\ Q' \end{bmatrix} = \begin{bmatrix} \cos(\phi) & -\sin(\phi) \\ \sin(\phi) & \cos(\phi) \end{bmatrix} \begin{bmatrix} I \\ Q \end{bmatrix} \tag{9.8}$$

and implemented with a structure shown in Figure 9.4. The first ($\phi = \pi$) and the second ($\phi = \pi/2$) stages are trivial because the sine and cosine terms are reduced to zero or ± 1. In the following stages, the sine and cosine multipliers are implemented using multiplier-free CSD coefficients. The complexity of the CSD taps is minimised and the approximations used are presented in Table 9.2. The third stage, which has the highest complexity, can be simplified using the fact that $\sin(\pi/4) = \cos(\pi/4)$ when the multiplication can be placed after the addition operation. The number of CSD multipliers is reduced from four to two. For small angles the cosine terms are approaching one and after the fifth stage ($\phi \leq \pi/32$) the cosine term no longer needs to be implemented.

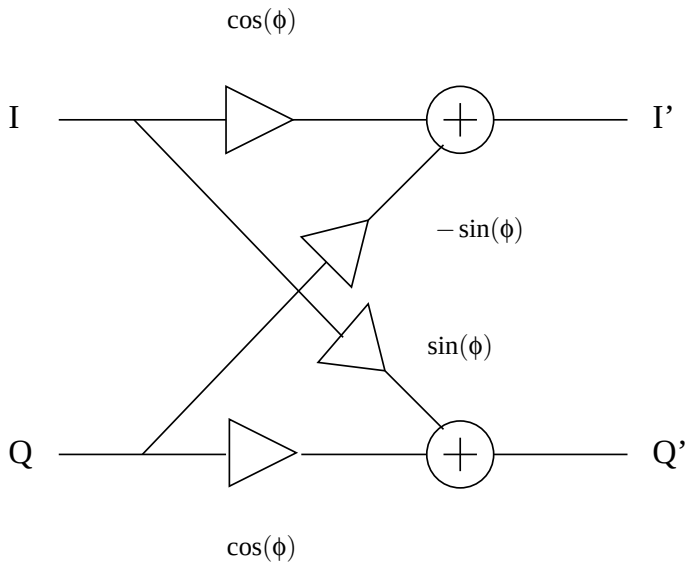

Figure 9.4 Block diagram of one rotation block.

Table 9.2 Realisation of the sine and cosine terms.

ϕ	$\cos(\phi)$	$\sin(\phi)$
π	-1	0
$\pi/2$	0	1
$\pi/4$	$2^0-2^{-2}-2^{-4}+2^{-6}$	$2^0-2^{-2}-2^{-4}+2^{-6}$
$\pi/8$	$2^0-2^{-4}-2^{-6}$	$2^{-1}-2^{-3}+2^{-7}$
$\pi/16$	$2^0-2^{-6}-2^{-8}$	$2^{-2}-2^{-4}+2^{-7}$
$\pi/32$	1	$2^{-3}-2^{-5}$
$\pi/64$	1	$2^{-4}-2^{-6}$
$\pi/128$	1	$2^{-5}-2^{-7}$
$\pi/256$	1	2^{-6}
$\pi/512$	1	2^{-7}
$\pi/1024$	1	2^{-8}

9.1.1.1 Error analysis

To analyse the error caused by the inaccuracy of the CSD coefficients the rotation is represented in the form

$$\begin{bmatrix} I' \\ Q' \end{bmatrix} = \begin{bmatrix} \cos(\phi)+e_1 & -(\sin(\phi)+e_2) \\ \sin(\phi)+e_2 & \cos(\phi)+e_1 \end{bmatrix} \begin{bmatrix} I \\ Q \end{bmatrix}, \tag{9.9}$$

where e_i is the difference between the ideal term and its CSD representation. The non-ideal rotation matrix can be decomposed to ideal rotation matrix Φ and error matrix $\mathbf{E}$ as follows

$$\begin{bmatrix} I' \\ Q' \end{bmatrix} = \left(\begin{bmatrix} \cos(\phi) & -\sin(\phi) \\ \sin(\phi) & \cos(\phi) \end{bmatrix} + \begin{bmatrix} e_1 & -e_2 \\ e_2 & e_1 \end{bmatrix} \right) \begin{bmatrix} I \\ Q \end{bmatrix}. \tag{9.10}$$

For simplicity, this is written as

$$\mathbf{a}' = (\Phi + \mathbf{E})\mathbf{a} = \mathbf{a}_1 + \mathbf{e}, \tag{9.11}$$

where $\mathbf{a}$ is the original vector to be rotated, $\mathbf{a}_1$ the ideally rotated vector and $\mathbf{e} = \mathbf{E}\mathbf{a}$ the error vector. Figure 9.5 clarifies the situation. Using the symmetry of the error matrix, it can be presented as a product of rotation matrix and constant term

$$E = \begin{bmatrix} e_1 & -e_2 \\ e_2 & e_1 \end{bmatrix} = G \begin{bmatrix} e & -ke \\ ke & e \end{bmatrix} = G \begin{bmatrix} \cos(\phi_e) & -\sin(\phi_e) \\ \sin(\phi_e) & \cos(\phi_e) \end{bmatrix}. \tag{9.12}$$

The rotation angle becomes

$$\phi_e = \arctan\left(\frac{e_2}{e_1}\right) \tag{9.13}$$

and the gain term

$$G = \frac{||\mathbf{e}||}{||\mathbf{a}||} = \frac{e_1}{\cos\phi_e}. \tag{9.14}$$

The sine of the angle between the actual and ideally rotated vectors can be solved from Figure 9.5

$$\sin(\Delta\phi) = \frac{||\mathbf{e}||\sin(\phi_e - \phi)}{\sqrt{||\mathbf{a}||^2 + ||\mathbf{e}||^2 - 2||\mathbf{a}||||\mathbf{e}||\cos(\phi_e - \phi)}}. \tag{9.15}$$

After further simplification and utilisation of the terms defined above, the rotation error caused by one stage becomes

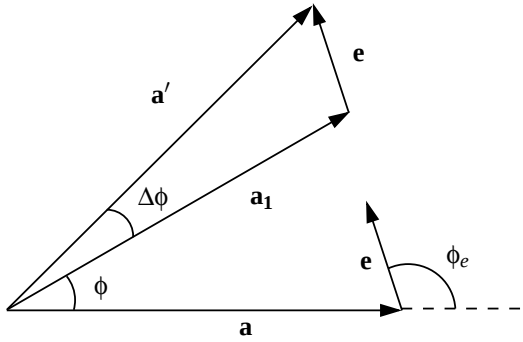

Figure 9.5 Non-idealities of the vector rotation.

$$\Delta\phi = \arcsin\left(\frac{G\sin(\phi_e-\phi)}{\sqrt{1+G^2+2G\cos(\phi_e-\phi)}}\right). \tag{9.16}$$

A bound for the total angular error $\Delta\phi_{tot}$ caused by the chain of rotations can be found by calculating the error for each stage separately using Equation 9.16 and composing the worst-case combination. The maximal angular errors are presented in Table 9.3. The number of stages K_{ROT} needed to implement the rotation in the case of $N = 2048$ is theoretically 11, but, in practice, only 10. This is because the error caused by the preceding stages is larger than the last rotation angle $360^\circ/2048 = 0.176^\circ$. Actually, this is true for the 10^{th} stage also, but it should be noticed that the $\Delta\phi_{tot}$ is the worst-case scenario and that most of the time the error can be significantly smaller. Simulations showed that the 11^{th} stage had no effect on the EVM of the system, but the 10^{th} stage still had an effect and therefore it was implemented.

9.1.1.2 Comparison

The main target of this error analysis is to compare the performances of the CORDIC rotator and the rotator discussed earlier in terms of complexity. To achieve the same accuracy, the number of CORDIC stages can be evaluated using the inequality

$$|\textstyle\sum_{i=1}^{K_{COR}} d_i\phi_i - \frac{n2\pi}{N}| < \varepsilon \quad , d_i \in \{-1,1\}, n = 0,1,2,...,N-1. \tag{9.17}$$

The number of stages K_{COR} is increased until the inequality is satisfied for all n. The results are shown in Table 9.3. Case $N = 8$ is tricky, because ideally there is no error in the reference case. In practice, the accuracy is limited due to finite word lengths in digital circuits, which can be assumed to be quite equal in both cases. However, it is justified to assume that at least as many CORDIC stages as in the next case $(N = 32)$

Table 9.3 Number of rotation stages needed to achieve equal accuracy

N	8	32	128	512	2048
K_{ROT}	3	5	7	9	11 (10)
$\Delta\phi_{tot}$	0°	0.068°	0.43°	0.49°	0.49°
K_{COR}	(>12)	12	9	9	9

is needed.

Another way to implement the $n2\pi/8$ rotation using CORDIC is to bypass the rotator or change the sign in the case of trivial rotations $(0,\pi)$, utilise one stage to implement rotations $\pm\pi/2$ and two stages in the case of $n \in \{1,3,5,7\}$. This approach has two problems. First, some extra control logic is needed, and second, more severe, the gain of the system is not constant but depends on the rotation angle. This means that a compensation system is needed. This extra hardware combined with a two-stage CORDIC rotator has a complexity comparable to the complexity of the rotator with three stages.

The effects of the finite word lengths are not included in this mathematical error analysis. The purpose is to find differences in these two implementations; it is reasonable to assume that both rotator structures show similar behaviour when the word length effects are included. Simulations support this assumption.

Another advantage compared with CORDIC is the simple control of the rotation angle. The rotation angle is determined by n in Equation 9.2 and this information must be converted to a corresponding control word in order to control the rotation stages. In our case, this becomes extremely simple because the control word is the digital presentation of n. The MSB and LSB in the control word corresponds to the first and the last stage of the rotator, respectively. The rotations are always made in the positive direction only, so the corresponding bit in the counter word indicates whether the rotation stage is bypassed or active. In the case of CORDIC, the control sequence d_i (see Equation 9.5) must either be computed real time from n, using a separate angle computation block, or pre-compute it for all n and utilise memories. In both cases, extra hardware is needed.

9.2 Inverse sinc

The sinc(x) frequency response distortion resulting from D/A-conversion is conventionally compensated by using filters [24], [25]. Compensation is needed to cancel the droop introduced by the sinc effect, especially in the case of very wideband signals. At the IF, the compensation can be achieved by using a real filter. If the compensation is in the baseband, a complex filter is needed. The drawback of the baseband com-

pensation is its increased complexity; on the other hand, the computation rate can be lower.

Here, a method suitable for the OFDM system is presented. This algorithm is applied prior to the Inverse Fast Fourier Transform (IFFT). Before the IFFT, the frequency response of the signal can be modified by scaling the powers of the different carriers. The easiest way to do this is to scale the data symbol of the corresponding carrier. In this specific case, the input data must be multiplied with a suitable inverse sinc function. If this is performed in serial mode, only one multiplier is needed. Another advantage is that this multiplier can operate with a lower computation rate than the solutions based on filtering. The inverse sinc function can be either read from a memory or approximated by using very simple ramp generator structures. In addition, this type of algorithm can be used to correct any kind of spectral distortion caused by a non-ideal transmitter if the non-idealities remain unchanged and are known beforehand. This Section is based on [41].

9.2.1 Compensation algorithm

The frequency response of the D/A-converter (zeroth-order hold) can be written as

$$H_{D/A} = \frac{\sin(\pi f/f_s)}{\pi f/f_s} e^{-j\pi f/f_s}, \tag{9.18}$$

where f_s is the sampling frequency. The distortion can be compensated by using a linear phase filter with frequency response

$$H(f) = 1/\mathrm{sinc}(f/f_s). \tag{9.19}$$

However, in the OFDM system, this frequency response can be implemented by adjusting the powers of the different carriers. The simplest way to adjust the power of a particular carrier is to scale the amplitude of the corresponding data symbol before the IFFT. This means that the serial form input data must be multiplied by a suitable function in order to achieve the wanted frequency response at the IF. This is presented in Figure 9.6.

If the centre frequency of the signal at the IF is f_c and the signal bandwidth is W, it means that the interesting frequency band is $[f_c - W/2, f_c + W/2]$, and the multiplying function needed is

$$H(f) = 1/\mathrm{sinc}(f/f_s), f \in [f_c - W/2, f_c + W/2]. \tag{9.20}$$

This must be presented in discrete form to find the coefficient for N carriers.

$$H(n) = 1/\text{sinc}(\frac{f_c - W/2}{f_s} + \frac{W}{f_s}\frac{n}{N}), n = 0, ..., N-1. \quad (9.21)$$

The ratio between the sample frequency and the signal bandwidth can be expressed as a function of the OSR

$$H(n) = 1/\text{sinc}(\frac{f_c}{f_s} - \frac{1}{2\text{OSR}} + \frac{1}{\text{OSR}}\frac{n}{N}), n = 0, ..., N-1. \quad (9.22)$$

The incoming data is cut onto blocks of N samples and multiplied sample-wise by $H(n)$ before the serial to parallel conversion.

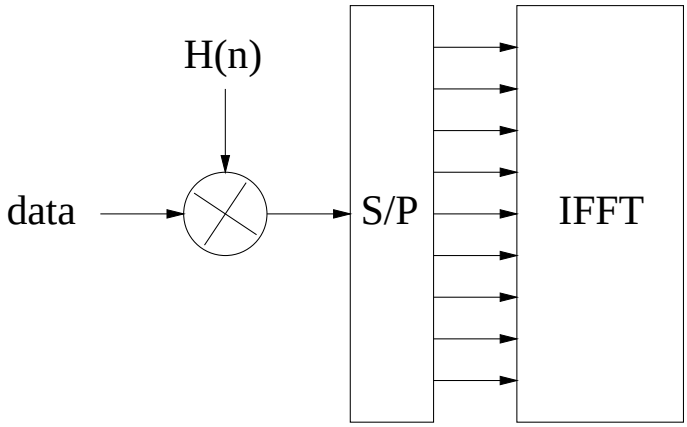

Figure 9.6 Block diagram of the compensation system.

9.2.2 Inverse sinc generation

Function $H(n)$ must be either read from a memory or approximated by using ramp generators. Here, two approximations, linear and parabolic, are studied. These approximations for $H(n)$ can be generated by structures shown in Figure 9.7 when the constants k_1, k_2 and k_3 are chosen properly. The constants needed are derived by using commonly known polynomial fitting methods.

The ideal $H(n)$, and the linear and parabolic approximations, are presented in Figure 9.8. In this example, $f_c/f_s = 1/4, N = 2048$ and OSR $= 8$. The constants are presented in Table 9.4. Note that the inverse sinc ramp is scaled so that its maximum does not exceed 1. As can be seen, the parabolic approximation gives very accurate results; in simulations, the performance of the parabolic ramp is equal to the ideal inverse sinc function.

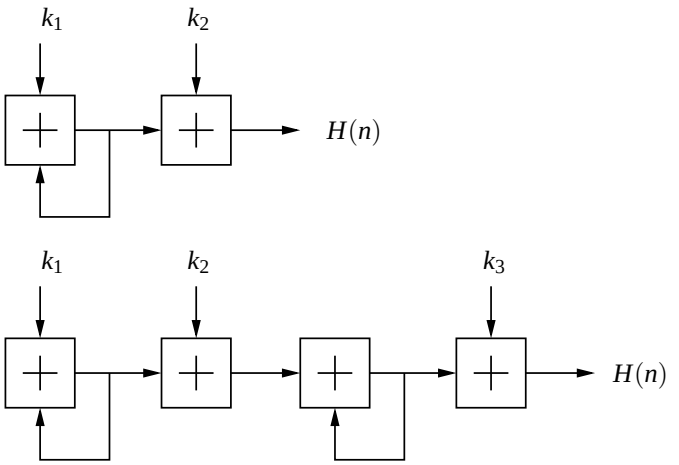

Figure 9.7 Linear and parabolic ramp generator.

Table 9.4 Ramp generator constants.

	k_1	k_2	$k3$
Parabolic	$1.5779 \cdot 10^{-8}$	$3.3453 \cdot 10^{-5}$	0.8982
Linear	$4.9603 \cdot 10^{-5}$	0.8927	

9.2.3 Performance

An OFDM modulator similar to that presented in Figure 9.1 and Table 9.1 is simulated. In this case, Equation 9.22 becomes

$$H(n) = 1/\text{sinc}(0.1875 + \frac{1}{8}\frac{n}{2048}), n = 0, ..., 2047. \quad (9.23)$$

The sinc effect caused by a D/A-converter is modelled with an FIR filter. The efficiency of the compensation is measured by calculating the EVM by comparing the received symbols to the ideal ones.

For comparison, a situation with no compensation, and one with compensation using a 7-tap FIR filter [24], are presented. The compensation filter is located at the IF before the D/A-conversion and it needs an eight-times-higher computation rate than the method presented in here.

The results are presented in Table 9.5. All compensation methods enhance the signal quality noticeably. Compared to [24], all methods presented here have better efficiency. The parabolic approximation gives as good results as the ideal inverse sinc, while the linear approximation is only slightly inferior. Due to the simulation non-idealities, i.e. limited numerical accuracy and finite length filters, the parabolic

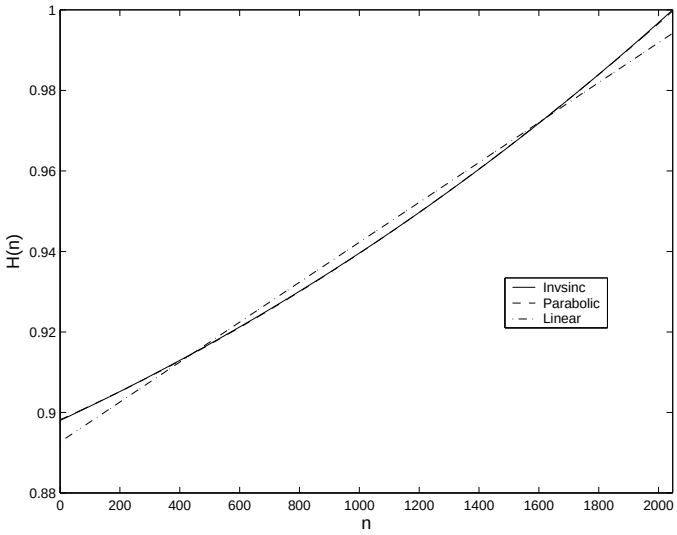

Figure 9.8 Parabolic and linear approximation of the inverse sinc ramp.

approximation seems to give a better result than the ideal inverse sinc. For the same reason, the result for the ideal inverse sinc is not zero, as it should ideally be.

The costs of the method presented are only one complex multiplier, which is reduced to two real multipliers because the other multiplicand, $H(n)$, is always real and a very simple ramp generator. Compared to the compensation methods based on filtering, the method presented uses a significantly lower computation rate, because the filtering is applied to an upsampled signal, unlike in this case.

Table 9.5 Simulated EVM.

Method	EVM (%)
None	2.742
7-tap FIR	1.148
Inverse sinc	1.108
Parabolic	1.107
Linear	1.117

9.2.4 Implemented algorithm

The inverse sinc compensation is done as presented above. However, this case differs from the one presented earlier in that the input samples are in bit-reverse-order due to the DIT implementation chosen for IFFT. The DIT implementation is chosen to decrease the amount of hardware needed in the sorting operation and therefore the

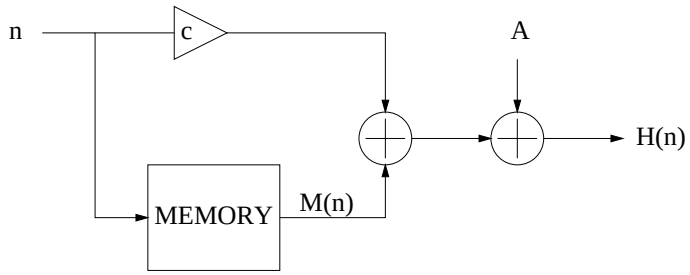

Figure 9.9 Generation of $H(n)$.

inverse sinc compensation must be placed after the sorting block. Otherwise, the increased wordlength needed to implement the inverse sinc compensation causes that no advantage is gained using DIT.

The fact that the input samples are not in order impedes the use of ramp generators. Instead, the weighting coefficient for a particular sample must be either calculated by using the sample number or read from the memory. To minimise the complexity of the calculation logic and the size of the memory a solution based on both calculation and memory is utilised. The inverse sinc ramp $H(n)$ is divided into a constant A, linear part and correction term $M(n)$ according to equation

$$H(n) = A + cn + M(n). \tag{9.24}$$

The linear term can be easily calculated using a CSD coefficient and the correction term is read from the memory using the sample number as an address. The structure used to obtain $H(n)$ is presented in Figure 9.9.

9.3 Upsampling and upconversion

The complex samples from the IFFT are split into real and imaginary parts. These I and Q branches are upsampled with a factor of 8. This is achieved in two steps. In the first phase, the signals are zero-padded and filtered with a 43 tap half band FIR filter. This doubles the sampling ratios of the signals and reduces the noise on the sidebands. All the odd taps of the half band filter, except the centre tap, are zeroes, and therefore only 22 taps need to be implemented. All the taps are implemented using CSD coefficients. In the second phase, three zeroes are placed between the adjacent samples and the resulting images are filtered out using a 29-tap FIR filter.

The upconversion is performed according to the equation

$$y(n) = I(n)\cos(2\pi\frac{f_c}{f_s}n) - Q(n)\sin(2\pi\frac{f_c}{f_s}n). \tag{9.25}$$

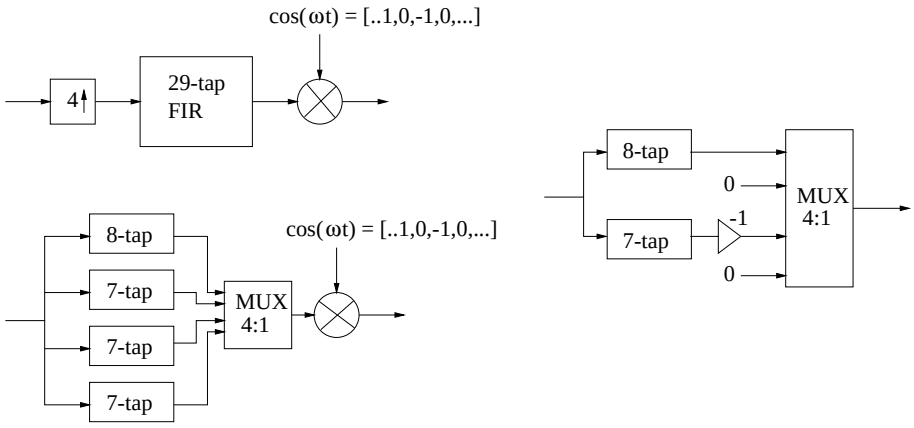

Figure 9.10 Simplification of the upconversion system presented step by step [61].

The carrier frequency (f_c) is chosen to be one quarter of the clock frequency (f_s). The advantage is that the sine and cosine waveforms needed in the upconversion are reduced to the sequences of ± 1 and zeroes. There is therefore no need for multipliers and the upconversion can be included in the preceding polyphase filtering stage. Previously, this kind of structure has been used in [61]. A 29 tap FIR filter is decomposed to four subfilters. Because the multiplicative carrier has a value of zero for every other sample, only two of the subfilters need to be implemented. Further, the multiplicand -1 can be implemented by changing the signs of the subfilter taps and the multiplicand 1 is trivial. For the *I* branch, this process is presented step by step in Figure 9.10.

When *I* and *Q* branches are combined according to Equation 9.25, we end up with the structure shown in Figure 9.1. The upsampling by a factor of four can be performed by using four filters, two for both (I and Q) branches, and the upconversion can be fully included in the filtering operation without extra hardware. The outputs of the subfilters are combined by using a multiplexer in order to generate a real valued IF frequency signal. In this structure, the multiplexer is the only block in the upconversion process that needs to operate at the full speed. The filters need to operate at the quarter of the clock frequency only: this structure is therefore very suitable for high-speed solutions.

9.4 Clipping

In OFDM transmission, several statistically independent sinusoidal signals are combined. The resulting signal is Gaussian distributed with a high PAR. According to simulations, the PAR of the IF signal in our case is around 13 dB. To relieve the linearity requirements of the PA, the signal is digitally clipped. As presented in Section

1.1.2, the requirement for the number of bits in the D/A-converter can be reduced also. Without clipping, the maximum value of the signal is unknown and, in order to prevent overflows, the full dynamic range of the digital circuitry cannot be effectively used. In practice, the back-off of the D/A-converter must be the nominal CF added with some margin.

The choice of the clipping algorithm is based on the following requirements. The OFDM modulation should remain untouched and no side information should be transmitted. This precludes the algorithms based on the modification of the modulation, e.g. Block Coding [19], Selected Mapping [20], Partial Transmit Sequence [21] and Tone Reservation [16]. The maximum value of the D/A-converter's input signal should be known in order to make the most of the D/A-converter's dynamic range. This precludes the methods that include filtering after the peak reduction, e.g. all baseband methods. Also, because of the high-speed requirements, the iterative methods are unpractical. Taking into account the aspects mentioned above, the windowing algorithm (Chapter 4) is chosen. The CF can be reduced down to 10 dB while still keeping the signal quality at a sufficient level. This enables the reduction of the number of bits in the D/A-converter from the eleven needed without clipping down to ten, which is a significant advantage when the sampling rate of the D/A-converter is as high as 800 MHz.

The windowing algorithm is implemented as presented in Chapter 4. An extra effort is made to implement the division operation in Equation 4.2. Implementing a division operation in a straightforward manner needs very complex hardware and problems arise from the high operation speed also. Therefore, a piecewise linear approximation is used for the function $1/x(n)$. The structure needed is shown in Figure 9.11. Constants a_n and b_n and the points of division are chosen to minimise the approximation error in the area of interest. A multiplexer is used to choose the right output, depending on the value of $x(n)$.

9.4.1 Window selection

Several window types were tested through simulations and even a triangular window with 31 samples proved to be sufficient. This fact gives a lot of freedom when selecting the window. To keep the hardware simple, the coefficients of the filter structure are realised as CSD taps. Because of the high sampling frequency, the CSD taps must be as simple as possible. Extra difficulties are caused by the feedback loop, which obstructs the utilisation of the conventional pipelining techniques. In order to reach the speed requirements, a window consisting of CSD taps with two terms maximum, preferably one, is designed. The window is designed by trial and error; the result is presented in Figure 9.12 and Table 9.6.

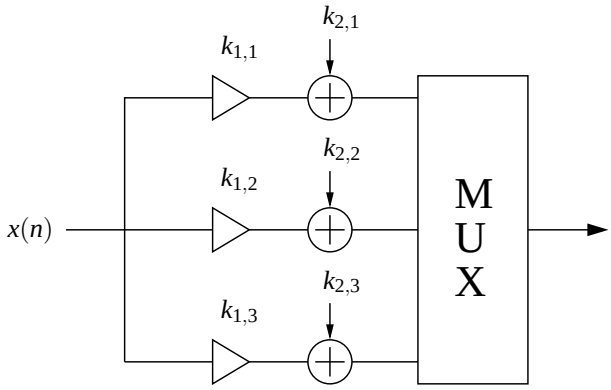

Figure 9.11 Approximation block for the division operation.

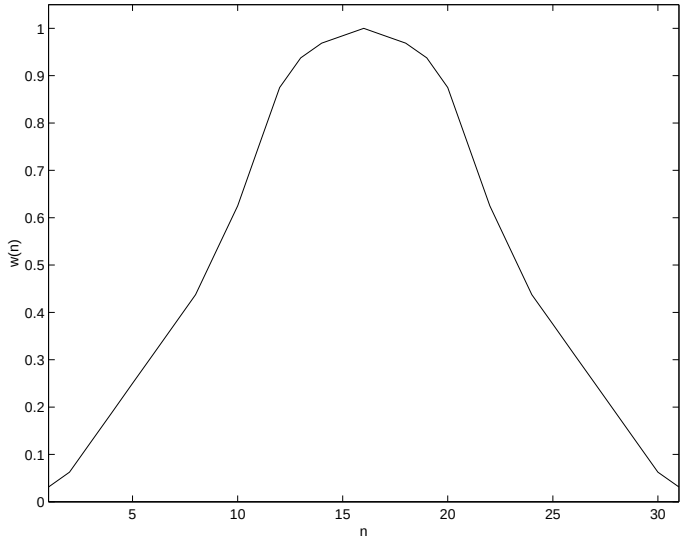

Figure 9.12 Window function.

Table 9.6 CSD presentation of the used window.

w(1)	2^{-5}	0.03125
w(2)	2^{-4}	0.0625
w(3)	2^{-3}	0.125
w(4)	$2^{-2}-2^{-4}$	0.1875
w(5)	2^{-2}	0.25
w(6)	$2^{-2}+2^{-4}$	0.3125
w(7)	$2^{-1}-2^{-3}$	0.375
w(8)	$2^{-1}-2^{-4}$	0.4375
w(9)	$2^{-1}+2^{-5}$	0.53125
w(10)	$2^{-1}+2^{-3}$	0.625
w(11)	$1-2^{-2}$	0.75
w(12)	$1-2^{-3}$	0.875
w(13)	$1-2^{-4}$	0.9375
w(14)	$1-2^{-5}$	0.96875
w(15)	$1-2^{-6}$	0.984375
w(16)	1	1

9.5 Implementation

At first, the system was tested through extensive Matlab and VHDL simulations. In these simulations, the functionality of the algorithms were verified and the optimal wordlengths were determined. The spectrum of the digital output with the inverse sinc response is presented in Figure 9.13.

The front-end of the system, namely the sinc compensation and the IFFT, was implemented using a Field Programmable Gate Array (FPGA). The interpolation filters, upconverter, clipping block and 12-bit D/A-converter were implemented on a 1 poly 6 metal 1.2V 90 nm CMOS and packaged to a 144 pin Ball Grid Array (BGA) package. The die area of the chip is 5 mm^2 (0.75 mm^2 digital parts, 1.2 mm^2 DAC, 0.9 mm^2 decoupling capacitors). The power consumption of the digital part is 85 mW with a 819.2 MHz clock frequency (34 mW for the clipper); the DAC consumes 46 mW with a 10 mA full output current. The IFFT and the sinc compensation were synthesised with the same process; the area estimate was 0.8 mm^2.

The original plan was to use a 10-bit D/A-converter, but, because there were problems in getting the clipper synthesised at the required frequency of 819.2 MHz, two extra bits were added. These extra bits were needed because the unclipped signal has a high dynamic range, and, because the maximum of the signal is not exactly known, it is impossible to utilise the full dynamic range of the D/A-converter efficiently. However, in the measurements, there were no problems with the clipper and only 10 bits

were used in the D/A-conversion because the output of the clipper was only 10 bits.

The VHDL code was written by J. Lindeberg M.Sc, who also did the layout synthesis; the D/A-converter was designed by J. Pirkkalaniemi M.Sc. A detailed description of the circuit implementation will be published later by the aforementioned contributors.

9.6 Measurement results

The OFDM signal with a centre frequency of 204.8 MHz measured at the DAC output is shown in Figure 9.14. Curve 1 stands for the unclipped signal with a CF of 12.7 dB and curve 2 stands for the clipped signal with a CF of 10 dB. The increment of the signal power gained by clipping is 4.0 dB, of which 2.7 dB comes from the CF improvement, while the rest comes from the efficient utilisation of the DAC's dynamic range enabled by clipping. This is achieved at the cost of a slightly-decreased ACP, but still the advantage gained by the clipping is obvious. Here, it must be taken into account, that with the clipping the D/A-conversion is performed at 10-bit accuracy, but, without the clipping, the accuracy is 12-bits.

Because the D/A-converter is the limiting factor for the signal quality, especially at the high frequencies, the correctness of the digital algorithms was verified by decreasing the clock frequency in the measurements so that the performance of the DAC was no more the limiting factor. The spectrum measured at the 100 MHz clock frequency is presented in Figure 9.15 and is very similar to the simulated spectrum (Figure 9.13). In Figure 9.15, the spectral widening caused by clipping is clearly visible. Due to the lack of a suitable receiver, the EVM could not be measured directly. Therefore the EVM results are based on VHDL simulations. The clipping level and the wordlengths were chosen to keep the EVM below 3.4%.

The modulator presented is a part of a full OFDM transmitter including RF parts. The digital part is designed to give a sufficient signal quality with enough margin for the DAC and the following RF parts. The output spectrum of the full transmitter chain is presented in Figure 9.16, where the distortion caused by the RF parts is clearly visible. The ACP specification at the RF output was 35 dB with a 25 dBm output power level. The output power shown in Figure 9.16 is only 6.27 dBm because an attenuator was used in front of the spectrum analyser.

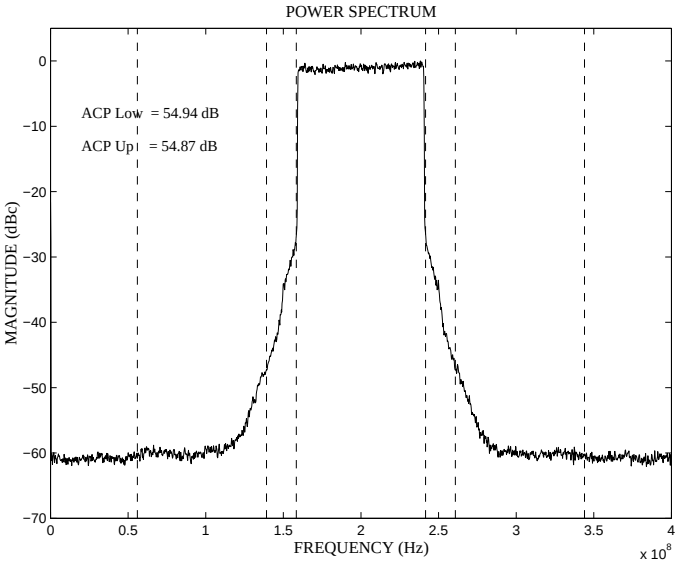

Figure 9.13 Simulated digital output with inverse sinc response.

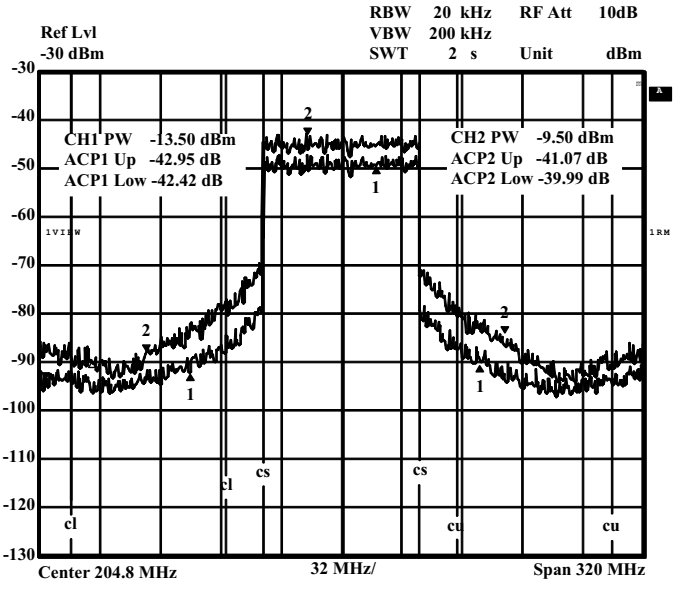

Figure 9.14 Measured spectrum with and without clipping.

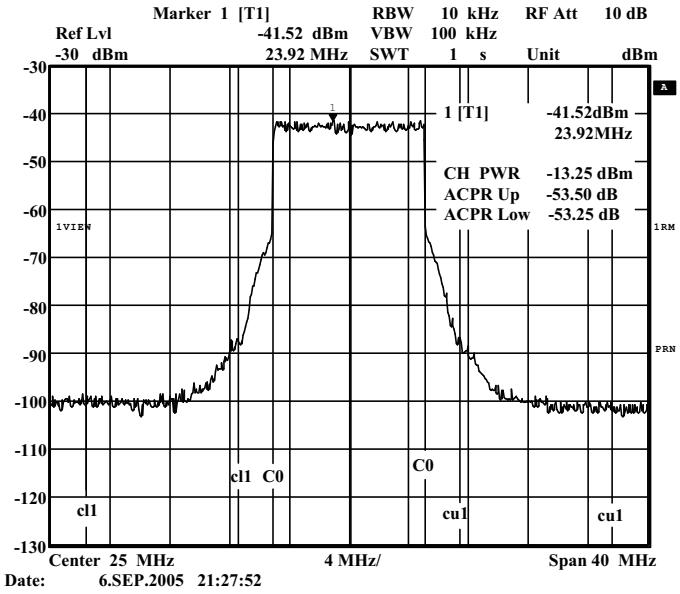

Figure 9.15 Measured output at 100 MHz clock frequency.

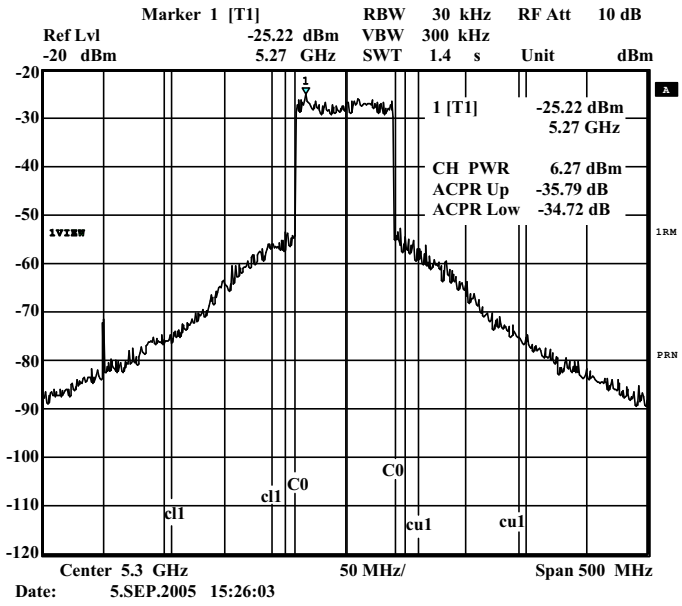

Figure 9.16 Measured RF output of the modulator.

9.7 Conclusions

A digital OFDM modulator with an 83.2 MHz bandwidth and 819.2 MHz sampling frequency was designed and implemented. This design also included an implementation of the windowing algorithm. The modulator was tested in measurements and it met the target specifications. Also, the advantage gained by clipping can be seen from the measurement results.

Chapter 10

Conclusions

In this thesis, methods for reducing the PAR of the signal in order to enhance the efficiency of the power amplifier were presented. WCDMA, OFDM, multicarrier GSM and multicarrier EDGE systems were covered. The methods presented were used to minimise the crest factor of the signal in such a way that the signal quality still fulfils the specifications. Two digital modulators, a multimode GSM/EDGE/WCDMA modulator and an OFDM modulator were designed and implemented. A specialised method of compensating the sinc distortion in the OFDM system was presented also.

It was shown that, in the WCDMA transmission, the quality metrics used do not guarantee an adequate signal quality for every user. The quality metrics EVM and PCDE are related in such a way that one can be derived from the other, which makes one of them unnecessary. Instead of using the PCDE, it might be more reasonable to calculate the SNR for each code channel separately, and set the minimum requirement for that quantity. Despite this fact, elsewhere in this thesis, the quality metrics were used as they are specified in the WCDMA standards.

An algorithm to implement the windowing method was proposed. It was tested in cases of WCDMA, OFDM, GSM and EDGE transmission. In the case of WCDMA, the algorithm was compared to other commonly known clipping methods and it was shown to be efficient, giving about 1 dB better crest factor reduction than the other methods analysed. In the case of multicarrier GSM and EDGE, where only the IF clipping methods seem to be reasonable solutions, the windowing method was utilised because the conventional clipping was out of question due to the spectral splattering problem. It was shown that a multicarrier GSM signal can be efficiently clipped by several decibels, depending on the number of carriers, but the EDGE signal still remains a challenge. An implementation of the windowing method was included in the OFDM modulator design. A special effort was made to simplify the algorithm enough to meet the high speed requirements. A new window with an efficient CSD

implementation was presented also.

Also, an approach totally different from to the conventional clipping methods of reducing the CF of the WCDMA signal was presented. This method, called the projection method, exploits the properties of the WCDMA modulation in such a way that, despite the high error measured by using the EVM and PCDE, the receiving user does not experience any error. The algorithms presented in this thesis were developed for practical implementations and are not optimal solutions. However, this algorithm can be expressed as a mathematical multivariable optimisation problem and can be solved exactly. In this work, the most simple clipping problem was solved mathematically in order to test the real potential of the presented idea. Results show that the CF can be reduced by some dBs, depending on the number of active codes and the definition used for the residual signal. The mathematical solution shows that there are still margins between the optimal solution and the solution achieved by the presented methods: this gives rise to fertile ground for further research.

References

[1] J. Vankka, J. Ketola, O. Väänänen, J. Sommarek, M. Kosunen and K. Halonen, "A GSM/EDGE/WCDMA Modulator with On-Chip D/A Converter for Base Station," *ISSCC Digest of Technical Papers*, February 3 - 7, 2002, San Francisco, USA, pp. 236-237.

[2] J. Vankka, J. Pyykönen, J. Sommarek, M. Honkanen, and K. Halonen, "A Multicarrier GMSK Modulator for Base Station," *ISSCC Digest of Technical Papers*, February 5 - 7, 2001, San Francisco, USA, pp. 354-355.

[3] P. B. Kenington, *High-Linearity RF Amplifier Design*, Artech House, 2000.

[4] S. C. Cripps, *Advanced Techniques in Power Amplifier Design*, Artech House, 2002.

[5] T. Sato, *Code division multiple access bas station transmitter*, United States Patent, 5751705, 1996.

[6] H. Muto, *Peak clipping in a quadrature modulator*, European patent application, EP0874501A2, 1998.

[7] R. Creighton, *System and method to reduce the peak-to-average power ratio in a DS-CDMA transmitter*, European patent application, EP0940925A1, 1999.

[8] S. L. Miller and R. J. O'Dea, "Peak Power and Bandwidth Efficient Linear Modulation," *IEEE Transactions on Communications*, Vol. 46, No. 12, Dec. 1998, pp. 1639 - 1648.

[9] Yang Hong-Kui, *Method & apparatus for reducing the peak power probability of a spread spectrum signal*, European patent application, EP1058400A2, 2000.

[10] M. Pauli and H.-P, Kuchenbecker, "Minimization of the Intermodulation Distortion of a Nonlinearly Amplified OFDM Signal," *Wireless Personal Communications* 4, 1996, pp. 90-101.

[11] R. van Nee and A. de Wild, "Reducing the Peak-to-Average Power Ratio of OFDM," *IEEE Vehicular Technology Conference*, 1998, vol. 3, pp. 2072-2076.

[12] M. Pauli and H.-P. Kuchenbecker, "On the reduction of the out-of-band radiation of OFDM-signals," *IEEE International Conference on Communications*, 1998, vol. 3, pp. 1304-1308

[13] M. Birchler, *Low-splatter peak-to-average signal reduction*, United States Patent, US5287387, Motorola, Inc., 1994.

[14] R. Prasad, *OFDM for Wireless Communication Systems*, Artech House, 2004.

[15] T. Wada, T. Yamazato, M. Katayama and A. Ogawa, "A Constant Amplitude Coding for Orthogonal Multi-code CDMA Systems," *IEICE Trans. fundamentals*, Vol. E80-A, No. 12, Dec. 1997, pp 2477-2484.

[16] J. Tellado, *Multicarrier Modulation with Low PAR*, Kluwer Academic Publishers, 2000.

[17] V. K. N. Lau, "Peak-to-average ratio (PAR) reduction by Walsh-code selection for IS-95 ans CDMA2000 systems," *IEE Proceedings Communications*, Vol. 147, No. 6, Dec. 2000, pp. 361-364.

[18] R. Braithwaite, "Using Walsh Code Selection to Reduce the Power Variance of Band-Limited Forward-Link CDMA Waveforms," *IEEE Journal on selected areas on communications*, Vol. 18, No. 11, Nov. 2000, pp.2260-2269.

[19] A.E. Jones, T.A Wilkinson and S.K Barton, "Block coding scheme for reduction of peak to mean envelope power ratio of multicarrier transmission schemes," *Electronics Letters*, Vol. 30, No. 25, Dec. 1994, pp. 2098 - 2099.

[20] R.W. Bauml, R.F.H Fischer and J.B. Huber, "Reducing the peak-to-average power ratio of multicarrier modulation by selected mapping," *Electronics Letters*, Vol. 32, No. 22, Oct. 1996 pp. 2056 - 2057.

[21] S.H. Muller and J.B. Huber, "OFDM with reduced peak-to-average power ratio by optimum combination of partial transmit sequences," *Electronics Letters*, Vol. 33, No. 5, Feb. 1997, pp. 368 - 369.

[22] Y.-W. Lin, H.-Y. Liu, and C.-Y. Lee, "A 1-GS/s FFT/IFFT processor for UWB applications," *IEEE Journal of Solid-State Circuits*, Vol. 40, No. 8, Aug. 2005, pp. 1726 - 1735.

[23] K. Maharatna, E. Grass and U. Jagdhold, "A 64-Point Fourier Transform Chip for High-Speed Wireless LAN Application Using OFDM," *IEEE Journal of Solid-State Circuits*, Vol. 39, No. 3, March 2004, pp. 484-493.

[24] H. Samueli, "The Design of Multiplierless FIR Filters for Compensating D/A Converter Frequency Response Distortion," *IEEE Transactions on Circuits ans Systems*, Vol. 35, No. 8, Aug. 1988, pp. 1064 - 1066.

[25] J. Vankka, J. Lindeberg and K. Halonen, "FIR Filters for Compensating D/A-Converter Frequency Response Distortion," *IEEE International Symposium on Circuits and Systems*, May 2002, Vol. 4, pp. 105-108.

[26] O. Väänänen, J. Vankka and K. Halonen, "Performance of EVM and PCDE Quality Metrics in a WCDMA Downlink," *Electronics Letters*, Vol. 38, No. 22, Oct. 2002, pp. 1386-1387.

[27] *Digital cellular telecommunications system (Phase 2+); Radio Transmission and reception* (GSM 05.05) V8.3.0 European telecommunications Standards Institute 1999.

[28] 3GPP Technical Specification Group Access Network *Base station conformance testing*, TS 25.141 V3.2.0. 2000.

[29] A. Papaoulis, *Probability, Random Variables, and Stochastic Processes*. McGraw-Hill, 1965.

[30] O. Väänänen, J. Vankka and K. Halonen, "Effect of Baseband clipping in Wideband CDMA System," *IEEE International Symposium on Spread Spectrum Techniques and Applications*, September 2-5, 2002, Prague, Czech Republic, proceedings Vol.2, pp.445 - 449.

[31] A. B. Carlson, *Communication Systems*. McGraw-Hill International Editions, Third Edition, 1986.

[32] O. Väänänen, J. Vankka and K. Halonen, "Effect of Clipping in Wideband CDMA System and Simple Algorithm for Peak Windowing," *World Wireless Congress*, May 28-31, 2002, San Francisco, USA, pp.614-619.

[33] E. C. Ifeachor and B. W. Jervis, *Digital Signal Processing, A Practical Approach*, Addison-Weshley Publishing Company, 1993.

[34] O. Väänänen, J. Vankka and K. Halonen, "Simple Algorithm for Peak Windowing and its application in GSM, EDGE and WCDMA systems", *IEE Proceedings Communications*, Vol. 152, No. 3, June 2005, pp. 357-362.

[35] R. Gross and D. Veeneman, "SNR and Spectral properties for a Clipped DMT ADSL Signal," *IEEE International Conference on Communications*, 1994, vol.2, pp. 843-847.

[36] O. Väänänen, J. Vankka, T. Viero and K. Halonen, "Reducing the Crest Factor of CDMA Downlink Signal by Adding Unused Channelization Codes," *IEEE International Symposium on Spread Spectrum Techniques and Applications*, September 2-5, 2002, Prague, Czech Republic, proceedings Vol.2, pp.455-459.

[37] O. Väänänen, J. Vankka, T. Viero and K. Halonen, "Reducing the Crest Factor of CDMA Downlink Signal by Adding Unused Channelization Codes," *IEEE Communication Letters*, Vol. 6, No. 10, Oct. 2002. pp. 443-445.

[38] R. J. Vanderbei, *Linear Programming: Foundations and Extensions*, Springer, Second edition, 2001.

[39] O. Väänänen, J. Vankka and K. Halonen, "Reducing the Peak to Average Ratio of Multicarrier GSM and EDGE Signals," *IEEE International Symposium on Personal, Indoor and Mobile Radio Communications*, September 15-18, Lisbon, Portugal, 2002, proceedings Vol.1, pp. 115-119.

[40] *Digital cellular telecommunications system (Phase 2+); Modulation* (GSM 05.04) V8.1.0 European telecommunications Standards Institute 1999.

[41] O. Väänänen, M. Kaltiokallio, J. Vankka and K. Halonen, "A Method for Compensating the D/A Converter Frequency Response Distortion in the OFDM System," *IEEE European Conference on Circuit Theory and Design*, Cork, Ireland, 2005, vol. 2, pp. 247-250.

[42] J. Ketola, *GSM/EDGE/WCDMA modulator for a base station*, Master's thesis, Helsinki University of Technology, 2001.

[43] J. Vankka, J. Ketola, J. Sommarek, O. Väänänen, M. Kosunen and K. Halonen, "A GSM/EDGE/WCDMA Modulator With On-Chip D/A Converter for Base Stations," *IEEE Transactions on Circuits and Systems*, Vol. 49, No. 10, Oct. 2002, pp. 645 - 655.

[44] 3GPP Technical Specification Group Access Network *Spreading and modulation*, 25.213 V3.2.0. 2000.

[45] 3GPP Technical Specification Group Access Network *Radio Transmission and Reception*, TS 25.104 V3.3.0. 2000.

[46] N. J. Fliege *Multirate Digital Signal Processing*, John Wiley & Sons, 1999.

[47] Z. Jiang and A. Willson, "Efficient Digital Filtering Architectures Using Pipelining/Interleaving," *IEEE Transactions on Circuits and Systems-II*, Vol. 44, No. 2, Feb. 1997, pp. 110-119.

[48] *Digital cellular telecommunications system (Phase 2+); Multiplexing and multiple access on the radio path* (GSM 05.02) V8.0.1 European telecommunications Standards Institute 1999.

[49] J. G. Proakis and D. G. Manolakis, *Digital Signal Processing*, third edition, Prentice Hall, 1996.

[50] F. M. Gardner, "Interpolation in Digital Modems-Part I: Fundamentals," *IEEE Transactions on Communications*, Vol. 41, No. 3, March 1993, pp. 501-507.

[51] L. Erup, F. M. Gardner and R. A. Harris, "Interpolation in digital modems-Part II: Implementation and performance," *IEEE Transactions on Communications*, Vol. 41, No. 6, June 1993, pp. 998-1008.

[52] C. W. Farrow, "A continuously variable digital delay element," *IEEE International Symposium on Circuits and Systems*, 7-9 June, 1988, vol.3, pp. 2641 - 2645

[53] J. Volder, "The CORDIC Trigonometric Computing Technique," *IRE Transactions on Electronic Computers*, Vol. EC-8, September 1959, pp. 330-334.

[54] J.W. Cooley and J.W. Tukey, "An Algorithm for Machine Computation of Complex Fourier Series," *Mathematical Computation*, Vol. 19, Apr. 1965, pp. 297-301.

[55] R.N. Bracewell, "Fast hartley Transform," *Proceedings of IEEE*, Vol. 72, No. 8, Aug. 1984, pp. 1010-1018.

[56] S. Winograd, "On Computing the Discrete Fourier Transform," *Mathematics of Computation*, Jan. 1978, pp. 175-199.

[57] M. Balducci, A. Choudary and J. Hamaker, "Comparative Analysis of FFT Algorithms in sequential and Parallel Form," Parallel DSP Group, Mississippi State University, 1996.

[58] M. Balducci, A. Ganapathiraju, J. Hamaker, J. Picone, A. Choudary and A. Skjellum, "Benchmarking of FFT algorithms," *IEEE Proceedings Southeastcon 97*. 12-14 April 1997, pp. 328-330.

[59] A. Ganapathiraju, J. Hamaker, A. Skjellum and J. Picone, "Contemporary View of FFT Algorithms," *Proceedings of the IASTED International Conference on Signal and Image Processing*, Las Vegas, Nevada, USA, October 1998, pp. 130-133.

[60] H. Shousheng and M. Torkelson, "A new approach to pipeline FFT processor," *The 10th International Parallel Processing Symposium*, Proceedings of IPPS ’96, 15-19 April 1996, pp. 766 - 770.

[61] J. Vankka, J. Sommarek, J. Ketola, I. Teikari and K. Halonen, "A Digital Quadrature Modulator With On-Chip D/A Converter," *IEEE Journal of Solid State Circuits*, Vol. 38, No. 10, Oct. 2003, pp. 1635 - 1642.